POLITECNICO
MILANO 1863

SCUOLA DI INGEGNERIA INDUSTRIALE
E DELL'INFORMAZIONE

Development of alternative plasmonic Ta:TiO_2/TiN multilayers as a platform for novel hyperbolic metamaterials

TESI DI LAUREA MAGISTRALE IN
MATERIALS ENGINEERING AND NANOTECHNOLOGY

Author: **Simone Bossetti**

Student ID: 991723
Advisor: Andrea Li Bassi
Co-advisor: Name Cristina Mancarella
Academic Year: 2022-2023

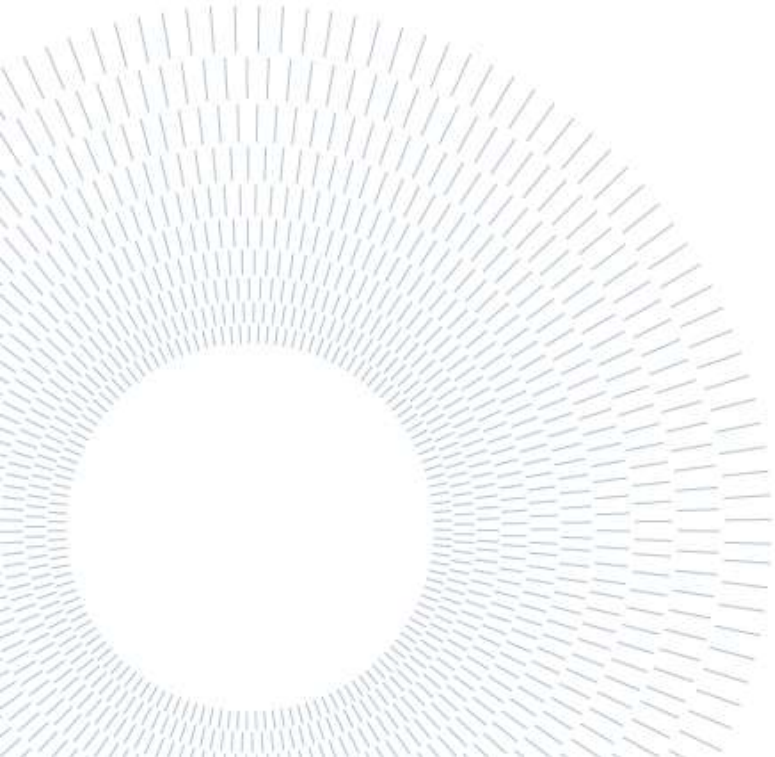

Abstract

Plasmonics is a branch of photonics that deals with the interaction between an electromagnetic field and metals, focusing on the possibility of overcoming the problems related to the diffraction limit of light. In the recent years novel plasmonic material, such as semiconductors and transition metal nitrides, have been investigated to overcome the limitations related to the use of the traditional plasmonic materials, such as gold and silver.

These novel plasmonic materials have attracted the attention of the researchers for the possibility of developing a new class of materials called metamaterials (MMs), which are structures artificially fabricated modulating, at the mesoscopic scale, specific features, such as density or composition, to obtain properties that cannot be found in nature. Among these, there is an interesting sub-class for its peculiar optical and plasmonic properties called hyperbolic metamaterials (HMMs), which are highly anisotropic structures with relatively simple geometry. The term "hyperbolic" is referred to the typical shape of the dispersion relation that can be achieved when a condition of dielectric anisotropy is satisfied. There are two main structures developed to obtain a hyperbolic behaviour: alternation of sub-wavelength layers of metal and dielectric or arrays of nanorod placed in a dielectric matrix.

During this project, several hyperbolic multilayers based on titanium nitride (TiN) and tantalum doped titanium oxide (Ta:TiO_2) have been modelled, deposited through Pulsed Laser Deposition (PLD) and characterized with the objective of understanding the effects of the deposition temperature, geometry and materials selected on the optical, electrical and plasmonic properties of the structures.

To model HMMs, the deposition and characterization of reference samples, made of single layer of TiN and Ta:TiO_2 have been necessary to investigate the electrical, optical and plasmonic properties of the single components of the multilayered structures.

Then two sets of multilayers have been deposited and characterized focusing the attention firstly on the effect of the order of the layers and of the deposition temperature on the optical properties of the multilayers, and secondly on the effect of the materials selected and the thickness of the layers on the plasmonic and optical properties of the samples.

The effects of the substrate temperature on the deposition of single layers of TiN and Ta:TiO_2 has been explored, highlighting the fact that a deposition temperature of 350°C is enough to promote the development of a stronger metallic behavior in TiN films and

to promote the crystallization of Ta:TiO_2 films without needing a post-deposition thermal treatment. A positive effect of the deposition temperature has been noticed also for the multilayered structures; indeed, several detachments of the films have been noticed, after the annealing, only the samples deposited at room temperature. The hyperbolic behaviour of the different structures has been predicted by means of simulations, noticing that structures with metallic layers thicker than the dielectric ones can show a wider range of hyperbolicity. A geometry dependence of the optical response of multilayers has been observed through simulations and confirmed by experimental data. In view of the results obtained, possible future perspectives could lie in the selection of different materials to enlarge the range of wavelengths in which a hyperbolic behaviour is shown, and in a deeper analysis of the effects of the geometry on the plasmonic properties of the multilayered structure. Finally, the use of a substrate heater should be extended to different materials and structures to exploit the positive effects highlighted during this work.

Key-words: titanium nitride, metamaterials, multilayers, plasmonics, hyperbolic behviour

Abstract in Italiano

La plasmonica è una branca della fotonica che si occupa dell'interazione tra un campo elettromagnetico e i metalli, concentrandosi sulla possibilità di superare i problemi legati al limite di diffrazione della luce. Negli ultimi anni sono stati studiati nuovi materiali plasmonici, come i semiconduttori e i nitruri di metalli di transizione, per superare i limiti legati all'uso dei materiali plasmonici tradizionali, come l'oro e l'argento.

Questi nuovi materiali plasmonici hanno attirato l'attenzione dei ricercatori per la possibilità di sviluppare una nuova classe di materiali chiamati metamateriali (MMs), le quali sono strutture fabbricate artificialmente modulando, alla scala mesoscopica, caratteristiche specifiche, come la densità o la composizione, per ottenere proprietà che non si trovano in natura. Tra questi, esiste una sottoclasse interessante per le sue peculiari proprietà ottiche e plasmoniche, chiamata metamateriali iperbolici (HMMs), che sono strutture altamente anisotrope con una geometria relativamente semplice. Il termine "iperbolico" si riferisce alla tipica forma della relazione di dispersione che si può ottenere quando è soddisfatta una condizione di anisotropia dielettrica. Esistono due strutture principali sviluppate per ottenere un comportamento iperbolico: l'alternanza di strati di metallo e dielettrico di spessore inferiore alla lunghezza d'onda o un'ordinata disposizione di nanofili posti in una matrice dielettrica.

Nel corso di questo progetto, sono stati modellati diversi multistrati iperbolici basati su nitruro di titanio (TiN) e ossido di titanio drogato con tantalio (Ta:TiO_2), depositati mediante deposizione laser pulsata (PLD) e caratterizzati con l'obiettivo di comprendere gli effetti della temperatura di deposizione, della geometria e dei materiali scelti sulle proprietà ottiche, elettriche e plasmoniche delle strutture.

Per modellare gli HMMs, la deposizione e la caratterizzazione di campioni di riferimento, costituiti da singoli strati di TiN e Ta:TiO_2, sono state necessarie per studiare le proprietà elettriche, ottiche e plasmoniche dei singoli componenti delle strutture multistrato.

Sono stati poi depositati e caratterizzati due set di multistrati, concentrando l'attenzione in primo luogo sull'effetto dell'ordine degli strati e della temperatura di deposizione sulle proprietà ottiche dei multistrati, e in secondo luogo sull'effetto dei materiali selezionati e dello spessore degli strati sulle proprietà plasmoniche e ottiche dei campioni.

Sono stati esplorati gli effetti della temperatura del substrato sulla deposizione di

singoli strati di TiN e Ta:TiO2, evidenziando che una temperatura di deposizione di 350°C è sufficiente a promuovere lo sviluppo di un comportamento metallico più marcato nei film di TiN e a favorire la cristallizzazione dei film di Ta:TiO_2 senza bisogno di un trattamento termico post-deposizione. Un effetto positivo della temperatura di deposizione è stato notato anche per le strutture multistrato; infatti, sono stati notati diversi distacchi dei film, dopo la ricottura, solo nei campioni depositati a temperatura ambiente. Il comportamento iperbolico delle diverse strutture è stato previsto mediante simulazioni, notando che le strutture con strati metallici più spessi di quelli dielettrici possono mostrare una gamma più ampia di iperbolicità. Una dipendenza della risposta ottica dei multistrati dalla geometria è stata osservata attraverso le simulazioni e confermata dai dati sperimentali. Alla luce dei risultati ottenuti, le possibili prospettive future potrebbero risiedere nella selezione di materiali diversi per ampliare la gamma di lunghezze d'onda in cui si manifesta un comportamento iperbolico e in un'analisi più approfondita degli effetti della geometria sulle proprietà plasmoniche della struttura multistrato. Infine, l'uso di un riscaldatore di substrato dovrebbe essere esteso a diversi materiali e strutture per sfruttare gli effetti positivi evidenziati in questo lavoro.

Parole chiave: nitruro di titanio, metamateriali, strutture multistrato, plasmonica, comportamento iperbolico.

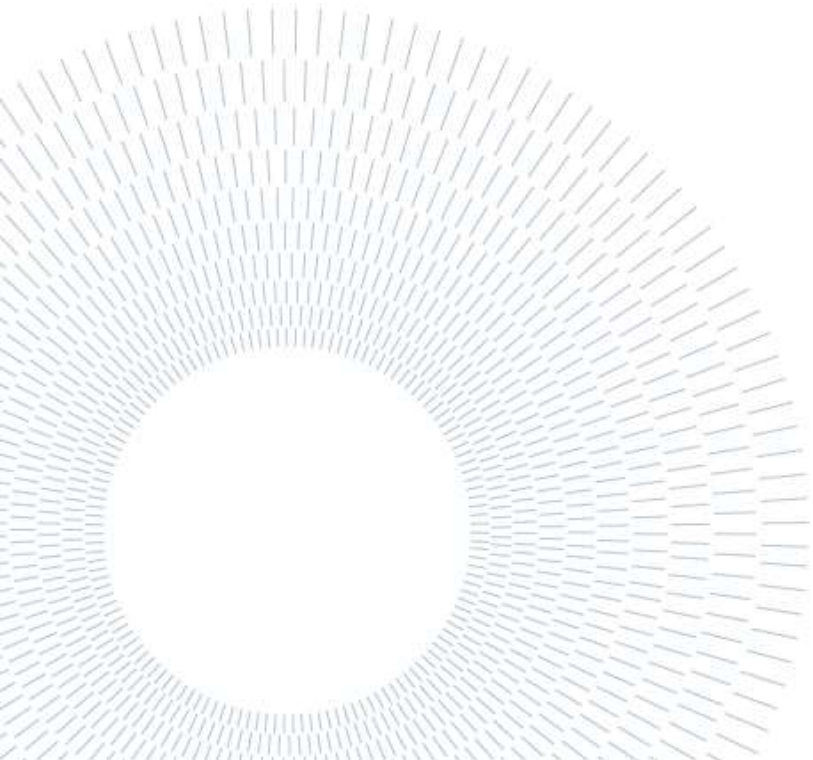

Contents

Introduction

Plasmonics is a branch of photonics that deals with the interaction between an electromagnetic field and metals, focusing on the possibility of overcoming the problems related to the diffraction limit of light [1]. The research in this field started in the 1950s after the discovery of the surface plasmon polaritons (SPPs). During the following decades, plasmonics became more and more of interest due to some discoveries, such as surface-enhanced Raman spectroscopy (SERS). Nowadays, the research on plasmonics is focused on the overcoming of the typical limitations of electronics and photonics, such as losses and diffraction limit.

The plasmonic devices that are intended to overcome these limitations are based on the excitation of sub-wavelengths modes due to the coupling between photons and free electrons. A peculiar feature of these modes is their dependence on the geometry of the device. Indeed, in presence of a metal-dielectric interface, the oscillations called surface plasmon polaritons (SPPs) are confined in a region close to the interface and exponentially decaying fields are established in both materials. While, in presence of metal nanoparticles (NPs), the modes, called localized surface plasmon resonances, are confined only inside the NPs. It is possible to identify two common effects related to the excitation of plasmon resonances: the intensification of the electromagnetic field in a region close to the metal-dielectric interface (SPPs) or to the metal nanoparticle surface (LSPR) and the subwavelength confinement of light[1]. Exploiting these effects could be of interest for many applications, such as photovoltaic, photocatalysis, sensing, surface enhanced Raman scattering and in general for application in the optoelectronics field.

The most common materials used for the development of plasmonic devices are noble metals, in particular gold and silver, because of their large electrical conductivity and small ohmic losses. On the other hand, these materials are characterized by several drawbacks, such as large optical losses (quite large values of the imaginary part of the dielectric function), low thermal and chemical stability, low compatibility with the conventional fabrication processes (problems related to the high percolation threshold) low tunability of optical and electrical properties (the carrier concentration is already large even without doping). For the reasons, the research on new noble-metal-free plasmonic materials became fundamental.

One of the most interesting categories of noble-metal-free plasmonic materials is semiconductors, such as transparent conductive oxides (TCOs). The most important feature of this type of materials is the versatility. Indeed, their properties can be easily

tuned through doping, obtaining several materials with different characteristics that can be adapted for various applications [2].

Another important alternative plasmonic material, titanium nitride (TiN), that belongs to the class of transition metal nitrides, is considered one of the most promising alternative plasmonic material [3] because of its good optical (relatively small negative dielectric permittivity and low interband losses) and electrical properties (relatively high electron conductivity and mobility), good chemical and thermal stability, high hardness and low friction coefficient and for its good compatibility with standard silicon manufacturing processes (CMOS).

These novel plasmonic materials have attracted the attention of the researchers for the possibility of developing a new class of materials called metamaterials (MMs), that are characterized by structures and properties never found in nature. In the first years of the 21st century, researchers have been interested in the development of metamaterials that can exhibit negative refractive index and negative electric permittivity to obtain the phenomenon of negative refraction. Since the high complexity of the structures required for this purpose, the research has shifted towards the development of simpler geometries that are characterized by tuneable optical properties, such as hyperbolic metamaterials [4]. HMMs are highly anisotropic structures with relatively simple geometry. The term "hyperbolic" is referred to the typical shape of the dispersion relation that can be achieved when one of the principal components of the electric or magnetic effective tensor has opposite sign with respect to the other two components. As a result, the material behaves as a metal ($\varepsilon<0$) along one direction and as a dielectric ($\varepsilon>0$) in the other one. An important effect related to this new shape of the dispersion relation consists in the possibility of having propagation of high-wavevector modes, that are typically forbidden in isotropic structures, making these materials interesting for several applications, such as high-resolution imaging and lithography, or thermal and spontaneous emission engineering [4]. The range of wavelengths in which the structure assumes a hyperbolic behaviour is strongly affected by the materials selected for the development of HMMs. Indeed, transition metal nitrides and transparent conductive oxides can be used as plasmonic building blocks to promote the development of a hyperbolic behaviour in the near-infrared (NIR) range, while III-V doped semiconductors, SiC and graphene favour this behaviour in the far-infrared range.

In the recent years, several structures based on TiN have been developed and studied proving that the multilayers or the superlattices can be considered more promising for future applications than the nanorod arrays. Nowadays, a deep understanding of the tunability of the optical and plasmonic properties of TiN-based multilayered structures has not been already reached.

Hence, this master thesis project has been carried out with the aim of developing and characterizing multilayers based on TiN and Ta:TiO_2 to investigate the effect of the

geometry (varying the number and the order of the layers), of the materials selected (changing the deposition condition for TiN and the content of tantalum for Ta:TiO_2) and the deposition temperature (using a substrate heater) on the optical, electrical and plasmonic properties of the multilayered structures. The choice of Ta:TiO_2 as a component of multilayered metamaterial structure represents a novelty and could be interesting for its peculiar plasmonic properties. Indeed, Ta:TiO_2 can behave as a metal in the IR because of its plasma frequency that is around 4100 nm, leading to the obtainment of a metamaterial multilayer with optical and plasmonic properties never explored.

The deposition of the samples has been performed by means of Pulsed Laser Deposition (PLD). The main deposition parameters, such as laser fluence, target-substrate distance, atmosphere and pressure have been retrieved from previous works carried out by the Nanolab research group. A thermal treatment has been performed on all the multilayers produced.

The morphology and the stoichiometry of the films deposited have been investigated by means of Scanning Electron Microscopy (SEM), Energy Dispersive X-ray Spectroscopy (EDXS) and Raman spectroscopy. The optical properties of the samples have been analyzed through UV-Vis-NIR spectroscopy and ellipsometry. Finally, electrical measurements have been performed by means of the four-probe Van der Pauw method.

The thesis is divided into five chapters and the principal contents are listed below:

- In Chapter 1, theoretical basis of plasmonics are presented in addition with a description of the principal phenomena of plasmonic resonances (SPPs and LSPR). A review on the traditional and alternative plasmonic materials in proposed, with particular attention to titanium nitride (TiN) and tantalum doped titanium oxide (Ta:TiO_2). Moreover, metamaterials (MMs) and in particular hyperbolic metamaterials, with their principal applications, are described. Finally, the goals of this thesis are declared.
- In Chapter 2, the experimental techniques adopted during this project are presented starting with the Pulsed Laser Deposition (PLD), adopted for the deposition of the sample. Then the ones employed for the characterization of specimens are described.
- In Chapter 3, the deposition parameters of the reference samples, composed by a single layer of TiN or Ta:TiO_2, are presented. Then, the experimental results obtained during the characterization of the specimens are proposed, analysed, and commented.
- In Chapter 4, the deposition parameters of the multilayered structures, made of TiN and Ta:TiO_2, are described. Then the experimental results obtained during the characterization are presented and commented, focusing on the simulations

performed to assess the hyperbolic behaviour of the structures and the geometry dependence of the optical response of the multilayers.

- In Chapter 5, a summary of the results obtained during the project is proposed and some possible future perspectives are introduced.

During this master thesis project, the process of deposition through PLD has been carried out by me at the Nanolab laboratory in Milan. I performed the characterization of the morphology and stoichiometry by means of SEM and Raman spectroscopy, and of the electrical properties through the four-probe Van der Pauw method, using the apparatus present at the Nanolab laboratory. The optical properties of the samples have been investigated by Dr. C. Mancarella at the Center for Nanoscience and Technology (CNST) of the Italian Institute of Technology (IIT) in Milan.

1 Plasmonics fundamentals, plasmonic materials and applications

In chapter 1, fundamentals of plasmonics are described, and a review of traditional and alternative plasmonic materials with their limitations and advantages is presented, with a focus on the materials studied in this thesis. After that, the possible applications of these materials are described. Finally, the objectives of this thesis project are explained.

1.1. Fundamentals of plasmonics

Plasmonics is a branch of photonics that deals with the interaction between an electromagnetic field and metals, focusing on the possibility of overcoming the problems related to the diffraction limit of light [1].

Since the high density of free carriers leads to a small spacing of the electron energy levels compared to the thermal excitation energy (k_BT) at room temperature, it is possible to describe the interaction between metals and electric fields using a classical approach based on Maxwell's equations of electromagnetism [1]:

$$\nabla \cdot \boldsymbol{D} = \rho,$$
$$\nabla \times \boldsymbol{E} + \frac{\partial \boldsymbol{B}}{\partial t} = 0,$$
$$\nabla \cdot \boldsymbol{B} = 0,$$
$$\nabla \times \boldsymbol{H} - \frac{\partial \boldsymbol{D}}{\partial t} = \boldsymbol{J}$$

where ϱ represent the charge volume density, **J** is the current density, **E** and **H** represent the macroscopic electric and magnetic field, **D** stands for the electric displacement and **B** is the magnetic induction and are described by the following equations:

$$\boldsymbol{D} = \varepsilon_0 \boldsymbol{E} + \boldsymbol{P}$$
$$\boldsymbol{B} = \mu_0 (\boldsymbol{H} + \boldsymbol{M})$$

where **P** represents the polarization or volume density of electric dipoles, **M** stands for the magnetization or volume density of magnetic dipoles, while ε_0 and μ_0 are respectively named the electric permittivity and the magnetic permeability of vacuum.

In case of a linear, isotropic, and nonmagnetic media, the two previous equations can be simplified to [1]:

$$\boldsymbol{D} = \varepsilon_0 \varepsilon \boldsymbol{E}$$

$$\boldsymbol{B} = \mu_0 \mu \boldsymbol{H}$$

where ε is the dielectric constant of the medium and μ is the relative permeability of the non-magnetic medium.

It is possible to obtain a different expression for the polarization **P** rearranging the previous equations (for a more detailed description see [1]) and introducing a new quantity, the electric susceptibility χ.

$$\boldsymbol{P} = \varepsilon_0 \chi \boldsymbol{E}$$

$$\varepsilon = 1 + \chi$$

To proceed with this description, it is fundamental to recall the Ohm's law, a constitutive linear relationship that highlights the direct proportionality between the applied electric field and the current density produced:

$$\boldsymbol{J} = \sigma \boldsymbol{E}$$

where σ is the conductivity of the medium.

Finally, it is possible to introduce a crucial optical property, the refractive index N, that can be expressed by the following equation:

$$N(\omega) = \sqrt{\varepsilon(\omega)}$$

Since the dielectric permittivity ε is a frequency dependent function [1], also N depends on the frequency ω. Seeing that the dielectric permittivity function ε(ω) is complex, also the function that describes the refractive index is complex:

$$N = n + ik$$

where the real part describes the phenomena of dispersion and propagation, while the imaginary part describes the phenomenon of absorption.

Adopting two different models, Lorentz and Drude ones respectively, it is possible to derive an analytical expression for the dielectric function ε(ω). In case of a dielectric material, the Lorentz model is more suitable, and it can be used to derive the following equations:

$$\varepsilon(\omega) = \varepsilon_1(\omega) - i\varepsilon_2(\omega)$$

$$\varepsilon(\omega) = 1 + \frac{\frac{Ne^2}{m\varepsilon_0}}{(\omega_0^2 - \omega^2) - i\gamma\omega}$$

where ω is the frequency of the electric field, N is the electron density, m is the electron mass, ω_0 represents the natural frequency of the system, that describes the transition between two subsequent vibrational energy levels, and γ is the coefficient of damping that is related to the scattering phenomena of the system, and it is expressed as the inverse of the relaxation time.

Knowing ε_1 and ε_2, it is possible to derive the real and imaginary part of the refractive index through the following expressions [1]:

$$\varepsilon_1 = n^2 - k^2$$

$$\varepsilon_2 = 2nk$$

$$n^2 = \frac{\varepsilon_1}{2} + \frac{1}{2}\sqrt{\varepsilon_1^2 + \varepsilon_2^2}$$

$$k = \frac{\varepsilon_2}{2n}$$

where k is also called the extinction coefficient and determines the absorption of an electromagnetic field that passes through the medium.

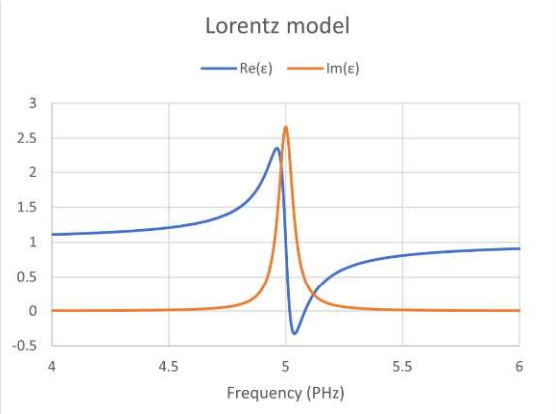

Figure 1.1 Schematic representation of the trend of complex dielectric function according to Lorentz model.

If the system is characterized by one Lorentz oscillator, it is possible to represent graphically (Figure 1.1) the trend of the dielectric function versus the frequency. An anomalous dispersion region is noticeable, and its width is related to the value of the damping factor γ. The graph of the imaginary part is centred on the natural frequency ω_0, representing the value at which the phenomenon of absorption is predominant.

In case of a system characterized by many natural frequencies, it is necessary to introduce a more general formula:

$$(\omega) = 1 + \sum_{j=1}^{m} \frac{f_j \frac{Ne^2}{m\varepsilon_0}}{\omega_{0j}^2 - \omega^2 + i\gamma\omega}$$

where j are the Lorentz oscillators, characterized by a proper oscillator strength f_j, a damping coefficient γ_j and natural frequency ω_{0j}.

Considering a metal, the Drude model can be used to describe its optical properties. The result is similar to the one discussed before, but now the natural frequency ω_0 is equal to zero, meaning that the electrons are not considered anymore bounded to the

nuclei. In reality, metals and dielectrics are more complex and so these models are not capable of describing precisely their optical behaviour. To overcome this problem, it is needed to make some corrections and to combine the two models.

1.1.1. Plasmonic resonances

Before proceeding with the analysis of the optical response of a material, it is necessary to introduce a new quantity that is present in the previous expressions of the dielectric function [1]. This quantity is called plasma frequency ω_p and it is expressed by the following equation:

$$\omega_p = \sqrt{\frac{Ne^2}{m\varepsilon_0}}$$

It is possible to attribute a physical meaning to this value of frequency because it corresponds to the characteristic frequency of collective oscillation of conduction electrons with the respect to the fixed positive ions.

According to the expression of ω_p, it is possible to state that the optical behaviour of a material can be tuned modifying the mass m of the electrons or, for example in case of semiconductors, increasing the carrier concentration through a process of doping.

This expression is valid only for a free electron gas, while if the effect of the potential related to the presence of the positive ions is considered, a new quantity called unscreened plasma frequency ω_{pu} needs to be introduced, and it is expressed by the following equation:

$$\omega_{pu} = \sqrt{\frac{Ne^2}{\varepsilon_0 m^*}}$$

where m^* is the effective mass of the electrons, which takes in account the contribution of the potential of the lattice.

Depending on the region of the material in which plasmonic excitation and propagation occurs, it is possible to distinguish two main cases:

- the bulk or volume plasmons
- the surface plasmons

The last class can be further divided in two subclasses depending on the dimensions of the material considered.

1.1.1.1. Bulk plasmon

It is possible to substitute the value of the frequency of plasma inside the dielectric function derived using a combination of Drude and Lorentz model, obtaining the following expression:

$$\varepsilon(\omega) = 1 - \frac{\omega_p^2}{\omega^2 + i\gamma\omega} = 1 - \frac{\omega_p^2}{\omega^2 + \gamma^2} + i\frac{\omega_p^2\gamma}{\omega(\omega^2 + \gamma^2)}$$

Since the damping coefficient is inversely proportional to the average collision time ($\tau \approx 10^{14}$s), γ is in the order of 10^{-14} s^{-1} and so can be neglected, obtaining the following expression:

$$\varepsilon(\omega) \cong 1 - \frac{\omega_p^2}{\omega^2}$$

Analysing this expression, it is possible to notice that when frequency of the incident electric field is equal to the plasma frequency the dielectric function is equal to zero. If $\varepsilon = 0$, also the refractive index N is null.

The refractive index N is related to the phase velocity of the electrons through the following expression:

$$N = \frac{c}{v_{phase}}$$

Hence, if N = 0 so the phase velocity tends to infinity. The phase velocity is linked to the wavelength of the electron through the wavevector:

$$v_{phase} = \frac{\omega}{k} = \frac{\omega\lambda}{2\pi}$$

If v_{phase} tends to infinite, also the wavelength λ tends to infinite. This implies that the electrons are oscillating all together collectively with the same phase at a frequency equal to ω_p. The quanta of oscillation of free electrons in a metal at the plasma frequency are called plasmons. It is possible to define it as a bulk plasmon when the material considered is not dimensionally limited.

The justification of this excitation can be found in the fact that an incident electric field provokes the displacement of the free charges present in material (Figure 1.2). Between the charges, a restoring force is created to restore the original unpolarized condition, leading the establishment of free charges oscillation.

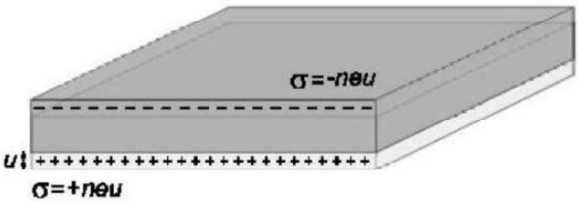

Figure 1.2 Longitudinal collective oscillations of the conduction electrons of a metal [1].

Combining the wave equation for the electric field with the simplified expression of the dielectric function [1], it is possible to derive the dispersion relation of a free electron gas:

$$\omega = \sqrt{\omega_p^2 + c^2 k^2}$$

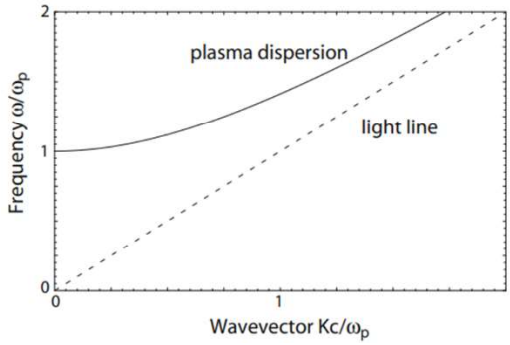

Figure 1.3 The dispersion relation of the free electron gas. Electromagnetic wave propagation is allowed only when ω is larger than ω_P [1].

1.1.1.2. Surface Plasmon Polaritons (SPPs)

Surface Plasmon Polaritons (SPPs) are electromagnetic excitations propagating at the interface between a dielectric and a conductor, evanescently confined in the perpendicular direction [1]. The electromagnetic surface waves are excited by the coupling between the incident electromagnetic field and the oscillating electrons of the metal.

As represented in Figure 1.4, the main features of SPPs are: the intensification of the electric field in the proximity of the metal-dielectric interface; the confinement of the surface wave along the normal direction with the respect to the interface; the wavelength dependency of the width of the confinement region. These characteristics can be relevant for several innovative applications, such as confinement of light below the diffraction limit [5].

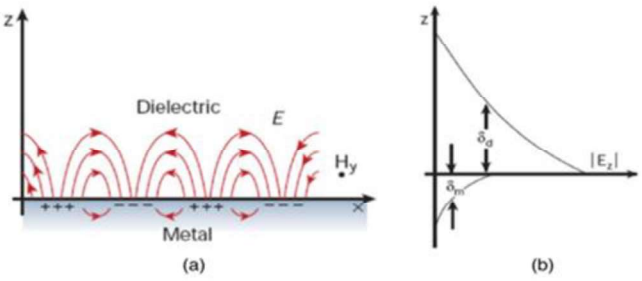

Figure 1.4 Schematic representation of the propagation of SPPs along the metal-dielectric interface; (b) representation of the increase in the electric field in the proximity of the interface during the propagation of SPPs[5].

Applying Maxwell's equations to the flat metal-dielectric interface, it is possible to retrieve expressions that link the different components of the wavevectors and the dielectric functions of the metal and dielectric:

$$\frac{k_{zm}}{\varepsilon_m} = \frac{k_{zd}}{\varepsilon_d}$$

$$k_{xm} = k_{xd} = \frac{\omega}{c}\sqrt{\frac{\varepsilon_m \varepsilon_d}{\varepsilon_m + \varepsilon_d}}$$

where z and x represent the two different directions of propagation, as shown in Figure 1.5; d and m stand for dielectric and metal.

Figure 1.5 Schematic representation of the geometry of propagation of SPPs along the interface [1].

Since k_{zm} and k_{zd} have opposite sign, also the product between ε_m and ε_d is negative. In general, for frequency below the plasma frequency the metal has a negative dielectric function (ε_m).

To have propagation along the direction x, the values of wavevectors must be real. Hence, the argument of the square root must be positive. Since $\varepsilon_m \cdot \varepsilon_d < 0$, also $\varepsilon_m + \varepsilon_d$ must be negative [1].

Analysing the expression of the wavevector along the x direction, it is noticeable that when $\varepsilon_m = -\varepsilon_d$ the values of k tend to infinite. This happens at a specific value of resonance frequency called surface plasmon frequency ω_{sp} and it is defined by the following equation:

$$\omega_{sp} = \frac{\omega_p}{\sqrt{1 + \varepsilon_d}}$$

The dispersion relation of SPPs and Radiative Plasmon Polaritons (or bulk plasmon) can be represented graphically, highlighting the presence of three different regions (Figure 1.6):

- $\omega < \omega_{sp}$, only SPPs are allowed, and they can propagate in confined region in proximity to the metal-dielectric interface with an intensity that decays exponentially.

- $\omega_{sp} < \omega < \omega_p$, nomode is allowed leading to the formation of a forbidden region.
- $\omega > \omega_p$, only radiative plasmon polaritons are allowed.

For SPPs, it is possible to define a length, called propagation length, at which the intensity is decreased by a factor of 1/e through the following equation:

$$L_x = \frac{1}{2Im(k_x)}$$

The values of L_x are different depending on the type of material: for metals is in the order of tenths of nanometres, while for dielectrics is in the order of hundreds of nanometres.

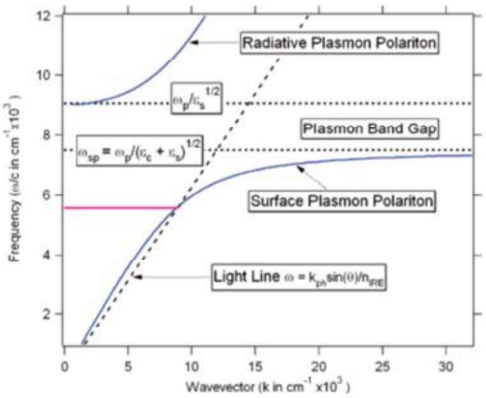

Figure 1.6 Schematic representation of the theoretical dispersion relation of SPPs and radiative plasmon polaritons [6]

The previous representation (Figure 1.6) is valid for ideal metal described by Drude model. In a real metal, the contribution of losses must be considered. Hence, the value of wavevector k cannot tend to infinite for frequencies close to the surface plasmon frequency, but it reaches a maximum value k_{max} (Figure 1.7) [1].

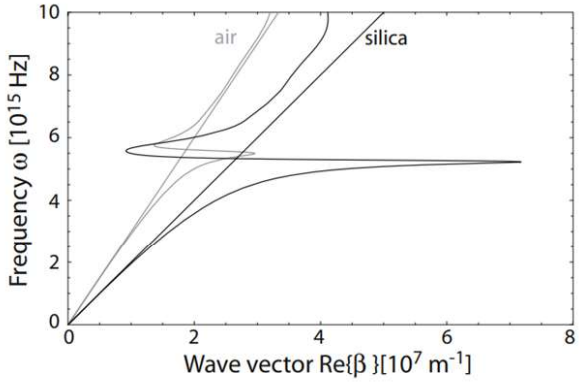

Figure 1.7 Dispersion relation at silver-air and silver-silica interface [1]

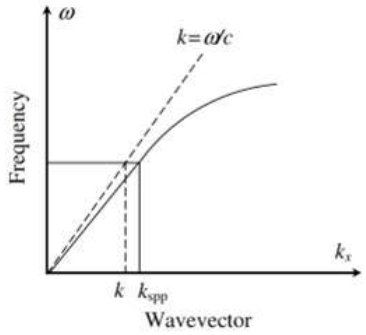

Figure 1.8 Representation of the dispersion relation of SPPs and light line in air [1].

To promote the excitation of SPPs a phase matching condition must be satisfied. In particular, the projection of the incident exciting photon must be equal to the x-component of the surface plasmon wavevector ($k_x = k_{x,SPPs}$).

As shown in Figure 1.8, the light line of air does not cross the dispersion relation of SPPs. Hence, a direct excitation of SPPs using a light beam coming from the air is not possible [5].

There exist different solutions that can be adopted to satisfy the phase matching condition, the most used are the following:

- *Prism coupling*, in which the light passes through a prism (Figure 1.9) made of a dielectric material characterized by a refractive index larger than the air one. In this way, the slope of the light line decreases leading to an interception with the dispersion relation of SPPs.

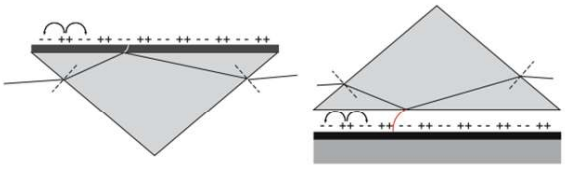

Figure 1.9 Schematic representation of the prism coupling technique. It can be perfomed adopting two different configurations: Kretschmann (left) and Otto (right) [1].

- *Grating coupling*, in which a grating of grooves or holes (Figure 1.10), patterned upon the metal surface, is used to favour the phase matching condition through diffraction of the imping photon.

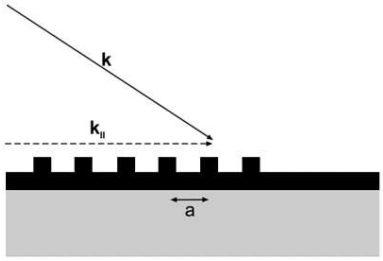

Figure 1.10 Schematic representation of the grating coupling method [1].

- *Near-field excitation*, in which, using scanning near-field optical microscopes probes that emit light from a subwavelength aperture (Figure 1.11), it is possible to promote a local SPPs exciton instead over a macroscopic area as in the case of prism coupling.

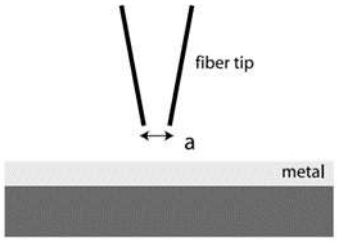

Figure 1.11 Schematic representation of a local SPPs excitation using near-field illumination with a sub-wavelength aperture [1].

Finally, considering a multilayered structure, the number of metal-dielectric interfaces increases. The study of this structure could be interesting because, if the thickness of the layers is lower than the propagation length L_x, it is possible to have coupling between different SPPs that are excited at different interfaces.

The efficiency of plasmonic resonances can be evaluated introducing a quality factor Q_f, that is defined as the ratio between the enhanced electromagnetic field and the incident one [7].

$$Q_f = \frac{Enhanced\ local\ field}{Incident\ field}$$

The quality factor for SPPs can be defined as the ratio between the real part of k_x ($k_1(\omega)$) and its imaginary part ($k_2(\omega)$) [8]

$$Q_f = \frac{k_1(\omega)}{k_2(\omega)}$$

If the absolute value of the real part of the dielectric function of the metal is much larger than the real part of the dielectric function of the dielectric medium ($|\varepsilon_{1m}| >> \varepsilon_{1d}$), the previous expression can be simplified to:

$$Q_{f,SPPs} = \frac{\varepsilon_{1m}^2(\omega)}{\varepsilon_{2m}(\omega)}$$

As discussed before, the propagation of SPPs is controlled by two main parameters: propagation length and confinement width. A compromise between these two concepts is needed because the larger is the propagation length, the lower is the confinement width and vice versa [9].

1.1.1.3. Localized Surface Plasmon Resonance (LSPR)

Localized Surface Plasmon Resonance is a non-propagating excitation caused by the coupling of the incident electromagnetic field and the conduction electrons of a nanostructured system [1].

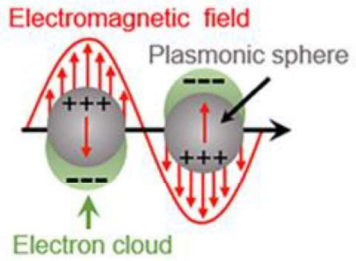

Figure 1.12 Schematic representation of LSPR [2].

The interaction between the light and surface electrons provokes the localized plasmon excitation (Figure 1.12), characterized by a resonant frequency that is related to the composition, size and geometry of the nanoparticles [10] Since the dimensions of the interacting particle are much smaller than the wavelength of the imping photon, the physics of the interaction can be described through the quasi-static approximation. According to this theory, the phase of the oscillating incident field is considered constant over the volume of the particle [1].

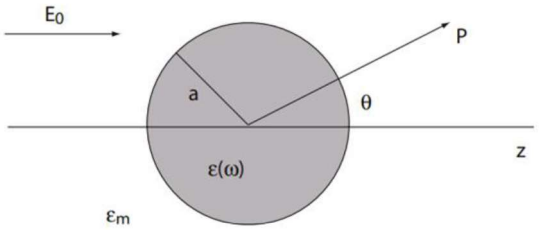

Figure 1.13 Schematic representation of a nanoparticles located at the origin of an external electric field.

Adopting an electrostatic approach, it is possible to retrieve a solution of the Laplace equation for the potential ($\nabla^2\phi=0$) that can be used to the define the electric field through the following expression:

$$\boldsymbol{E} = -\nabla\phi$$

Proceeding with the description (for a more detailed analysis see [1]), a relationship between the dipole moment **p** and the electric field $\mathbf{E}_0$ can be derived:

$$\boldsymbol{p} = 4\pi\varepsilon_0\varepsilon_m a^3 \frac{\varepsilon - \varepsilon_m}{\varepsilon + 2\varepsilon_m}\boldsymbol{E_0}$$

where a is the radius of the nanoparticle; ε is the dielectric permittivity of the particle that describes its interaction with the electric field; ε_m is the dielectric permittivity of the medium that contains the nanoparticle, as shown in Figure 1.13.

The electric field and the dipole moment are linked also through the following expression:

$$\boldsymbol{p} = \varepsilon_0 \varepsilon_m \alpha \boldsymbol{E_0}$$

where α is the polarizability and it is equal to:

$$\alpha = 4\pi a^3 \frac{\varepsilon - \varepsilon_m}{\varepsilon + 2\varepsilon_m}$$

From this last expression, it is evident that the polarizability experiences a resonant increase when the denominator is equal to zero ($\varepsilon = -2\varepsilon_m$). This relationship can be simplified to the Frohlich condition:

$$Re\,[\varepsilon(\omega)] = -2\varepsilon_m$$

The Frohlich condition is satisfied at specific value of frequency, called localized surface plasmon resonance frequency ω_{LSPR}:

$$\omega_{LSPR} = \frac{\omega_p}{\sqrt{1 + 2\varepsilon_m}}$$

As is noticeable from the last expression, the ω_{LSPR} depends on the material of the nanoparticle through ω_p and on the surrounding environment through ε_m.

From an optical point of view, the resonant increase of the polarizability α is related to the increase in the scattering and absorption efficiency of the nanoparticle. The enhancement of the efficiency can be evaluated using the following expressions for the scattering and absorption cross section:

$$C_{sca} = \frac{k^4}{6\pi}|\alpha|^2 = \frac{8\pi}{3} k^4 a^6 \left|\frac{\varepsilon - \varepsilon_m}{\varepsilon + 2\varepsilon_m}\right|^2$$

$$C_{abs} = kIm[\alpha] = 4\pi k a^3 Im\left[\frac{\varepsilon - \varepsilon_m}{\varepsilon + 2\varepsilon_m}\right]$$

In case of small particles ($a \ll \lambda$), the cross section for the scattering is much lower than the one for the absorption. Analysing the expressions presented is possible to notice that the Frolich condition is not dependent on the size of the nanoparticles, but proceeding with a more accurate description, introducing the concepts of scattering and absorption efficiency, the resonant increase in the polarizability becomes strictly related to the dimensions of NPs.

The efficiency of LSPR excitation can be assessed in the same way as for SPPs, introducing the concept of quality factor Q_f.

The quality factor for LSPR can be expressed as the ratio between the real part and imaginary part of the complex dielectric function:

$$Q_{f,LSPR} = \frac{-\varepsilon_1}{\varepsilon_2}$$

Since, in case of nanoparticles, the shape can affect the dielectric function also the quality factor results to be influenced by the geometry of NPs [7].

In case of too large or too small NPs, the quasi-static approximation described in the previous section is not valid anymore. Now the Mie theory [1] is used to describe scattering, absorption, and extinction efficiencies of NPs. The latter is a parameter used to quantify the ability of a particle to attenuate a radiation [11], while the former is adopted to evaluate the efficiency for far field enhancement applications.

The characteristic enhancement of the electric field related to the excitation of LSPR can be used to produce sensors with a resolution that can be in the order of a single molecule [10], [12], [13]. Other main features of LSPR can be exploited to produce advanced photovoltaic [14] and photocatalytic [15] systems, Surface Enhanced Raman Scattering (SERS) [10], [12], [16], and waveguides with a significant reduction of the losses [10], [12].

1.2. Traditional plasmonic materials

The most common plasmonic materials are noble metals, in particular gold and silver. They are widely used for plasmonic applications because of their large electrical conductivity and small ohmic losses. But these materials are also characterized by some drawbacks that can limit their applications.

The dielectric function describes the optical response of a material in presence of an electromagnetic field. The imaginary part ε_2 can be used to describe optical losses that can be related to the extension of the plasmonic field to wavelengths that do not belong to the visible regime, and to the presence of defects in the crystalline structure of the material. It possible to define three different contributions to optical losses: intra-band transitions occurring in the infrared range; inter-band transitions that occur at UV-Vis wavelengths and scattering that is related to the presence of defects inside the material.

In case of noble metals, the value of ε_2 arises when an electron is excited from the valence band to the conduction band because of the absorption of a photon. The larger is ε_2, the lower is the characteristic enhancement of the electric field exploitable for specific applications [17].

In addition, noble metals are characterized by large negative values of ε_1. Hence, it is more difficult to satisfy the phase matching condition to promote the excitation of SPPs.

Another limitation lies in the fabrication process because the deposition of thin films made of noble metals present problems related to the high percolation threshold [17].

Since the carrier concentration of noble metals is already large, the optical properties cannot be tuned through doping. Moreover, they are characterized by reactivity in presence of oxygen and humidity leading to a possible depletion of optical properties.

1.3. Innovative plasmonic materials

For the reasons described above, the research on new noble metal-free plasmonic materials became fundamental. One of the most interesting categories of materials that can overcome the problems just mentioned is semiconductors. The most important feature of this type of materials is the versatility. Indeed, their properties can be easily tuned through doping, obtaining several materials with different characteristics that can be adapted for various applications [2].

Because of what have just been described, plasmonic semiconductors can be adopted for several applications, such as photovoltaics, bioscience, and integrated photonics [2].

Another advantage of using plasmonic semiconductors lies in their higher chemical and physical stability. In addition, they can be easily deposited through physical or chemical techniques without the development of structural e morphological problems.

According to the Drude model described above, it is noticeable that the values of ε_1 and ε_2 can be controlled acting on ω_p. In particular, the plasma frequency increases with the charge carrier density, that is controllable with doping [18]. Hence, it is necessary to reach a compromise between the required electrical and optical properties for the plasmonic applications.

The most common classes of plasmonic semiconductor are: conductive metal oxides (CMOs); refractory nitrides; III-V semiconductors; 2D materials; transition metal oxides (TMOs) [2]. In the following sections, a more detailed description of a case of refractory nitrides (TiN) and conductive metal oxides (Ta:TiO_2) is presented because they have been deposited during this thesis project.

1.3.1. Titanium nitride (TiN)

Titanium nitride (TiN) is a non-stoichiometric refractory material compound. Titanium belongs to the class of transition metals of the fourth group of the periodic table of elements [19]. Indeed, it has four valence electrons, its configuration is $3d^2\ 4s^2$ and can form bonds with nitrogen (with a valence electronic configuration equal to $2s^2\ 2p^3$). TiN can be present in different phases, such as Ti_3N_4 or Ti_2N, but the most stable one is the cubic rocksalt B1-TiN structure, named δ-TiN [19].

The main characteristics of this material are: gold-yellow like appearance; high hardness [20]; good thermal stability with a melting temperature of 2930°C for the δ-phase; good electrical conductivity; good abrasion resistance and low friction coefficient; it is biocompatible and non-toxic [19].

The several properties of TiN allow its adoption for several applications, such as protective coatings and cutting tools, or for biomedical purposes. Due to its compatibility with CMOS technology, TiN can be used also as diffusion barrier layer,

while, thanks to its good electrical conductivity, it can be used as contacts in the electronic industry.

The most important application for the objectives of this work is the one related to the plasmonic field. This compound can offer a good plasmonic response in the visible and NIR regime, with optical properties easily tuneable controlling its stoichiometry [3]. In addition, titanium nitride can be deposited in thin films using chemical or physical vapour deposition techniques without significant problems.

In the following subsections the main properties of TiN, investigated during this work, are presented.

1.3.1.1. Optical properties and electrical properties of titanium nitride (TiN)

The optical properties of δ-TiN, fundamental for its plasmonic applications, can be investigated through ellipsometry and spectral reflectivity measurements [19]. As described more precisely in the following chapter, spectroscopic ellipsometry is performed to retrieve the dielectric function of the material, analysing and modelling its response to an incident electromagnetic field characterized by a specific angle of incidence and polarization.

The optical properties of TiN can be analysed studying the electron density of state (DOS), represented in Figure 1.14, where the zero represents the Fermi energy E_F. It is possible to divide the graph in two different regions:

- -3 eV < E < 0 eV, where Ti-d electrons are present in a large quantity. The onse that are not responsible for the formation of bonds with N-p electron can contribute to the electrical conductivity of the material.
- -8 eV < E < -3 eV, where a strong ibridization between Ti-3d and N-2p electrons is well established. In the graph, two distinct transitions are indicated (E_{01} and E_{02}) representing inter-band transitions that can occur in accordance with the selection rules for photonic excitation.

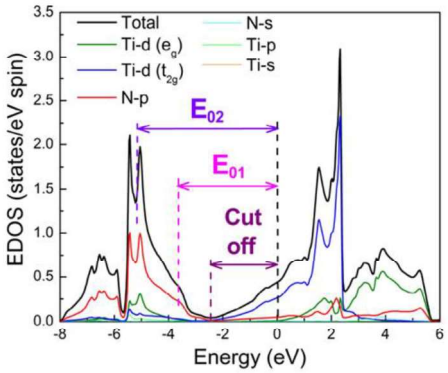

Figure 1.14 Schematic representation of DOS of TiN, in which the peaks representing the inter-band transition are highlighted by the red circles, and where 0 stands for the Fermi energy value

The most important quantity that can describe the optical response of a material is the complex dielectric function. To produce a good optical conductor in a determined frequency range, the real part ε_1 must assume negative values, while ε_2 must be as low as possible [19]

Recalling the Drude and Lorentz model described before, it is possible to derive an expression that describes the complex dielectric function for titanium nitride (TiN) that considers inter- and intra-band transitions:

$$\varepsilon(\omega) = \varepsilon_\infty - \frac{\omega_{pu}^2}{\omega^2 - i\Gamma_D\omega} + \sum_{j=1}^{m} \frac{f_j\omega_{0j}^2}{\omega_{0j}^2 - \omega^2 + i\gamma_j\omega}$$

where ε_∞ is a positive background constant that considers all the possible high energy transition. The second term of the expression represent the contribution of the Drude model, where ω_{pu} stands for the unscreened plasma frequency and Γ_D for the damping coefficient. The last term describes the presence of j Lorentz oscillators that contribute to the total dielectric function of the material. In this term, ω_0 represents the natural resonance frequency of the single Lorentz oscillator. In the analysis of the dielectric function of TiN, two different Lorentz oscillators are considered, to consider the two transitions discussed above.

Since ω_{pu} is directly linked to the density of free electrons, it can be used to have indication about the metallicity of the compound [19]. In the case of TiN, the unscreened plasma energy E_{pu} ($E_{pu} = \hbar\omega_{pu}$) can assume values from 2 eV to 2.95 eV [19]. This parameter can be also used as index for the stoichiometry of the compound and its value for a perfectly stoichiometric TiN is equal to 2.65 eV. In particular, the unscreened plasma frequency of titanium decreases when the content of nitrogen increases. This phenomenon is related to the decrease in the free electron density due to the lower content of titanium.

As mentioned before, the optical properties of a material can be also investigated by means of reflectivity measurements. In general, looking at the results of the measurement it is possible to retrieve information about the unscreened plasma frequency of the material in the point in which the reflectance reaches its minimum. In particular, a blue-shift of the position of the minimum of reflectance suggests an increase in the plasma frequency, while a red-shift suggests a decrease in the plasma frequency.

For wavelength higher than the unscreened plasma one, TiN is characterized by a large value of reflectance. This is in accordance with what have been described before, indeed it assumes a metallic behaviour for frequencies lower than the unscreened plasma one.

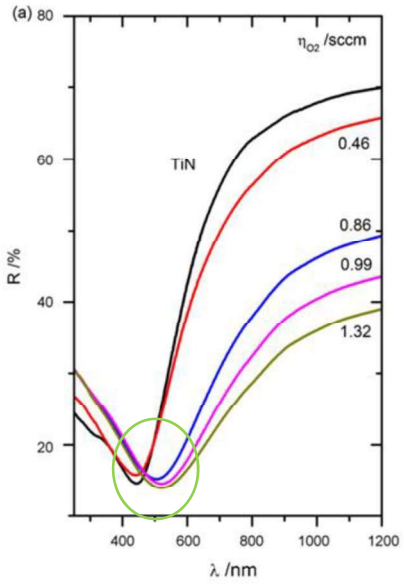

Figure 1.15 Reflectance curves of TiN films deposited with different oxygen flows, where the minimum are highlighted by the green circle [21].

Concerning the electrical properties, it is possible to define a relationship between the damping term and the electron average relaxation time, since Γ_D is directly related to the phenomenon of electron scattering [19]:

$$\tau_D = \frac{\hbar}{\Gamma_D(eV)}$$

where ħ is the reduced Planck constant.

Both the unscreened plasma frequency and damping coefficient are directly linked to the resistivity of the material through the following relationships:

$$\rho = \frac{4\pi}{\hbar} \cdot \frac{\Gamma_D}{\omega_{pu}^2} = \frac{m^*}{\tau_D N e^2}$$

According to the previous expression, ω_{pu} can be used as an index of the metallic behaviour of TiN through the value of the resistivity ϱ and the value of the damping coefficient Γ_D. In case of titanium nitride, ϱ can assume values from 10 to 600 μΩcm [8]. The electrical conductivity of TiN is based on the partially filled valence orbitals (Ti-3d) that are completely hybridized with the orbitals of the nitrogen (N-2p) [22].

Summarizing what have been just described, the optical and electrical properties of TiN can be tuned controlling the composition of the compound. In addition, the quality of the material (i.e. impurities and porosity) can affect the mean free path of the electrons and so also the resistivity.

1.3.1.2. Reflectance of titanium nitride (TiN)

The complex refractive index can be used to evaluate the reflectance of a material in normal incidence condition through the following expression:

$$R = \frac{(n-1)^2 + k^2}{(n+1)^2 + k^2}$$

here n and k are the real and imaginary part of the refractive index, respectively.

Several measurements of TiN reflectance have been performed by different authors [19], [21], obtaining the results shown in Figure 1.16 and 1.17.

Observing the results, it is possible to notice a minimum in the reflectance in correspondence to a specific value of frequency. This value is the plasma frequency characteristic of the material. Indeed, below this value the value of reflectance is significantly high meaning that the material behaves as a metal.

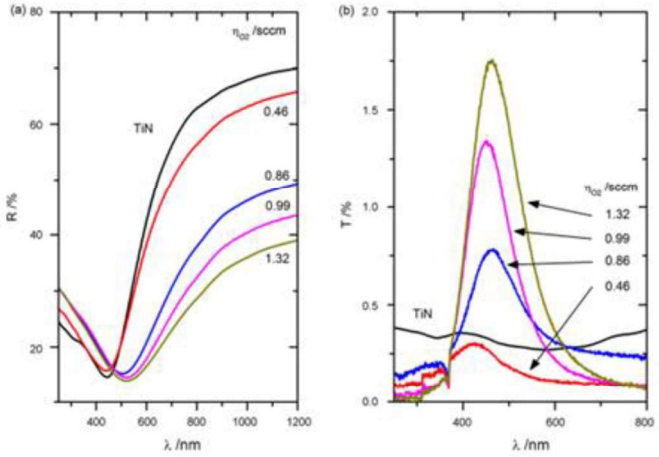

Figure 1.16 Plot of reflectance (a) and transmittance (b) of TiN deposited with different flows of oxygen [21].

The position of the minimum of reflectance is around 400 nm and it undergoes a redshift in presence of a reduction in the free charge carrier density, that could be related to an increase in the nitrogen content, to an oxidation of the surface or to a lower quality of the film [23].

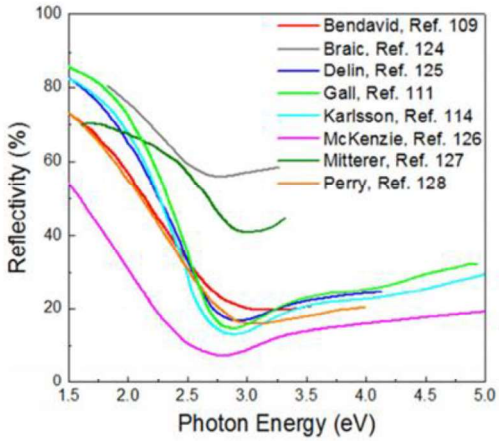

Figure 1.17 Representation of reflectance curves of different TiN samples measured by several research groups [19].

Theoretically, for very large wavelengths, the value of R(%) should be equal to 100%. In reality this is not true, and it decreases with an increasing concentration of impurities. Hence, it can be a quality indicator of the material. In addition, below 500 nm the value of reflectance should tend to zero, but in the real case this does not happen due to some inter-band transitions.

1.3.1.3. Raman spectroscopy of titanium nitride (TiN)

As mentioned in section 1.3.1, the most stable phase of TiN is characterized by a fcc rock-salt structure (Figure 1.18) that is part of the O_h symmetry point group. Hence, in principle, titanium nitride does not present active modes for Raman spectroscopy [24].

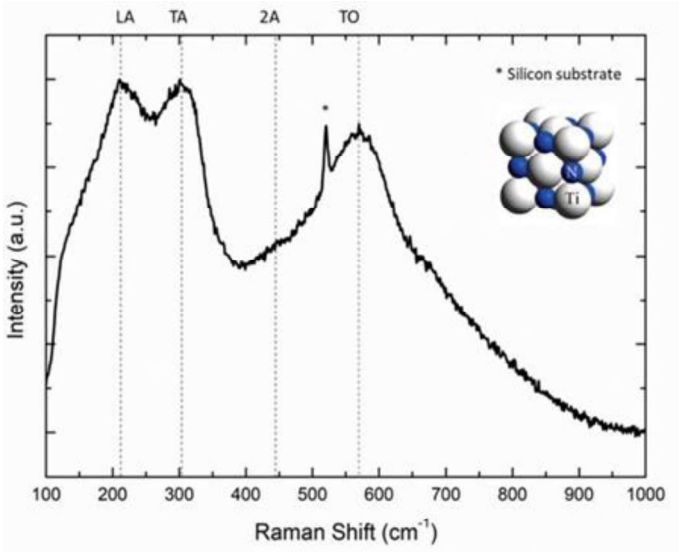

Figure 1.18 Typical Raman spectrum of TiN and schematic representation of its atomic structure [25].

However, the process of deposition of TiN causes the formation of several defects and vacancies in the film. This provokes a reduction in the symmetry of the system leading to the obtainment of vibrational modes that have non-zero first-order polarizability derivatives and so detectable with Raman spectroscopy.

In addition, the introduction of defect and vacancies leads to a relaxation of the selection. Hence, not only the phonons at the centre of the Brillouin zone contribute to Raman processes, but also other modes are involved. In general, disorder-activated Raman modes lead to of Raman spectra characterized by broad bands instead of sharp peaks [24], [26].

The phonons bands of titanium nitride have been studied by several authors [21], [24], [26], [27], leading to the definition of three principal spectral regions (Figure 1.19):

- below 400 cm^{-1}, it is possible to notice two bands. The first at ≈ 200-215 cm^{-1} is associated to the transverse acoustic phonons (TA), while the second one at ≈300-350 cm^{-1} is related to longitudinal acoustic modes (LA). The formation of these bands is mainly related to the vibration of Ti^{4+} ions and they can be

observed to investigate the presence of nitrogen vacancies inside the crystalline lattice [26].

- between 400 cm^{-1} and 450 cm^{-1}, a peak related to TA phonons is noticeable [26]
- between 500 cm^{-1} and 600 cm^{-1}, it is possible to observe a band related to transverse optical modes (TO). The presence of this band is caused by the vibration N^{3-} ions due to Ti vacancies [26].

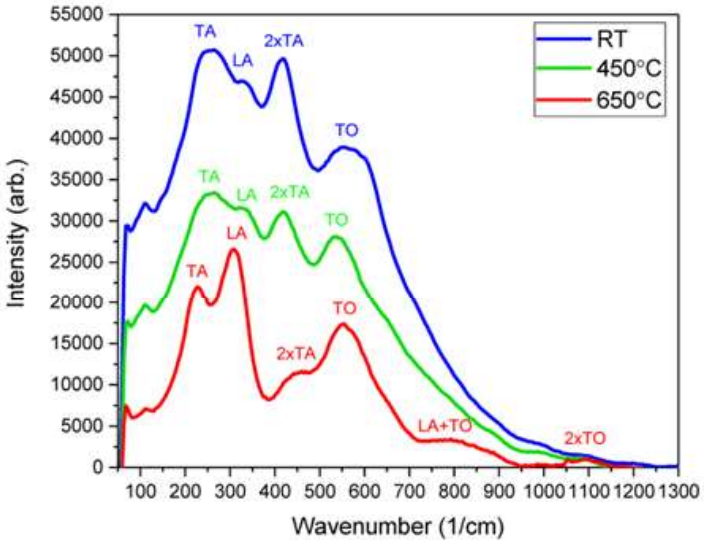

Figure 1.19 Raman spectra of TiN deposited at different temperatures [26].

The analysis of Raman spectra can be useful to retrieve qualitative information about the stoichiometry of titanium nitride. In particular, the bands observed are the ones present below 400 cm^{-1}, related to nitrogen vacancies, and the one present in the range between 500 cm^{-1} and 600 cm^{-1}, related to titanium vacancies.

Analysing these bands, it is possible to define three different cases of stoichiometry:

- if the bands related to nitrogen vacancies are more intense than the one related to titanium vacancies, the compound is sub-stoichiometric in nitrogen.
- if the bands related to nitrogen vacancies is less intense than the one related to titanium vacancies, the compound is over-stoichiometric in nitrogen.
- if the intensity of the bands is the same, the compound is stoichiometric.

In addition, observing the Raman spectrum it is possible to retrieve information about possible phenomenon of oxidation that occurs on the surface of TiN. In particular, it has been found that the larger is the content of oxygen, the broader are the bands below 400 cm^{-1}. This is related to the fact that oxygen reacts with titanium leading to an increase in the nitrogen vacancies. In addition, it is possible to observe two bands at ≈520 cm^{-1} and 520 cm^{-1} that are characteristics of titanium oxynitride compounds [21].

1.3.1.4. Plasmonic applications

Since TiN is characterized by good metallic behaviour, it has been proved that films and nanoparticles can withstand SPPs and LSPR excitation, respectively. In this sense, TiN can be considered a promising material to substitute noble metals for plasmonic applications in the visible and NIR range of frequency.

The performances of titanium nitride as plasmonic material can be assessed by means of the quality factor introduced in Subsection 1.1.1.2.

Thin films of TiN can be used to exploit the excitation of SPPs. This type of plasmon can be excited at a metal-dielectric interface. Since, the TiN constitutes the metal part of the system, its electrical and optical properties can affect significantly the SPPs excitation and propagation at the interface. In addition, the easy tunability of its properties make titanium nitride a very promising material that can offer a good tailoring potential for SPPs systems [8]. Titanium nitride is characterized by a lower propagation length than gold, but by a better confinement [9].

Titanium nitride can be also deposited in forms of nanoparticles to favour the excitation of LSPR exploiting their main characteristics for specific applications.

Analysing the case of titanium nitride, it is possible to notice that TiN is characterized by a lower maximum enhancement of field than gold, but by a larger width of the characteristic peak that is also redshifted with the respect to gold. Hence, making a compromise, the performances of gold and TiN are comparable [28].

It is noticeable that the quality factor is defined by the same expression both for SPPs and LSPR.

Analysing the expression of the quality factor Q_f, presented above, it is noticeable that higher is the value of imaginary part of TiN dielectric function, higher is the contribution of optical losses. Hence, the quality factor is lower. In addition, to increase the performance a material with a large negative value of the real part ε_1, and so with a distinct metallic behaviour, is required.

Titanium nitride is characterized by a low absolute value of ε_1 and by a quite large value of ε_2, limiting it applicability to photothermal or photocatalysis fields [29], [30], instead of the optical one (i.e. waveguides) where materials with lower losses and higher efficiencies are required.

Summarizing what have just been described, TiN can offer plasmonic performances, in the visible and NIR range, comparable to gold ones. Hence, it could be considered a valid substitute for noble metals in specific applications, such as for the production of new generation solar cells [29] or photocatalysis [15].

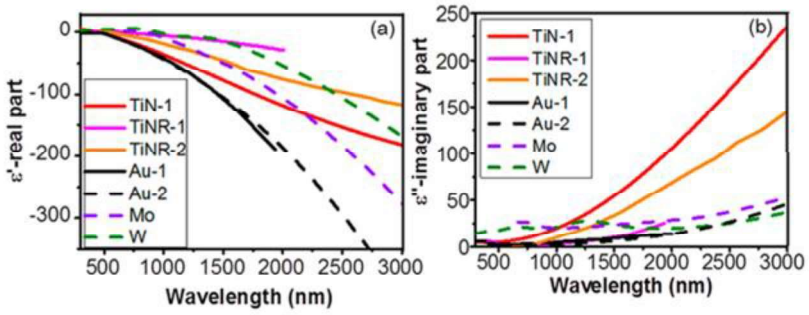

Figure 1.20 Schematic representation of the real part (left) and imaginary part (right) of TiN dielectric function with the respect to traditional plasmonic materials [30].

1.3.2. Tantalum doped titanium oxide (Ta:TiO_2)

Another important class of innovative plasmonic materials is that of Transparent Conductive Oxides (TCOs). The two main features of this type of material are: large enough band gap to guarantee transparency in visible regime; free charge carriers to be a conductor comparable to metals, but not too much to obtain a plasma frequency in the visible range limiting the reflectivity of the material. These characteristics can be found for example in doped metal oxides. They are characterized by a sufficiently large bandgap and their conductivity can be easily tuned through doping. The charge carrier density in a wide bandgap material can be controlled introducing oxygen vacancies or introducing substitutional atoms with a larger number of valence electrons than the metal present in the original compound [31].

The most common and studied material that is characterized by the properties just mentioned is Indium Tin Oxide (ITO). It has very low conductivity (10^{-4} Ωcm) and very good transmittance (80-90%) that can guarantee a high efficiency in optical and electrical applications. The main problem related to the production of this material is the availability and the high cost of recycling of indium, causing a significant increase in the price [Sputter deposition and computational study of M-TiO2]. A possible alternative, that has been studied in the last years is titanium oxide (TiO_2), that is characterized by a good transparency in the visible regime and by a good chemical stability in a reducing environment [32].

It is possible to obtain titanium oxide in its three different crystalline phases: rutile, anatase and brookite. The first one, characterize by a cubic cell, is the stable phase, while the remaining, characterized by a tetragonal cell, are metastable (Figure 1.21) [33].

Since it is a wide bandgap oxide ($E_g \approx 3.2$ eV), it is characterized by a good transparency in the visible range. TiO_2, and in particular its anatase phase, is characterized by good electron-transport properties. Hence, in the last years, it has been widely used to produce photoanodes for water splitting [34] and dye sensitized solar cell (DSSCs) [35].

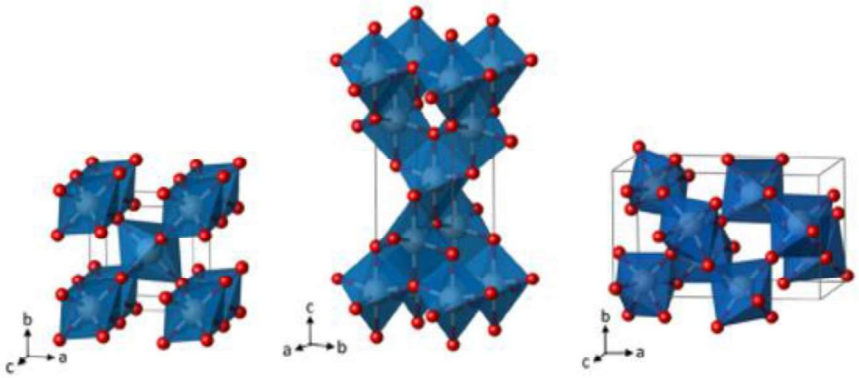

Figure 1.21 Schematic represation of the crystalline structure of the three different phases: rutile (left), anatase (middle), brookite (right) [33].

A process of doping is necessary to enhance its electrical properties. Because Ti belongs to the fourth group of the periodic table, doping can be performed introducing elements of the fifth group [36], such as tantalum (Ta) or niobium (Nb). Ta is characterized by a higher solubility than Nb. In addition, tantalum is characterized by a lower theoretical electron effective mass, that in principle leads to better electron mobility. For these reasons it is considered a better doping agent than Nb, although it is less analysed than niobium [32].

In the following sections are presented only the main properties of tantalum doped titanium oxide because it is the material analysed during this thesis work.

Thin films of tantalum doped titanium oxide can be obtained through several deposition techniques (i.e. pulsed laser deposition) in presence of a reducing atmosphere, that is required to obtain a conductive film. If the deposition takes place at temperatures below 350-400°C, the film is characterized by an amorphous structure [37]. Hence, a post-deposition thermal treatment is necessary to obtain a crystalline structure leading to an increase in the electrical conductivity [32].

In the following sections a description of the principal properties of transparent conductive oxides is presented, with particular attention to the properties of tantalum doped titanium oxide.

1.3.2.1. Optical and electrical properties of tantalum doped titanium oxide (Ta:TiO_2)

In principle, TCOs are semiconductors so their properties can be described using the Lorentz model. Increasing the concentration of doping agent, the material tends to assume a more metallic behaviour, leading to the adoption of a combination of Drude and Lorentz model. Hence, for doped TCOs, the optical and electrical properties are strongly correlated.

Since TCOs are characterized by a large bandgap, they are expected to be transparent in the visible and NIR range. At low wavelengths, and so at high energy, TCOs start to absorb, while at high wavelengths the reflective behaviour becomes predominant.

Optical and electrical properties are strongly linked by the carrier density through the plasma frequency.

Through doping, it is possible to increase the carrier density and so the conductivity. But, in this way also the plasma frequency raises, causing the narrowing of the transmission range. The limit in the UV range, at which absorption starts, decreases with an increase in carrier concentration. This phenomenon is explained by Burnstein-Moss model, for which the increase in the optical band gap is in some way proportional to $N^{3/2}$.

According to what have just described, a compromise between electrical and optical properties must be considered.

Another important parameter that can be used to tune the electrical properties of a material is the mobility μ, that is described through the following expression:

$$\mu = \frac{e\tau}{m^*}$$

where m* is the electron effective mass, e is the electron charge and τ is the average relaxation time.

The conductivity of material σ is directly proportional to the mobility μ by the following equation:

$$\sigma = Ne\mu$$

The mobility can be used to increase the increase the conductivity of TCOs without significantly affecting the transmission window.

According to the previous expression of the mobility, its value can be raised increasing the average relaxation time, reducing the impurities and the degree of disorder of the system, or reducing the electron effective mass, selecting a proper semiconductor.

The degree of disorder of the crystalline lattice can be controlled adopting the proper technique for the fabrication of the films and performing thermal treatments after the deposition to promote the crystallization.

Optical and electrical properties of tantalum doped titanium oxide have been widely investigated by Mazzolini et al [32], [38] and Bricchi et al. [39], [40] during studies carried out in Nanolab research group laboratories.

Mazzolini found out, as it is noticeable in Figure 1.22, that the resistivity decreases from around 10 Ωcm to 10^{-3} Ωcm after thermal treatment in vacuum. In addition, it seems that the annealing has a stronger effect on the doped semiconductor with the respect to sub-stoichiometric TiO_2.

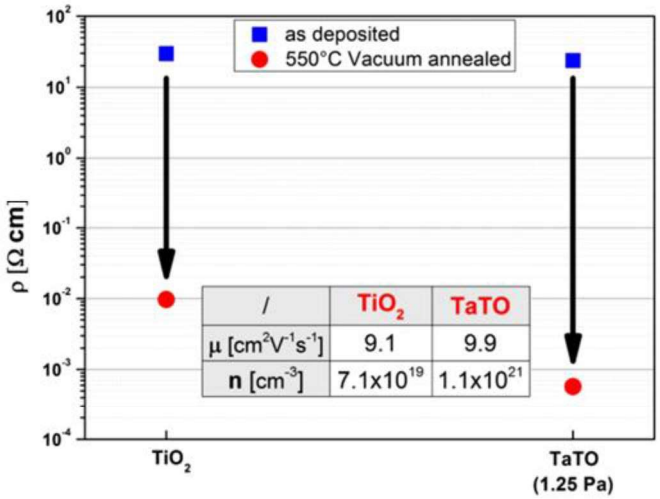

Figure 1.22 Schematic representation of the effect of the doping and of the thermal treatment on the resistivity and mobility of titanium oxide films [32].

In addition, it is possible to notice an influence of the deposition parameters [32] on the electrical properties of Ta:TiO_2 films annealed in vacuum (Figure 1.23). In particular, the resistivity increases with the O_2 deposition pressure, while the mobility and carrier density tend to reduce.

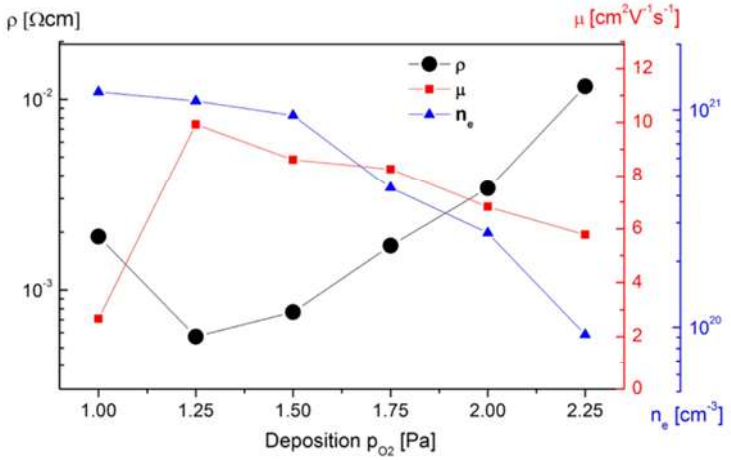

Figure 1.23 Schematic representation of the effect of the deposition pressure on the resistivity of Ta:TiO_2 films annealed at 550°C [32]

Analysing the results, it is noticeable that the resistivity increases with the deposition pressure, while the mobility and carrier density tend to reduce.

Bricchi found out that the resistivity, the carrier density and the mobility of the film are influenced by the thickness. (Figure 1.24)

In Figure 1.24, it is possible to notice that the electrical properties can be considered thickness dependent only for values below 50 nm. Above this threshold, the resistivity, carrier density and mobility can be considered constant. This phenomenon could be related to the fact that the crystalline structure of a Ta:TiO_2 film, deposited at room temperature through PLD and subsequently annealed, is polycrystalline. Increasing

the content of the doping agent seems to not cause a significative variation of the resistivity, while, considering carrier density and mobility, the effect is more evident. As it is expected, an increase in the degree of doping causes a decrease in the mobility which is compensated by an increase in the carrier density.

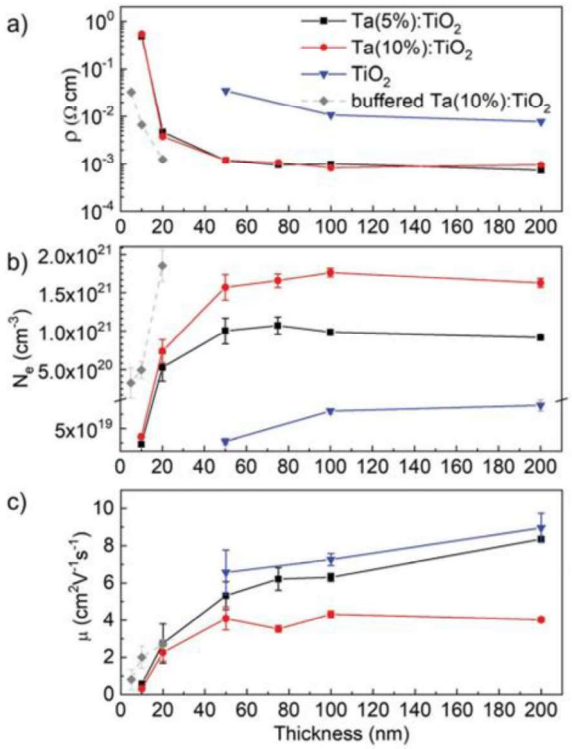

Figure 1.24 Representation of the effect of thickness and doping on the electrical properties of the films [40].

The dependence between mobility and thickness is in accordance with the model developed by D. Look, et al. [Model-for-thickness-dependence-of-mobility-and-concentration-in-highly-conductive-zinc-oxideOptical-Engineering], which states that the mobility of a very thin film (below 50 nm) is more or less equal to half of the bulk case.

Concerning the optical properties of Ta:TiO_2, Mazzolini measured an average value of transmission in the visible range that is around 75% and it can increase to 80% after the thermal treatment [32]

Bricchi performed several ellipsometric measurements to investigate the dielectric function of Ta:TiO_2 films, obtaining the following results presented in Figure 1.25.

Analysing the results, it is evident that the introduction of doping agent inside the crystalline lattice caused a shift of the absorption limit to higher energies (UV). This phenomenon can be explained by the Burnstein-Moss effect described above.

In Figure 1.25.b, ε_2 is equal to zero in the visible energy range. Hence, it is assumed that the samples are characterized by low absorption coefficients.

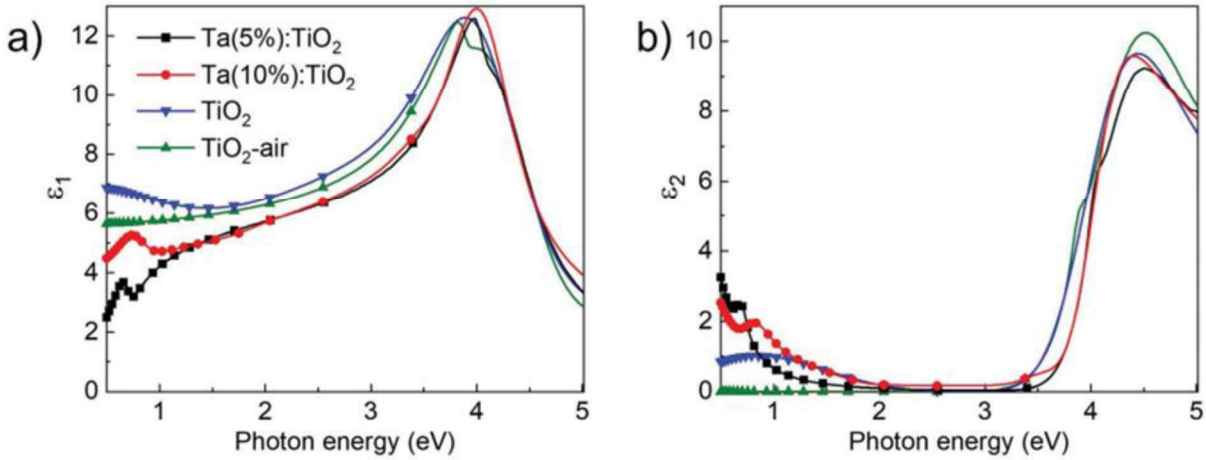

Figure 1.25 Representation of the effect of the dopant content on the real and imaginary part of the complex dielectric function of titanium oxide after annealing[40].

1.3.2.2. Raman spectroscopy of tantalum doped titanium oxide (Ta:TiO_2)

Raman spectroscopy can be performed on Ta:TiO_2 film to investigate its crystallinity [38]. As mentioned before, the TiO_2 transition from an amorphous to a crystalline structure occurs at temperatures equal to 350-400°C. If the deposition temperature is lower, the film grows in amorphous phase that is not able to produce distinct signal during Raman spectroscopy.

A crystallization process, leading to the obtainment of the anatase phase, can be promoted through an annealing process at temperatures higher than the transition ones. In general, after that, Ta:TiO_2 films exhibit a different Raman spectrum characterized by four main peaks, one strong at 140-150 cm^{-1} (E_g) and three weaker at 400 cm^{-1} (B_{1g}) , at 520 cm^{-1} (B_{1g} (2)-A_{1g}) and at 650 cm^{-1} (E_g). The most interesting and important peak is the strongest one. (Figure 1.27)

Bricchi and Mazzolini investigated the effect of the Ta content on the most intense signal, noting that the position of the peak changes with different concentrations of tantalum [38].

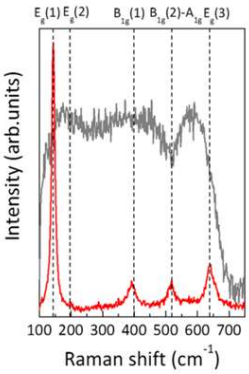

Figure 1.26 Raman spectra of Ta:TiO_2 films before and after annealing : red (annealed), grey (as dep).

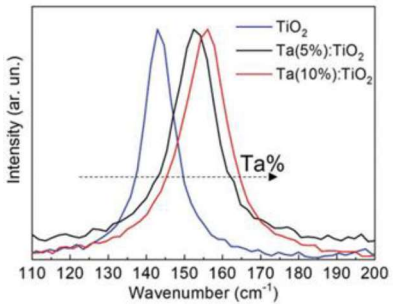

Figure 1.27 Raman spectra of the most intense peak of Ta:TiO2 of films with different concentrations of tantalum [40]

As it is noticeable from Figure 1.27, increasing the concentration of tantalum the peak is shifted from the characteristic position of titanium oxide at 140 cm^{-1} to values of 150-155 cm^{-1}. In addition, Mazzolini et al. founded a monotone relationship between the position of the peak and the content of tantalum (Figure 1.27)

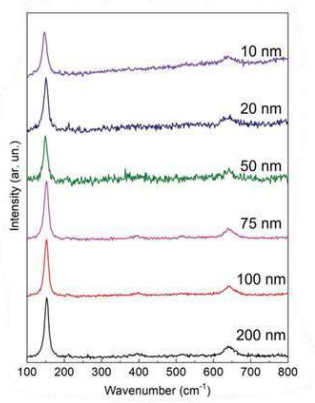

Figure 1.28 Raman spectra of Ta:TiO2 films with different thicknesses [32].

In addition, Bricchi studied the effect of the thickness of the film on the signal to noise ratio of the Raman spectra, noting that increasing the thickness the quality of the Raman spectra increases. (Figure 1.28)

1.3.2.3. Plasmonic applications

In recent years, TCOs started to be considered for plasmonic applications since they can guarantee a better control of the light-matter interaction with their tuneable properties.

It is possible to define three main plasmonic research fields, in which the introduction of transparent conductive oxide can be considered of interest:

- optical metamaterials [41].
- optical modulators [42] [43]
- TCOs nanocrystals for LSPR [44], [45]

In the first two applications, TCOs can be introduced both as films and nanoparticles. Considering the films, the thickness represents a crucial parameter for plasmonic

applications for what has been described in the subsection 1.3.2.1. Indeed, if the thickness is below 50 nm it is possible to have a significant drop in the mobility of the material causing a degradation of the electrical properties.

Another important feature of TCOs is their compatibility with other plasmonic materials, such as gold or silver. In some cases, it has been demonstrated that the introduction of a thin metallic film in TCOs can cause an increase in the electrical conductivity without significantly affecting the typical transparency of the conductive oxide [46].

It is possible also to integrate metals, in general gold and silver, nanoparticles into conductive oxides film to combine the transparency of the oxide with the plasmonic properties of metals [39], [47].

1.4. Metamaterials

A metamaterial is structure artificially fabricated modulating, at the mesoscopic scale, specific features, such as density or composition, to obtain properties that cannot be found in nature [48]. The prefix "meta" derives from Greek word "μετά", which means "beyond", highlighting the will of overcoming the limit of the traditional materials with the development of this new class of materials.

Metamaterials can be characterized by extraordinary magnetic, electronic, and optical properties that can be exploited for many applications, such as advanced biosensors [49], novel devices for nanolithography [4], innovative waveguides and super lenses [4], [50], [51].

The term metamaterial has been introduced for the first time by a physics professor at the University of Texas called Walser in 1999 and it has been adopted in literature in 2000. [Composite Medium with Simultaneously Negative Permeability and Permittivity]. The first appearance of this class of material can date back to the IV century with the Lycurgus Cup [52].

At the beginning of the 21st century, metamaterials features started to be investigated more deeply. One of the most important research projects, carried out in these years, consisted in modelling, and producing metamaterials with negative electric permittivity and negative refractive index to achieve the phenomenon of negative refraction [53], [54].

Currently it is possible to gather different classes of materials under the category of metamaterials. They are characterized by different properties that can be exploited for various applications.

Since the high complexity of the structure required for this purpose, the research has shifted towards the development of simpler geometry that are characterized by tuneable optical properties, called hyperbolic metamaterials (HMMs) [4], [50].

1.4.1. Hyperbolic metamaterials

Hyperbolic metamaterials constitute an interesting sub-class of metamaterials due to their anisotropic and tuneable optical and electrical properties. This new class of materials is called hyperbolic due to the shape of its dispersion relation (Figure 1.29), defined by the effective electric and/or magnetic tensors [4]. Since the modelling and realization of novel HMMs is the main objective of this project, it is fundamental to introduce the main features of these structures.

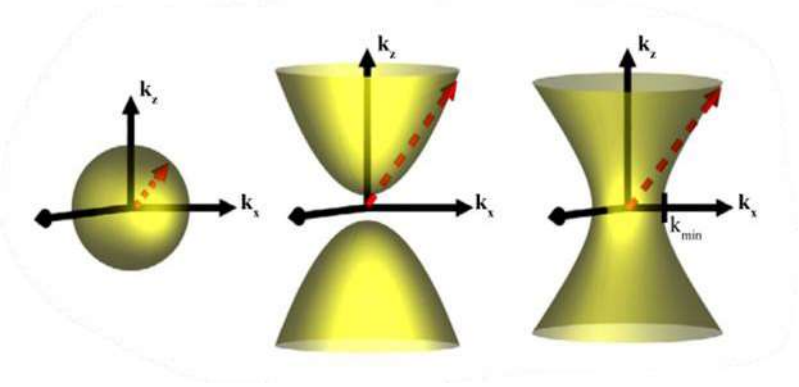

Figure 1.29 Schematic representation of dispersion relations of different materials: isotropic (a), HHMs type I (b), HHMs type II (c) [4].

HMMs can be considered as the ultra-anisotropic limit of traditional uniaxial crystals, in which one the principal components of the permittivity ε and permeability μ tensors is different from the two remaining.

If the material is considered uniaxial, these tensors can be represented by the following expressions:

$$\hat{\varepsilon} = \begin{pmatrix} \varepsilon_{\perp} & 0 & 0 \\ 0 & \varepsilon_{\perp} & 0 \\ 0 & 0 & \varepsilon_{\parallel} \end{pmatrix}, \quad \hat{\mu} = \begin{pmatrix} \mu_{\perp} & 0 & 0 \\ 0 & \mu_{\perp} & 0 \\ 0 & 0 & \mu_{\parallel} \end{pmatrix}$$

where the subscript ⊥ and || indicates the components that are perpendicular and parallel to the anisotropy axis, respectively.

If the non-local effects and electromagnetic coupling can be neglected and supposing that $\mu_{\parallel} = \mu_{\perp} = 1$, it is possible to define the dispersion relation of the material starting from the Maxwell's equations, described in the section 1.1, obtaining the following expression:

$$\left(k_x^2 + k_y^2 + k_z^2 - \varepsilon_{\backslash\backslash} k_0^2\right)\left(\frac{k_x^2 + k_y^2}{\varepsilon_{\perp}} + \frac{k_z^2}{\varepsilon_{\backslash\backslash}} - k_0^2\right) = 0$$

where k_x,k_y and k_z are the components of the wavevector **k**, and k_0 is the wavevector in free space.

The terms in brackets of the dispersion relation represent spherical and ellipsoidal surfaces in the reciprocal space (k-space). The former describes waves polarized in the xy plane (transverse-electric (TE) waves), while the latter describes waves that exhibit a magnetic field polarized in xy (transverse-magnetic (TM) waves) [50].

If both $\varepsilon_{\parallel}$ and $\varepsilon_{\perp}$ are positive, the material is considered isotropic, and it is characterized by the dispersion relation described in Figure 1.30.a. If the components of the dielectric permittivity ε have opposite sign, it is necessary to distinguish two possible cases:

- If $\varepsilon_{\parallel} > 0$ and $\varepsilon_{\perp} < 0$, TE and TM modes can coexist (HMMs type I).
- If $\varepsilon_{\parallel} < 0$ and $\varepsilon_{\perp} > 0$, only TM modes are present (HMMs metal-type or type II)

Analysing the various dispersion relations depicted in Figure 1.30, it is evident that for HMMs a limit for the value of wavevector cannot be found. This means that these materials can sustain the propagation of high-k waves that are forbidden in the isotropic case [50]. In addition, it is possible to notice an increase in the optical density of states (DOS) of the material that leads to a strong improvement of the phenomenon of spontaneous emission. According to what have been just described, HMMs could be promising for several applications, such as high-resolution imaging and lithography, or thermal and spontaneous emission engineering [4].

The structure of HMMs is based on the achievement of dielectric anisotropy. Along one direction a metal behaviour is wanted ($\varepsilon < 0$), while along the other direction a dielectric is needed ($\varepsilon > 0$). This condition can be satisfied adopting mainly two configurations (Figure 1.30).

The first configuration is based on the alternation of layers made of a metallic and dielectric material, while the second consists in the deposition of metal nanorods in a dielectric matrix.

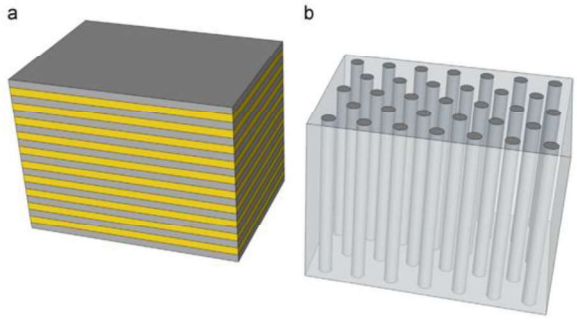

Figure 1.30 Schematic representation of the two possible configurations of HMMs: (a) multilayered structure, (b) nanorod array (b) [4].

The multilayered structure can be obtained through different experimental techniques, such as pulsed laser deposition or molecular beam epitaxy, while nanorods can be obtained using the dielectric matrix as a template. The geometry and the materials

adopted can be used to tune the optical response of the final structure enlarging its application and research fields.

1.4.1.1. Effective medium theory

Both multilayers and nanorod arrays can be considered quite complex structures. Hence, also the characterization of HMMs properties could present some problems. Since the dimensions of the components of the multilayers or the nanorod arrays are subwavelength, it is possible to apply the Bruggeman's effective medium theory (EMT) or Maxwell Garnett theory to predict the optical response of the total HMMs structure. The former is used for system in which the metallic and dielectric constituents have comparable dimensions (multilayers), while the latter is adopted to describe structures in which one of the components has larger dimensions with the respect to the other one (nanorod arrays) [4] Both theories are based on the possibility of describing the behaviour of the complete structure through the definition of effective parameters as a function of the properties of the single components.

During this thesis work, only multilayered structures have been studied. Hence, in this section the attention has been focused on the Bruggeman's effective medium theory (EMT).

According to Bruggeman's effective medium theory, it is possible to define the 'effective' parallel and perpendicular components of the dielectric permittivity tensor using the following expressions:

$$\varepsilon_{\backslash\backslash} = \frac{\varepsilon_m d_m + \varepsilon_d d_d}{d_m + d_d} \; ; \; \frac{1}{\varepsilon_{\perp}} = \frac{d_m/\varepsilon_m + d_d/\varepsilon_d}{d_m + d_d}$$

where ε_m and d_m are the dielectric permittivity and thickness of the metal component, respectively. ε_d and d_d are the dielectric permittivity and thickness of the dielectric constituent.

These expressions can be rewrote highlighting the dependence of the effective parameters on the dimensions of the metallic components, obtaining the following relationships:

$$\varepsilon_{\backslash\backslash} = p\varepsilon_m + (1-p)\varepsilon_d; \; \varepsilon_{\perp} = \frac{\varepsilon_m \varepsilon_d}{p\varepsilon_d + (1-p)\varepsilon_m}$$

where p is called filling ratio, defined by the following equation:

$$p = \frac{d_m}{d_m + d_d}$$

Analysing these results, it is possible to notice that the effective components of the dielectric permittivity tensor do not depend on the total thickness and number of layers of the structure.

In conclusion, adopting the effective medium theory model it is possible to predict the optical response of the HMMs multilayer evaluating the optical properties of the single components. In addition, the optical behaviour of the total structure can be tuned not only selecting different materials for the constituents, but also varying their dimensions.

The most common combination of materials for the fabrication of HMMs is gold or silver with alumina, obtaining a hyperbolic behaviour in the ultraviolet (UV) range. It is possible to substitute the dielectric component with titanium oxide (TiO_2) or silicon nitride (SiN) to shift the hyperbolicity range to the visible.

Since the problems, described above, related to the use of noble metals for plasmonic applications, it could be interesting to substitute the metal component with alternative plasmonic material, such as titanium nitride (TiN) C.Chen at al. demonstrated that sandwiching a layer of titanium nitride between two layers of indium tin oxide (ITO) is possible to obtain a hyperbolic material in the near-infrared range (NIR) [55]. Finally, the introduction of graphene as metallic component permits to shift the hyperbolic behaviour at far-infrared wavelengths.

1.4.1.2. Applications

In the high-resolution imaging field, the possibility of having propagation of high-k modes can be exploited to produce hyperlenses [4]. In general, the information about the object analysed are provided by scattered electromagnetic fields with different wavevectors. Since fine details are related to evanescent high-k modes, HMMs can be used to allow the propagation of these modes overcoming the problem related to the diffraction limit, leading to the obtainment of images with a higher resolution. For this type of application, it is possible to adopt the multilayered structure to produce cylindrical hyperlenses (Figure 1.31.a) or spherical ones (Figure 1.31.b) [56], [57].

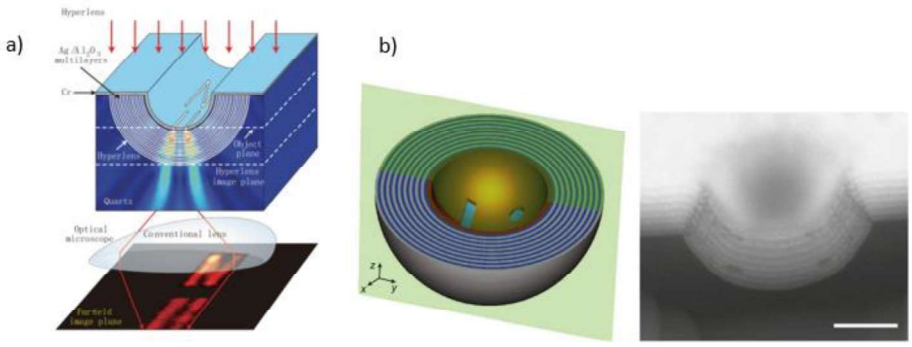

Figure 1.31 Schematic representation of a cylindrical (a) or spherical (b) hyperlens [4], [50].

For what concerns nanolithography, a nanorod array (Figure 1.32) can be used to overcome the diffraction limit reducing the dimensions of the features patterned [50], [58].

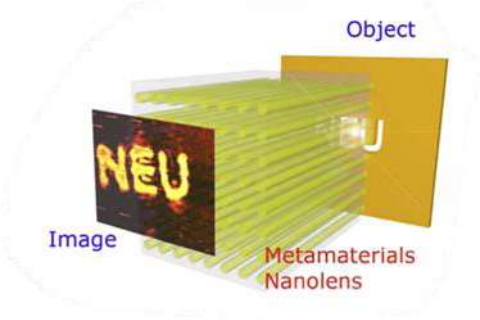

Figure 1.32 Schematic representation of a HMMs lens adopted for nanolithography [4].

One of the first investigated HMMs effect has been the negative refraction of TM modes. This phenomenon is related only to transverse-magnetic (TM) waves, hence the best materials for this type of application are the ones that allow the propagation only of this type of modes. As mentioned in section 1.4.1, these materials are the HMMs type II [53], [54], [59].

Another interesting application could be related to the energy transfer, since it has been proved that HMMs can solve the problem related to the short-range limitation of near-field coupling, on which dipole-dipole interactions are based. Indeed, the high-k modes, in which near-field are converted, can propagate for longer distances due to the properties of HMMs, leading to a great enhancement of energy transfer [60].

HMMs features can be exploited also to produce high-quality sensors, such as biosensors or refractive index sensors, that are based on the propagation of high-k modes [61], [62].

Lastly, HMMs can be adopted to produce peculiar waveguides that are not characterized by a fundamental mode and that can promote the propagation of surface modes [4].

1.5. Objectives of the thesis

The aim of this master thesis work consists in depositing and characterizing single layers of titanium nitride and tantalum doped titanium oxide, and multilayers made of these two materials to investigate their optical, electrical and plasmonic properties. The optical properties of the multilayers have been investigated to retrieve information about their dependence on the materials selected and on the geometry of the system. Indeed, the influence of the material adopted has been studied varying the deposition conditions of titanium nitride and varying the content of dopant in tantalum doped titanium oxide. All the samples produced have been obtained through pulsed laser deposition (PLD), on monocrystalline silicon and glass substrates, and characterized with the experimental methods described in Chapter 2. A new parameter of deposition has been introduced for fabrication of this type of material, the substrate temperature. During the project, the developed samples have been obtained with and without the

use of the substrate heater with the objective of investigating the effect of the substrate temperature on the morphology, electrical and optical properties of the system.

First, reference sample, constituted by a single layer of titanium nitride or tantalum doped titanium oxide, have been obtained and characterized to retrieve information about the effect of the substrate temperature, the materials selection and to derive the fundamental optical properties needed for the assessment of the hyperbolicity, according to the effective medium theory (Subsection 1.4.1.1). Moreover, the effect of the material selection has been investigated changing the type and the values of the deposition pressure for titanium nitride, while, for tantalum doped titanium oxide, two different targets with 5% of Ta and 10% of Ta have been used. The deposition parameters used have been retrieved from previous works performed by the Nanolab research group. Then, the first set of multilayered structures have been developed and characterized to investigate the effect of the substrate temperature and order of the layers on the morphology and on the optical response of the system.

Finally, the data obtained from the characterization of the reference samples have been used to determine, according to the effective medium theory, the best filling factors p (Subsection 1.4.1.1) that allow to obtain the wider range in which the system is expected to show a hyperbolic behaviour. And, after the definition of the geometry, a second set of multilayers has been produced with the aim of obtaining system characterized by the theoretical widest range of hyperbolicity.

2 Experimental techniques

In this chapter, the experimental techniques used for the production and characterization of the samples and the theoretical bases on which they are based are presented.

2.1. Pulsed Laser Deposition (PLD)

Pulsed Laser Deposition (PLD) is a growth technique in which the energy of a pulsed laser is coupled to a bulk target material via electronic processes [63] to produce species that are then deposited onto a substrate in the form of a thin film. This technique is based on the use of an intense laser pulse that passes through an optical window of a vacuum chamber and collides with the target material. When a threshold value of power density is overcome, the material starts to be ablated producing a plasma plume characterized by a shape and a direction of expansion that are related to the laser-target interaction and, above all, to the deposition pressure. The species that form the plume are characterized by a certain kinetic energy that allow them to reach the substrate, onto which they can recondense leading to the growth of a film.

The PLD apparatus, represented in Figure 2.1, is constituted by a laser source and a vacuum chamber containing the material target and the substrate [64].

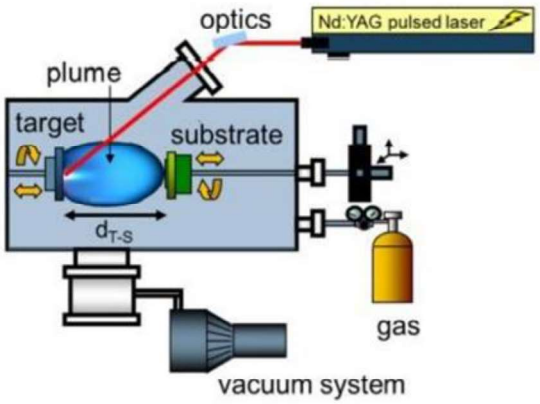

Figure 2.1 Schematic representation of the PLD apparatus [65].

In general, intense ns laser pulses are used which are focused on the target using an optical path made of lenses, mirrors and a viewport. The typical angle of incidence of the laser is 40-50° with the respect to the normal to the surface of the target. The vacuum chamber is connected to a vacuum system composed by a primary scroll pump that can reduce the internal pressure from the atmospheric one to few pascals,

and by a turbomolecular pump, able to reduce the pressure to values in the order of 10^{-3} Pa. The substrate and target holders are connected to rotational and translational motion controllers leading to the optimization of the processes of ablation and deposition. The apparatus is also equipped with pressure gauges to control the internal pressure during all the phases of the deposition.

The process can be performed in vacuum or in presence of a background gas that is injected into the chamber using a gas inlet system equipped with mass flow controllers. The gas used can be inert or reactive, in the last case the technique is called reactive PLD and it possible to have modifications of the target plume due to chemical reactions.

Once the material target has been selected, the deposition process can be controlled modifying mainly five important parameters that are:

- The *substrate temperature*, fundamental to enhance the mobility of the impinging atoms promoting the crystallization process of the deposited film. This parameter can be varied using a substrate heater composed by a resistance that, according to Joule effect, is able produce heat when a current passes through it. During this work a substrate heater has been used in some cases to analyse the effect of the deposition temperature on titanium nitride films, Ta-doped titanium oxide films and multilayer structures that have been deposited at room temperature during previous works at Nanolab [66], [67]. The heater has been set to a nominal value of 500°C, but, since the copper substrate holder is mounted on the heater, the temperature of the substrate is lower than the nominal one. This value has been measured using a thermocouple directly connected to the substrate holder surface, and it is more or less equal to 350°C.
- The *laser fluence* on the target surface, considered as the energy per unit surface of the laser pulses that hit the target. It can be evaluated as the ratio between the energy of the impinging laser, considering the transmittance of the vacuum chamber window, and the surface of the laser spot on the target. This parameter can be controlled modifying the energy of the laser or varying the laser spot on the surface of the target through the use of lenses. During this project, the values adopted are in the range between 2 J/cm^2 and 6.5 J/cm^2, that have been selected according to previous studies done by the Nanolab research group [66]–[68].
- The *base vacuum* reached in the chamber before the start of the ablation process. This parameter is important to control the degree of contaminations that can affect the quality of the film deposited (e.g. due to the presence of oxygen). If gases are not injected into the chamber, the base vacuum also represents the pressure at which the deposition process takes place. In this case, the base pressure can affect the shape of the plume generated as shown in Figure 2.2. During this thesis, the values of this parameter vary from 1*10^{-3} Pa to 0.4 Pa to

assess the effect of the presence of residual air inside the vacuum chamber, also considering the different deposition temperature.

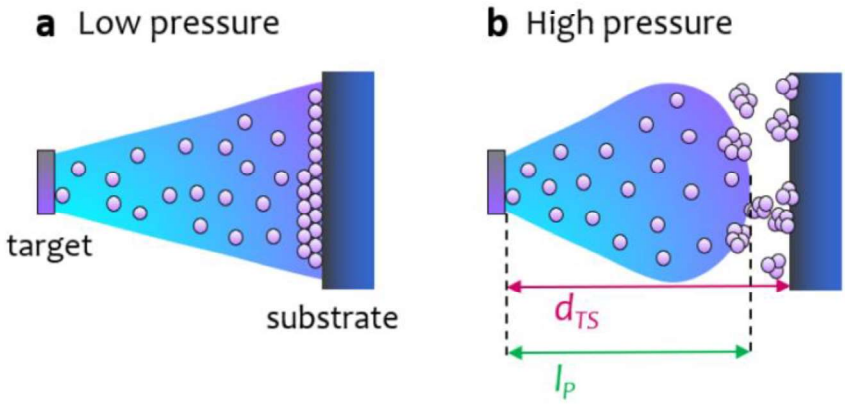

Figure 2.2 Representation of the effect of the deposition pressure on the morphology of the plume [65].

- The *deposition atmosphere* and *pressure*. If a gas is injected into the chamber during the ablation, its nature can affect the expansion of the plume. In presence of a reactive gas, it is possible to have chemical reactions depositing a film with a different composition than the one of the target. If the gas is inert, this can be used to confine the plume with a degree that is strictly related to the pressure of the gas. The higher is pressure, the larger is plume confinement induced by the gas. In addition, the pressure can affect the kinetic energy of the species of the plasma plume because increasing the pressure inside the chamber the collisions between them are favoured and so the velocity decreases. Another effect of pressure consists in the probability to have the formation of cluster or nanoparticles during the expansion of the plume towards the substrate: higher is the pressure, higher is the probability to have nucleation of cluster or nanoparticles. Both of these two last effects can lead to the deposition of a film with a significant degree of porosity. During my experiments, different atmospheres and pressures has been used to assess the effect of these parameters on the properties of the deposited samples. For the deposition of titanium nitride, a mixture of nitrogen and hydrogen (N_2-H_2, 95%-5% volume percentages) has been used with pressure of 1 Pa and 3 Pa. While, during the deposition of Ta-doped titanium oxide oxygen, O_2 has been used with a pressure of 1 Pa to obtain the best properties required for the objectives of this project. These values have been retrieved from previous research done by Nanolab group [66], [67], [69].
- The *target to substrate distance*, which affects, together with the laser fluence and deposition pressure, the way in which the atoms of the plume reach the substrate. This parameter can affect the morphology of the film deposited, as shown in the Figure 2.2. Increasing the distance, the atoms reach the substrate

with a lower kinetic energy leading to an increase in the porosity of the film deposited. During this thesis, the distance has been set to a value of 5 cm because, according to previous studies of the Nanolab research group[66], [67], [69], it has been found as the best value to obtain films with the optimal morphology for the purposes of this project.

This growth technique can offer several advantages: almost any condensed matter material can be ablated; the pulsed nature of PLD can be used to control in a proper way the growth rates of the films; the ablation of the target occurs only in the spot where the laser hits the surface; since the deposition occurs only in an isolated chamber, the stoichiometry of the target material is usually maintained also in the deposited films if no reactive gas are injected in the chamber; the kinetic energies of the ablated atoms are in a range of values that favours the surface mobility and avoids bulk displacement [63].

There are also some drawbacks related to the use of pulsed laser deposition: the production of droplets that can affect the homogeneity of the surface of the film; if the kinetic energy of the impinging atoms is too high it is possible to form some crystallographic defects in the film; the plume could be characterized by an inhomogeneous flux and energy distribution leading to inhomogeneous film thickness over large areas [63].

In this project, the PLD apparatus is composed by a Nd:YAG nanosecond pulsed laser, with second harmonic at wavelength equal to 532 nm, repetition rate equal to 10 Hz and with duration of the pulses that is around 6 ns. The vacuum system is constituted by an Agilent TriScroll 600 and a Pfeiffer Vacuum TMU 521 turbomolecular pump. The gas pressure is monitored by MKS Multi Gas Controller 647C.

A manually activable shutter has been mounted inside the chamber to allow a proper cleaning of the target before the depositions.

All the samples have been deposited upon silicon substrates (Si(100)) or soda-lime glass substrates. For the deposition of the reference samples, targets of TiN (2″), Ta:TiO_2 5% of Ta in mass (2″), Ta:TiO_2 10% of Ta in mass (2″) have been used. While for the production of multilayers structures, a TiN target (1″) has been mounted upon the previous mentioned target of Ta:TiO_2.

The substrate heater is not connected to the rotational motion controllers, so it can move only vertically and horizontally.

Before every deposition, a test sample has been deposited to estimate the growth rate and so the time required to obtain a specific thickness. The growth rate has been computed as the ratio between the thickness of the test sample, measured using SEM, and the time required for the test.

2.2. Annealing

During the annealing treatment process, the sample is exposed to high temperatures in vacuum (at pressure in the order of 10^{-5} Pa) or in presence of a controlled atmosphere. With this technique it is possible to modify the crystalline structure and the composition of the sample.

One of the most important components of the apparatus, shown in Figure 2.3, is the vacuum chamber that is connected to a pumping system, composed by a rotary and turbo pump. Inside the vacuum chamber there is the heating system that acts also as substrate holder. This component is made of pyrolytic boron nitride and pyrolytic graphite. It is also possible to put a molybdenum shield onto the heater to obtain a more uniform temperature during the treatment and to protect the components of the vacuum chamber. The heating system is connected to a PID controller (Yudian AI-518P), that is connected to a PC to control the treatment parameters. During the annealing the temperature is monitored using a C thermocouple and a pyrometer (Figure 2.3).

The vacuum chamber can be also connected to a gas tank if a controlled atmosphere is required during the treatment.

In this thesis work, the annealing process has been always performed in vacuum (at pressure in the order of 10^{-5} Pa), after the deposition process trough PLD, to promote the crystallization of the samples produced and not induce oxidation. During all the treatments the temperature has been set to 500°C, with a dwell time of 1 hour [66], [68], [69] and a heating rate of 10°C/min.

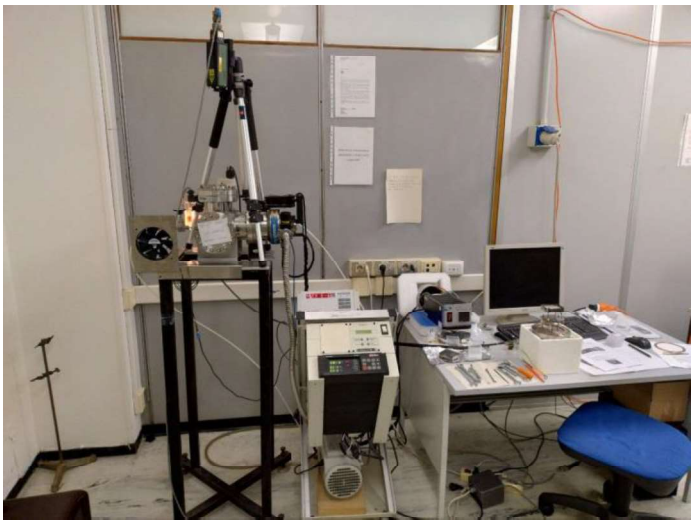

Figure 2.3 Photo of the apparatus used for the annealing.

2.3. Scanning Electron Microscopy (SEM)

Scanning Electron Microscopy (SEM) is a technique used to derive several information about the surface and the bulk of a sample, such as the surface and bulk morphology, the chemical composition, or the crystalline orientation of the specimen [70].

A schematic representation of the SEM system is shown in Figure 2.4. The SEM apparatus consists of an electron source, an accelaration system for the electron beam, a vacuum chamber in which a sample holder is placed, a vacuum pumping system, a deflection system made of scan coils, a control console and several detectors able to collect and analyse the signals generated. The electrons required can be generated by field emission or by thermoionic effect. Nowadays, the former is the most common process adopted for the electron beam generation. The path of the electrons between the gun and the sample is controlled by a deflection system and by one or two lenses. The system operates in vacuum to guarantee the largest mean free path and so the highest energy of the impinging electrons, that is required to have images with a good resolution [70]. When the electrons reach the surface of the sample they can interact with it in different ways leading to the formation of different signals as reported in Figure 2.4. The presence of an array of detectors is necessary to collect and analyze all the different signals, because they can be used to derive different information about the sample.

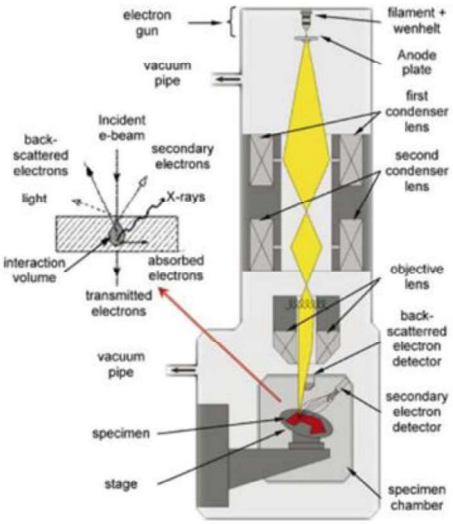

Figure 2.4 Schematic representation of a typical SEM and possible effects due to the interaction between the sample and the electron beam [71].

The two most common signals are the ones related to the secondary electrons (SE) and to the backscattered electrons (BSE). The former are related to the morphology and surface texture of the sample, while the latter are connected to the crystal structure and grain orientation.

Another important signal is related to the characteristic X-Rays, because it can be used to obtain some information about the elemental composition of the sample analysed.

During this thesis project, a Field Emission Zeiss SEM Supra 40 with a GEMINI column has been used to anlyse the cross section of the different samples produced. The voltage bias has been set at 5 kV with a typical maximum resolution in the order of few nanometres.

2.4. Energy Dispersive X-ray Spectroscopy (EDXS)

Energy Dispersive X-Ray Spectroscopy (EDXS) is a non-destructive technique that can be used to determine the elemental composition of materials. The system employed is directly embedded in the Scanning Electron Microscopy (SEM) instrument [72]. As a matter of fact, a detector for EDXS analysis (by Oxford Instruments) is connected to the SEM used during this thesis project.

This analysis consists in the detection of an X-ray signal that is characteristic of each element. The signal detected comes from the collision between the analysed sample and the impinging high energetic electron beam. The latter hit the core electrons of the material, provoking the emission of them. Other electrons that are present in the outer shell can replace the ejected electrons, leading to the emission of an X-Ray photon. The energy of the photon is equal to the difference between the energy levels of the inner and outer shells, and it is characteristic of the element. For this reason, it is possible to retrieve information about the elemental composition of a sample using a particular detector that can collect and measure the energy of the incoming X-rays [72].

The results obtained during the analysis are represented in a spectrum of the peaks that can be associated with the different elements. Making a comparison between the intensities of these peaks, it is possible to obtain an estimate of the elemental composition of the sample.

The accuracy of the elemental composition is limited [73]. Generally, it is of the order of some percent or even worse in the case of elements with low atomic number, such as oxygen or nitrogen. Therefore, during this thesis project, the EDXS analysis has been used to define trends and not precise elemental compositions of the sample. The targets used for the depositions are characterized by precise compositions that can be considered as reference values for the analysis.

2.5. Raman spectroscopy

Raman spectroscopy is a vibrational spectroscopy used to characterized molecules, crystalline structures and chemical reactions. During the analysis, the sample is irradiated by a monochromatic laser beam with frequency ν_0 [74]. This permits the excitation of the molecule, or crystal, analysed from the starting electronic energy level to a virtual one, then it decays instantly to the initial electronic energy level, but at a vibrational level that can be equal to the initial one or different (Figure 2.5). During the

decay process, a photon is emitted with an energy equal to the difference between the energy of the virtual level and the energy of the final vibrational level.

It is possible to define three different possible way in which the radiation interacts with the molecule (Figure 2.5) [74]:

- if the molecule decays to the initial energy level, elastic scattering occurs with the emission of a photon that has the same energy of the photon that caused the excitation. This type of interaction is also known as Rayleigh scattering and it happens for about 99% of the scattered light.
- If the molecule decays to a higher vibrational energy level, inelastic scattering occurs causing the emission of a photon with energy that is lower than the one of the incident photon. This type of interaction is also called Stokes scattering.
- If the molecule decays to a lower vibrational energy level, inelastic scattering occurs leading to the emission of a photon with an energy larger than the photon that caused the excitation. This kind of interaction is also named anti-Stokes scattering.

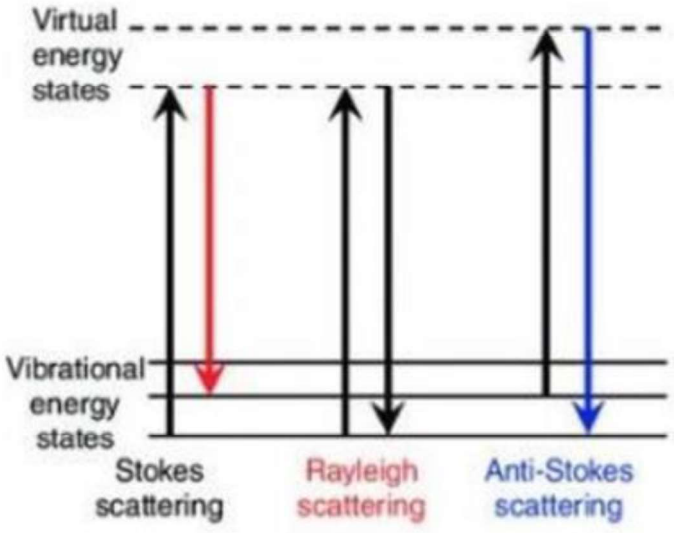

Figure 2.5 Schematic representation of the possible excitation and decay processes that can occur between virtual energy levels and vibrational ones [75].

If inelastic scattering occurs, the difference between the frequency of the incident photon and the frequency of the emitted one is equal to the vibrational frequency of the mode involved during the scattering process.

Since anti-Stokes scattering requires that molecules are in an excited starting vibrational state, intensity of anti-Stokes scattering is remarkably lower than the Stokes one because the ground vibrational level is more highly populated than the excited ones according to Bose-Einstein statistics (Figure 2.6) [74].

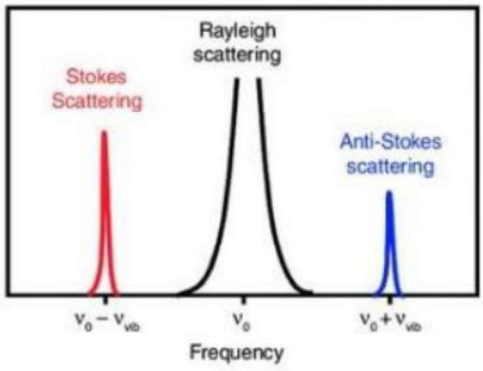

Figure 2.6 Raman spectra in which are presented all the signals related to the interaction between the molecule and the radiation [75].

The apparatus used for the spectroscopy, represented in Figure 2.7, consists in an optical microscope that is connected to a light source and to a Raman spectrometer. The former is responsible for the emission of the photons required for the excitation of the sample crystal, while the latter is responsible for the detection of the scattered photons.

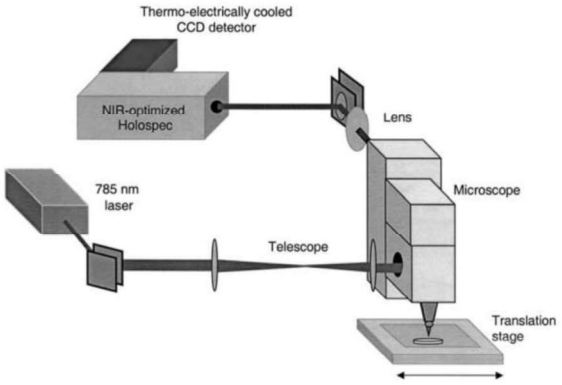

Figure 2.7 **7** Schematic representation of a Raman spectroscopy apparatus [76].

The results of the analysis are in general represented in a graph of Raman intensity over Raman shift. The first one corresponds to the number of photons emitted that are collected by the detector, while the second one corresponds to the difference between the wavenumbers of the scattered radiation and the incident one. The values of Raman shift are independent on the wavelength of the imping photons because they are related only to the frequency of the vibrational modes and thus to the nature of the chemical species of the sample.

Since the anti-Stokes lines have a lower intensity the Stokes one, usually only the Stokes part of a spectrum is acquired.

The normal modes of vibration of a molecule, or a crystal, must satisfy some conditions to be considered Raman active, hence detectable. A mode can be considered Raman active if it is characterized by a change in the polarizability α of the molecule during the oscillation [74]. The property of polarizability describes the dynamical response of

a molecule to an external field, hence the capability of the material to form instantaneous dipole and to distort its electronic cloud. Considering the crystalline solids, the larger is the degree of order of the structure, the sharper and more intense are the signals detected. Indeed, in presence of defects, such as point defects or grain boundaries, the propagation of the phonon is hindered causing an uncertainty in the phonon energy leading to the obtainment of a broader signal. In addition, due to the fact that photons with any frequency are characterized by a low momentum, the selection rule related to the wavevector conservation is less strict in case of disordered material, leading to possible couplings also with phonons with higher wavevector that cause the broadening of the signals.

To obtain Raman spectra during this project, a Renishaw InVia micro Raman spectrometer has been used. This instrument is directly connected to an optical microscope equipped with a 50x objective. The monochromatic light source adopted is an argon ion laser with a wavelength equal to 514 nm and a power set at 1 mW to avoid any laser-induced modification of the samples.

All the samples have been analysed in a range of Raman shift between 100 cm^{-1} and 1100 cm^{-1} with thirty accumulations of ten seconds. For each sample, a measurement in the full range (100-3200 cm^{-1}) has been performed, but it is not reported in the following chapters.

During this project, Raman spectroscopy has been used to retrieve information about the stoichiometry of titanium nitride, and to control the crystallinity of doped titanium oxide after the deposition and after the annealing treatment.

2.6. UV-Vis-NIR spectroscopy

UV-Vis-NIR spectrophotometry is a non-destructive technique performed to define the optical properties of a material. This technique is based on the interaction between light and matter [77]. The sample, constituted by the substrate and the film, is irradiated by light and then different phenomena can occur. A fraction of the light can be transmitted (T), reflected (R), absorbed (A) or diffused (D). The sum of all these fractions must be equal to unity. Thanks to this technique, it is possible to quantify the fraction of reflected and transmitted photons and so the reflection and the transmission. The results are expressed as a function of the wavelength of the incident photons over a range typical of the instrument used [77].

The measurement is performed using a spectrophotometer equipped with an integrating sphere internally covered with a polymer named Spectralon to reach an internal reflectance close to 100% (Figure 2.9). The sphere is characterized by two apertures that can be filled with the sample and with a Spectralon tap, depending on the property measured. The light source is a monochromator, which is able to generate a narrow light beam characterized by a defined wavelength. Then, the light beam

interacts with the sample, and it is reflected or transmitted. A detector, placed inside integrating sphere, is capable of computing the intensity transmitted or reflected.

Depending on the property measured there exist different configurations of the system, as shown in Figure 2.8:

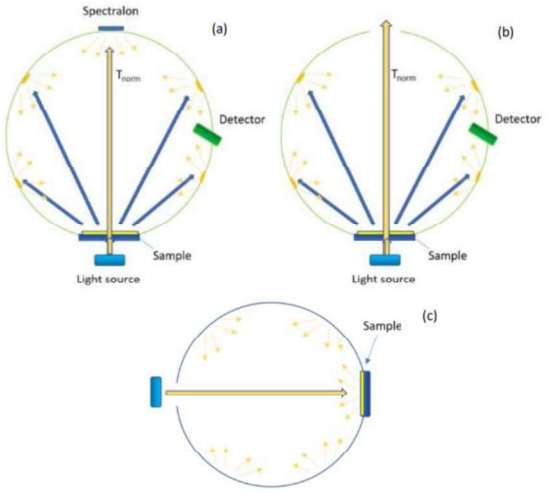

Figure 2.8 Schematic representation of the possible configurations used to derive different properties: (a) configuration used to compute the total transmission; (b) configuration adopted to evaluate the diffusive transmission, (c) configuration used to derive the reflectance [78].

To measure the transmittance, the sample is placed at one of the apertures with the film pointed to the centre of the sphere. At the second aperture a Spectralon tap is put in order to evaluate the direct and diffuse contribution to the transmission (Figure 2.8.a). To collect only the second contribution, it is possible to remove the tap permitting the light to exit from the sphere (Figure 2.8.b). In this way the detector can detect only the diffuse transmitted light that remains inside the sphere.

To measure the reflectance, the sample is placed in the same way as before, but the other aperture is open to permit the entrance of the light beam (Figure 2.8.c). In this way, the radiation directly hits the film.

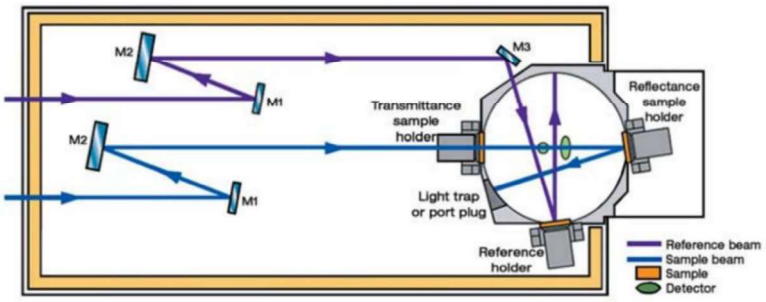

Figure 2.9 Schematic representation of the spectrophotometer equipped with a Perkin Elmer integrating sphere [79].

The analysis has been performed using a LAMBDA 1050 UV-Vis-NIR spectrophotometer equipped with Perkin Elmer 150 mm integrating sphere. This apparatus is hosted at the Centre for Nanoscience and Technology (CSNT) of the Italian Institute of Technology (IIT) in Milan. The measurements have been performed in a range of wavelengths between 250 nm and 2000nm with a data interval of 2 nm.

2.7. Ellipsometry

Ellipsometry is an optical characterization technique performed to determine an important property of a material, the dielectric function [80], in particular its real and imaginary part. Its name is related to the type of light polarization employed during the measurement.

The process is based on the evaluation of parameters that describe the interaction between the sample and the incident polarized radiation. Fitting these values with specific physical o mathematical models, it is possible to retrieve the material dielectric function.

The apparatus is constituted by a source and a detector that are characterized by their own polarizing systems. These instruments are employed to calculate the variation of the electric field after a specular reflection upon the surface of the sample analysed, varying the angle of incidence in a quite large range of values.

The change in the polarization can be quantified through the values of angles Δ and ψ, that represent the phase difference and the amplitude ratio of the reflection coefficients, respectively [80].These values are related to the variation of polarization through the following equation:

$$\frac{E_{rp}/E_{ip}}{E_{rs}/E_{is}} = \tan(\psi)e^{i\Delta}$$

where p and s represent two different orientations of polarization (Figure 2.10), while i stands for incident and r for reflected.

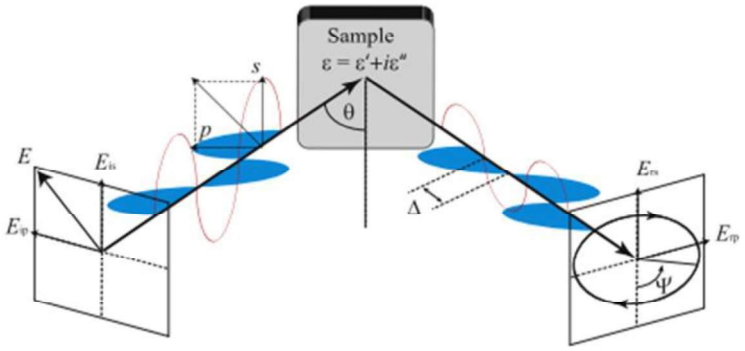

Figure 2.10 Schematic represenation of the geometry of the apparatus [80].

It is possible to obtain the dielectric function or refractive index through a direct interpolation of the raw data only if the material analysed is sufficiently thick, homogenous, and characterized by a flat surface. While, in the case of thin film, or rough surface or layered structures it is necessary to use some theoretical models, that describe properly the system, to retrieve the material properties. In general, these models are based on different parameters and optical constants of the sample. Typical models used are the Lorentz or Drude one or other oscillators models that can physically fit the data.

If it is not possible to derive the material properties, such as the plasma frequency, required for the interpolation using physical models, it is possible to adopt mathematical interpolating models. One of these models is based on the parametrization by B-Splines, able to describe the Kramers-Kronig relations between the real part and the imaginary one in the dielectric function [81].

The ellipsometric measurements have been performed using a J.A. Woollam Co. M2000 ellipsometer, hosted at the Centre for Nanoscience and Technology (CSNT) of the Italian Institute of Technology (IIT) in Milan. Lorentz model and the mathematical method based on B-splines have been used to fit the data obtaining the dielectric function of the materials analysed.

2.8. Van der Pauw method for resistivity measurements

The Van der Pauw method is a technique widely used to perform an electrical characterization of thin films that allows to obtain values of resistivity ϱ and Hall coefficients (carrier density n and mobility μ). During the project, the measurement has been performed to derive only the values of resistivity ϱ.

This method is applied to two-dimensional samples when specific conditions are satisfied:

- the sample must be isotropic and homogeneous.
- the sample must be continuous.
- the sample must be characterized by a uniform thickness.

In this specific type of measurement, four contacts (or probes) are used. There are conditions even on the probes that must be satisfied:

- the contact area must be lower than the area of the sample by at least one order of magnitude.
- the four probes must be placed at the edges of the sample.

The process consists in the application of a current between two neighbour electrodes and the consequent evaluation of a potential difference between the remaining electrodes (Figure 2.11). Since the probes are four, there are four possible configurations that duplicate just inverting the sign of the current applied.

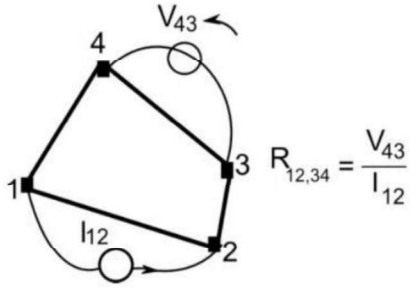

Figure 2.11 Schematic representation of a possible configuration adopted during the measurement[82].

According to symmetry conditions and reciprocity constraints, there are some equations that must be satisfied:

$$R_{21,34} = R_{12,43}$$

$$R_{32,41} = R_{23,14}$$

$$R_{43,12} = R_{34,21}$$

$$R_{14,23} = R_{41,32}$$

$$R_{21,34} + R_{12,43} = R_{43,12} + R_{34,21}$$

$$R_{32,41} + R_{23,14} = R_{14,23} + R_{41,32}$$

If these conditions are fulfilled, it is possible to introduce the concept of average resistances R_A,R_B, evaluated at the two edges of the sample, leading to the evaluation of the value of the sheet resistance R_s using the following equation:

$$e^{-\pi\frac{R_A}{R_s}} + e^{-\pi\frac{R_B}{R_s}} = 1$$

Knowing the sheet resistance, it is possible to derive the value of the resistivity of the material using the following equation:

$$\rho = R_S \cdot d$$

where d represents the thickness of the sample.

The instrument used to perform the measurements is constituted by a Keythley 2400 SourceMeter, for the generation of the current, and an Agilent 34970A voltage meter. The system is connected to a Keysight 34972A LXI Data acquisition unit. It is possible to change the configuration using a home-made switch. All the data acquired have been analysed later using a suitable Matlab code.

3 Materials selection and characterization

As described in Section 1.5, the final goal of this thesis is to model and develop multilayered structures, composed of TiN and Ta:TiO_2, that can show a hyperbolic behaviour. For this reason, the investigation of the properties of the single layers became crucial. Hence, before the deposition of the multilayered structures, reference samples of the different materials adopted have been fabricated and characterized. In this chapter, the parameters adopted during the deposition and the results of the characterization are presented.

3.1. Titanium nitride (TiN)

During the thesis, several reference samples of titanium nitride have been produced to investigate the effect of some deposition parameters on the morphology, optical and electrical properties of the single layer. The parameters changed during the fabrication process are the type and the values of the deposition pressure and the substrate temperature. To simplify the description, the samples have been divided into three different groups according to the different deposition pressure (high vacuum, low vacuum and reducing atmosphere).

All the reference samples of titanium nitride are presented below in Table 3.1.

Target	Atmosphere	Pressure	T_{nom} (°C)	T_{sub} (°C)	Fluence (J/cm^2)
TiN	Vacuum	$1.53*10^{-3}$	400	250	3.5
TiN	Vacuum	$1.29*10^{-3}$	500	350	3.5
TiN	Vacuum	$1.08*10^{-3}$	25	25	3.5
TiN	Vacuum	0.1	25	25	6.5
TiN	Vacuum	0.1	500	350	6.5
TiN	Vacuum	0.4	500	350	6.5
TiN	N_2-H_2	1	25	25	3.5
TiN	N_2-H_2	1	400	250	3.5
TiN	N_2-H_2	3	500	350	4

Table 3.1 List of TiN reference sample deposited.

where T_{nom} represents the nominal temperature set on the substrate heater and T_{sub} is the effective substrate temperature measured by an additional thermocouple mounted

on the substrate holder.

The deposition parameters that have not been changed during the fabrication process are listed below:

- Target: TiN (99% pure with a dimeter of 2 inches).
- Substrate: silicon wafer (110 crystal plane) and glass. The substrates have been heated through a substrate heater, as described in section 2.1.
- Target to substrate distance: 5 cm.
- Laser: pulsed green laser (532nm) with a frequency of 10 Hz.
- Sample thickness: ≈ 200 nm

Every sample deposited with the substrate heater have been extracted from the vacuum chamber only when the temperature measured through the thermocouple mounted on the substrate holder was around 50°C, to avoid oxidation of the film.

The deposition parameters have been retrieved from previous works carried out by the Nanolab research group except for the substrate temperature since the substrate heater has been used for the first in the Nanolab laboratories. These parameters have been selected to investigate the effect of the substrate temperature, atmosphere and pressure on the optical, electrical and plasmonic properties of titanium nitride.

A thermal treatment in vacuum and at around 500°C has been performed on the samples highlighted in Table 3.1.

3.1.1. TiN samples deposited in high vacuum

In this section the main features of the deposited samples are presented, focusing on the effect of the substrate temperature. All the samples have been produced in vacuum with pressure in the order of 10^{-3} Pa.

The titanium nitride reference samples deposited in high vacuum are listed in Table 3.2.

Target	Atmosphere	Pressure (Pa)	T_{nom} (°C)	T_{sub} (°C)	Fluence (J/cm^2)
TiN	Vacuum	$1.53*10^{-3}$	400	250	3.5
TiN	Vacuum	$1.29*10^{-3}$	500	350	3.5
TiN	Vacuum	$1.08*10^{-3}$	25	25	3.5

Table 3.2 List of TiN samples deposited in high vacuum.

The values of the laser fluence have been selected in accordance with previous works performed by the Nanolab research group [66], [67].

After the deposition, a thermal treatment, in vacuum at 500°C, has been performed on the samples deposited at 250°C and 25°C to investigate the influence of the substrate temperature on the effects of the annealing process.

The samples have been analysed using SEM to measure the thickness and verify the morphology of the sample produced. (Figure 3.1)

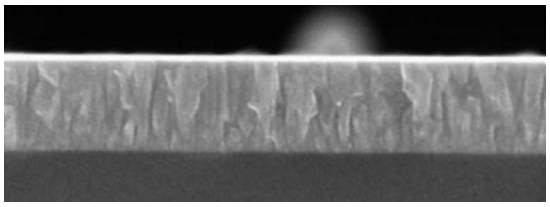

Figure 3.1 Cross-section image of TiN deposited in high vacuum at 350°C.

By means of scanning electron microscopy, it has been possible to verify the obtainment of an adherent and compact titanium nitride film with thickness around 200 nm. After the thermal treatment the sample have been analysed again through SEM, without noticing any differences with the samples on which the thermal treatment has not been performed.

Then, an EDXS analysis has been performed to retrieve qualitative information about the stoichiometry of the titanium nitride thin films. Even if the accuracy of the measurement is limited by the small atomic number of nitrogen and oxygen and by the similarity of the energies of their x-ray transitions, the data obtained are enough to define trends that can describe how the composition changes with the substrate temperature. The data obtained during the measurement are expressed in atomic percentage and they have been normalized with the respect to the atomic percentage of silicon to derive more precise information about the stoichiometry of the films excluding the contribution of the substrate. The results obtained are listed in Table 3.3.

Target	Pressure (Pa)	T_{sub} (°C)	C (%)	N(%)	O(%)	Ti(%)	N/Ti
TiN	$1.53*10^{-3}$	250	6.49	19.73	35.53	38.26	0.52
TiN	$1.29*10^{-3}$	350	5.35	21.20	33.53	39.92	0.53
TiN	$1.08*10^{-3}$	25	7.05	22.37	32.95	37.62	0.59

Table 3.3 List of elemental concentration and atomic ratios of different TiN samples deposited in high vacuum.

In Table 3.3, the atomic ratio N/Ti is computed, and it can be used as a stoichiometry index to investigate the intrinsic sub-stoichiometric nature of the titanium nitride that is described in literature [9]. From Table 3.3, it is possible to confirm that the titanium nitride deposit is sub-stoichiometric in nitrogen. In addition, the substrate temperature seems not to have a significant effect on the stoichiometry of the samples produced.

Target	Pressure (Pa)	T_{sub} (°C)	Status	C (%)	N (%)	O (%)	Ti (%)	N/Ti
TiN	$1.53*10^{-3}$	250	ann.	6.49	19.73	35.53	38.26	0.52
TiN	$1.29*10^{-3}$	350	ann.	5.35	21.20	33.53	39.92	0.53

Table 3.4 List of elemental compositions and atomic ratios of different TiN samples deposited in high vacuum after the annealing process.

The EDXS analysis on the annealed films provided the results that are listed in table 3.4.

Looking at the results, it is possible to notice that in the sample deposited at 250°C the content of oxygen decreased after the annealing and the ratio N/Ti increased with the respect to the as deposited sample.

The atomic ratios computed are larger than the ones obtained by L. Tovaglieri during her master thesis project [66]. Since there are no evidences of the effect of the substrate temperature on N/Ti, it is possible to assume that the improvement can be related to some changes in the pumping system with the respect to the one used by L.Tovaglieri.

The films have been analysed also by means of Raman spectroscopy, providing the results presented in Figure 3.2.

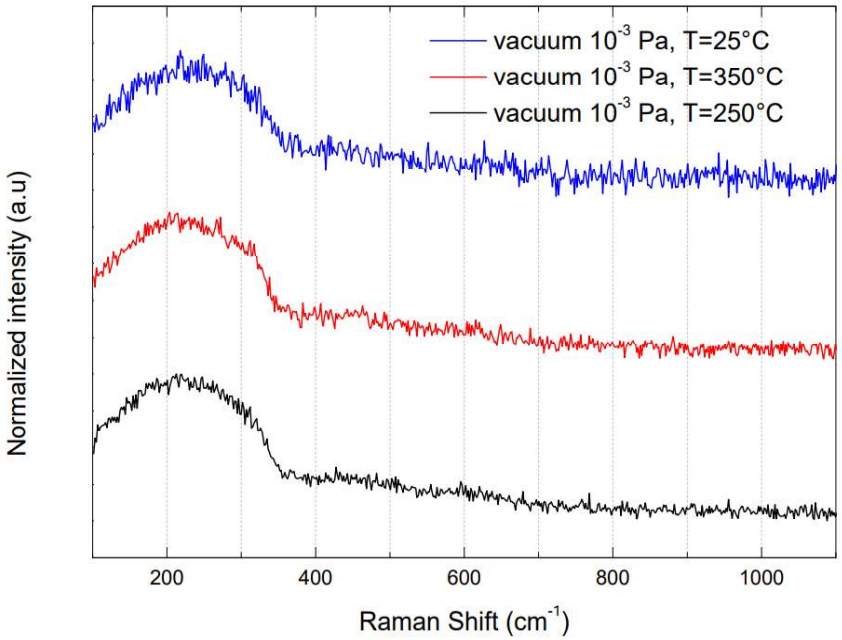

Figure 3.2 Raman spectra of TiN samples deposited in high vacuum.

In Figure 3.2, it is evident the presence of a broad band below 400 cm^{-1} that indicates the presence of nitrogen vacancies. Hence, the sub-stoichiometric nature of the compound is confirmed also by Raman spectroscopy. The Raman spectra of the samples deposited at 250°C and 350°C presented a better signal-to-noise ratio that the one deposited at room temperature. Hence, it could be assumed that the deposition at

350°C and 250°C allowed the achievement of a more ordered structure with the respect to the case deposited at room temperature.

The effect of the annealing process of the Raman spectra of the samples deposited at 25°C and 250°C is presented in Figure 3.3. Looking at the results obtained, it is noticeable a blue-shift of the acoustic band present below 400 cm^{-1} in the annealed samples with the respect to the as deposited ones. This effect is in accordance with the data obtained from previous work carried out by the Nanolab research group and could be related to phenomenon of partial oxidation occurred during the annealing. In addition, the thermal treatment caused a narrowing of the acoustic band and also a better signal-to-noise ratio. These effects allow to assume that the structure obtained after the annealing is more ordered with the respect to the as deposited samples. For what concerns the effect of the substrate temperature, it can be observed that after the thermal treatment the Raman spectra of the samples deposited at room temperature and at 400°C are even more similar than immediately after the deposition. Hence, it is possible to declare that the substrate temperature has not significantly affected the effects of the annealing on the titanium nitride thin films produced.

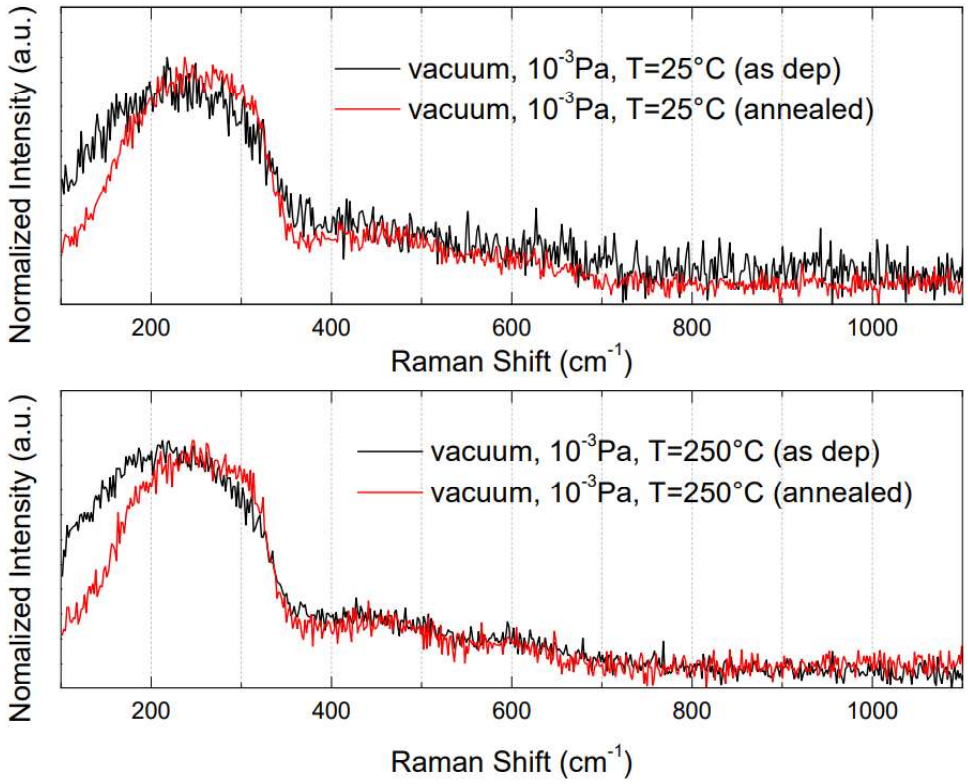

Figure 3.3 Effect of annealing on the Raman spectra of the samples deposited at 25°C and 250°C.

The optical properties of the samples have been investigated through reflectance measurements, and the results obtained through UV-Vis-NIR spectroscopy are presented in Figure 3.4

In Figure 3.4 it is evident that the minimum of reflectance, from which is possible retrieve information about the plasma frequency, is practically the same for all the samples deposited at different substrate temperatures, and it is around 320 nm. While, for large wavelengths, the reflectance of the material tends to increase with the substrate temperature. Since high reflectance is a typical property of metallic materials, it is possible to assume that the higher is the substrate temperature, the stronger is the metallic behaviour of the material deposited.

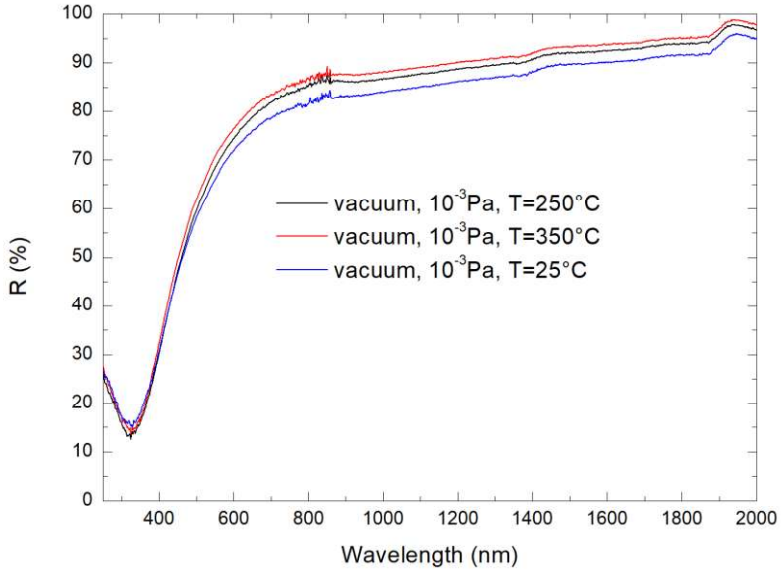

Figure 3.4 Plot of reflectance curves of TiN samples deposited in high vacuum at different substrate temperatures.

The effects of the thermal treatment on the reflectance curves of the samples deposited at 25°C and 250°C are presented in Figure 3.5.

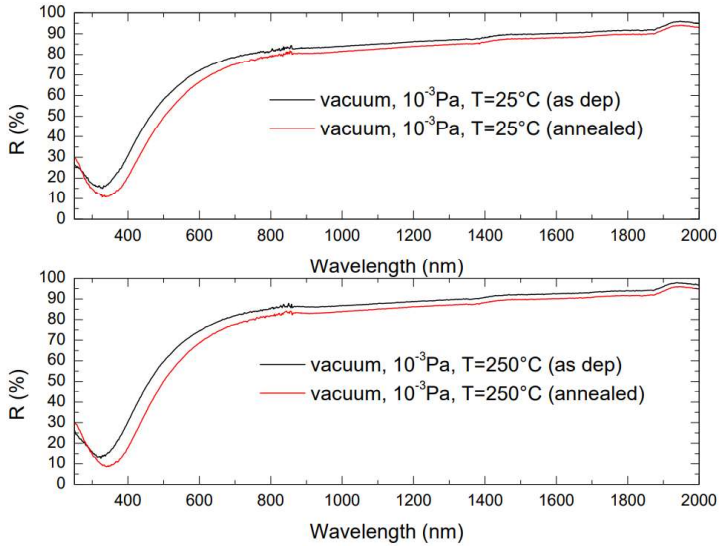

Figure 3.5 Effect of annealing on the reflectance curves of samples deposited at 25°C and 250°C.

Analysing the results, it can be observed that, after the annealing process, the minimum of reflectance is lower and red-shifted from around 320 nm to 340 nm, meaning that the plasma frequency could decrease during after the annealing. These effects are in accordance with what have been found during previous works carried out at Nanolab research laboratories [66]. Considering the effect of the substrate temperature, the position of the minimum of reflectance after the thermal treatment is practically the same for the two samples deposited at different temperatures, while the value of the minimum of R is lower in the case of the sample deposited at a temperature of 250°C. Moreover, the trend of the reflectance at high wavelengths with the respect of the deposition temperature is confirmed also after the thermal treatment. Indeed, it is evident that, increasing the substrate temperature, the values of reflectance at large wavelengths rise.

The dielectric complex function of the titanium nitride films has been retrieved through an ellipsometric measurement, described in Chapter 2, that provided the results represented in Figure 3.6.

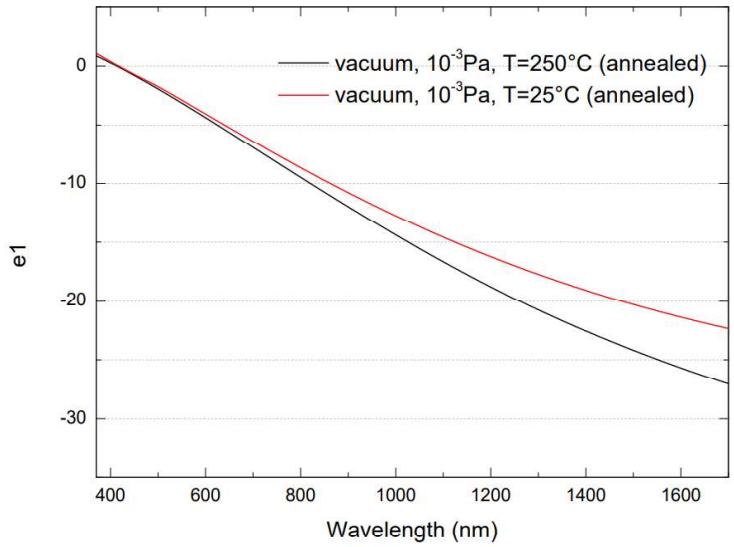

Figure 3.6 Plot of the real part of the dielectric complex function for different annealed TiN samples deposited at different substrate temperatures.

In these sections only the real part of the complex dielectric function is presented because it is the most significant part for the description of the plasmonic properties of a material. The dielectric function has been computed through the adoption of a combination of Drude and Lorentz model that was able to satisfactorily interpolate the date obtained during the measurements. Since the multilayered structure to develop needs to be thermal treated to improve the crystallinity of Ta:TiO_2, the ellipsometric analysis have been performed only the annealed samples. As described in Chapter 1, the point in which ε_1 is null can be associated with the plasma frequency of the material. The plasma wavelength seems to be independent on the deposition temperature. Indeed the ε_1 curves of the samples cross the x-axis practically in the same

point. The values of wavelengths at which the previous condition is satisfied are slightly different from the ones evaluated analysing the reflectance curves. Indeed, they shifted from 338 nm to 410 nm. It is possible to find three different reasons for this variation:

- The range of the ellipsometric measurement starts at 370 nm that is already beyond the plasma wavelength evaluated with the reflectance curves.
- As mentioned in Chapter 2, the derivation of the complex dielectric function implies the adoption of physical or mathematical models that can interpolate the values of angles obtained during the measurements. Hence, the variation could be caused by some approximation made by the model used for the interpolation.
- From the position of the minimum of reflectance is not possible to directly derive the value of the plasma frequency but is possible only to retrieve indication about how it varies changing different parameters.

Analysing the graph in Figure 3.6 at high wavelengths, it is possible to notice that the real part of the sample deposited at 250°C is lower than the one deposited at room temperature. This confirms the fact that the material fabricated with a higher substrate temperature has a stronger metallic behaviour.

Electrical properties of TiN films have been investigated through the four probe Van der Pauw method, described in Chapter 2, providing the results listed in Table 3.5.

Target	Pressure (Pa)	T_{sub} (°C)	Resistivity (Ωcm)
TiN	$1.53*10^{-3}$	250	$4.19*10^{-4} \pm 1.30*10^{-5}$
TiN	$1.29*10^{-3}$	350	$3.24*10^{-4} \pm 2.77*10^{-5}$
TiN	$1.08*10^{-3}$	25	$4.91*10^{-4} \pm 4.38*10^{-5}$

Table 3.5 List of values of resistivity for TiN samples deposited in high vacuum at different substrate temperatures.

Analysing the results presented in Table 3.5, it is possible to highlight a trend of the resistivity with respect to the temperature of the substrate. Indeed, the higher is the substrate temperature the lower is the value of resistivity. This confirms the effect noticed in analysis of the optical properties for which an increase in the substrate temperature can improve the metallic behaviour of the titanium nitride thin films produced.

Due to the low adhesion of the film on the glass substrate and due to the damages carried by the pin used for the measurements, the analysis of the electrical properties of the annealed samples could not have been performed.

3.1.2. TiN samples deposited in low vacuum

According to a previous work carried out by G.Baiardi [67] at the Nanolab research group laboratories, the deposition of TiN films in presence of certain quantity of residual air (low vacuum) causes the development of a double epsilon-near-zero behaviour, which means that the material is characterized by two distinct plasma frequencies, as represented in Figure 3.7. This phenomenon could be probably related to the obtainment of a new compound called titanium oxynitride (TiON).

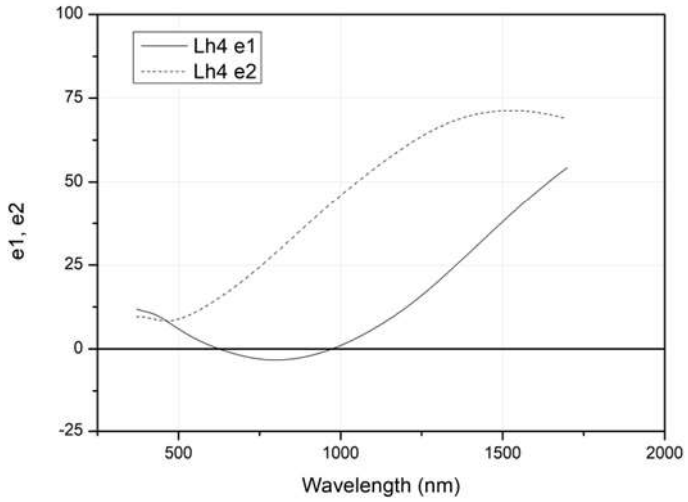

Figure 3.7 Example of components of the dielectric function computed by G.Baiardi during his master thesis project [67].

This peculiar behaviour could lead to two important advantages for the development of HMMs multilayers:

- Considering the limited positive values of the real part of ε of the dielectric component (Ta:TiO_2), having a less negative real part of ε for the metallic component could favour the achievement of the phase matching condition, described in Chapter 1, necessary for the excitation of SPPs.
- As described in Figure 3.7, this particular type of titanium nitride shows a positive ε_1 in the IR range, meaning that it behaves as a dielectric material. Hence, since the theoretical plasma frequency of Ta:TiO_2 is around 4100 nm, in principle it could be possible to develop a novel infrared HMMs multilayered structure in which the metallic component is the tantalum doped titanium oxide and the dielectric one is composed of titanium nitride.

On the other hand, the deposition of titanium nitride in presence of residual air leads to a partial oxidation of the films causing a depletion of electrical and optical properties. So, a trade-off between the positive and negative effects of residual air becomes necessary.

For the reasons just described, it has been decided to deposit different TiN films in presence of residual air to investigate their optical and electrical properties that are fundamental for the development of HMMs.

The reference samples produced, with their relative deposition parameters, are listed in Table 3.6.

Target	Atmosphere	Pressure (Pa)	T_{nom} (°C)	T_{sub} (°C)	Fluence (J/cm^2)
TiN	Vacuum	0.1	25	25	6.5
TiN	Vacuum	0.1	500	350	6.5
TiN	Vacuum	0.4	500	350	6.5

Table 3.6 List of TiN samples deposited at low vacuum with their relative deposition parameters.

The values of fluence have been derived from G. Baiardi's work because they have been found to be optimal for the deposition of this type of materials.

According to the study carried out by G.Baiardi, the maximum value of residual air to avoid the incorporation of oxygen in the structure in form of titanium oxide (TiO_2) has been evaluated around 0.5 Pa. Hence, I decided to adopt values of pressure below this threshold.

Due to the duration of the cooling process of the substrate holder, I decided to deposit only one sample at 0.4 Pa to permit the production of other reference samples fundamental to proceed with the thesis project.

The analysis of the thin films through scanning electron microscopy (SEM) confirmed the deposition of compact and adherent layers of TiN with thickness around 200 nm, without noting variations between the samples deposited at different substrate temperatures and pressures. (Figure 3.8)

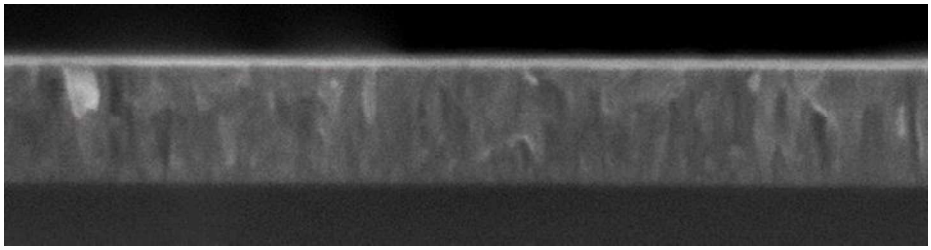

Figure 3.8 Cross-section image of TiN samples deposited in vacuum at 0.1 Pa and at 350°C.

Then, the elemental composition of the reference samples has been investigated by means of EDXS analysis. As mentioned before, this type of measurement can provide only qualitative information about the stoichiometry. However, they are enough to retrieve trends useful to understand the effect of the deposition pressure and the substrate temperature. The results obtained are listed in Table 3.7.

Target	Pressure (Pa)	T_{sub} (°C)	C (%)	N(%)	O(%)	Ti(%)	N/Ti
TiN	0.1	25	5.41	18.64	36.11	39.85	0.47
TiN	0.1	350	6.38	20.71	35.09	37.82	0.55
TiN	0.4	350	2.81	20.98	32.84	43.38	0.48

Table 3.7 List of elemental compositions for different TiN samples deposited in low vacuum.

As expected, the reference samples produced in low vacuum are sub-stoichiometric in nitrogen. Considering the samples deposited at 0.1 Pa, it is noticeable that the sample produced at 250°C is less sub-stoichiometric in nitrogen than the one deposited at room temperature. Hence, the substrate temperature could be used to favor the incorporation of nitrogen in TiN films.

The stoichiometry of the compounds has been analysed also by means of Raman spectroscopy, providing the results presented in Figure 3.9.

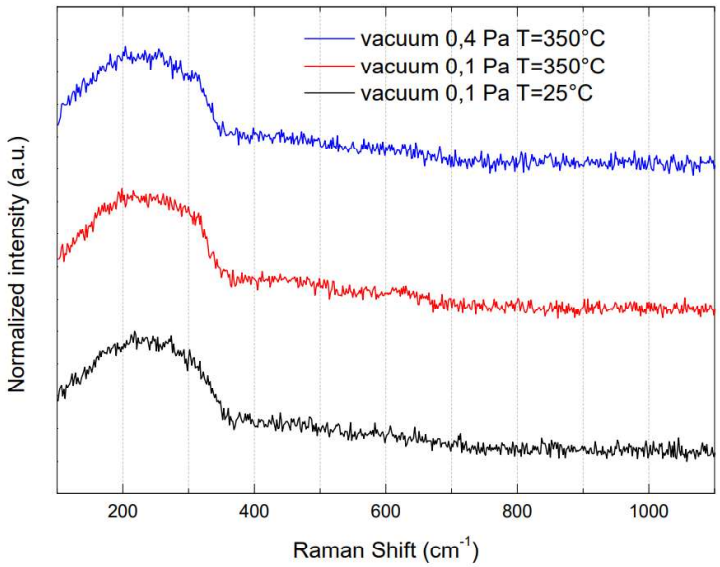

Figure 3.9 Raman spectra of TiN samples deposited in low vacuum.

As evident from the graph, the substoichiometric nature of the compounds is confirmed by the presence of a broad acoustic band below 400 cm^{-1}, highlighting the presence of nitrogen vacancies. In addition, it is noticeable that the variation of deposition pressure has not caused any changes in the Raman spectra of the samples. Even the substrate temperature seems non to affect the Raman spectra of the samples deposited at 0.1 Pa. Hence, the difference in stoichiometry noticed during the EDXS analysis could be not enough to promote a narrowing of the acoustic band below 400 cm^{-1}.

The optical properties of TiN samples have been investigated by means of UV-Vis-NIR spectroscopy and ellipsometry.

The reflectance curves retrieved through the UV-Vis-NIR analysis are presented in Figure 3.10

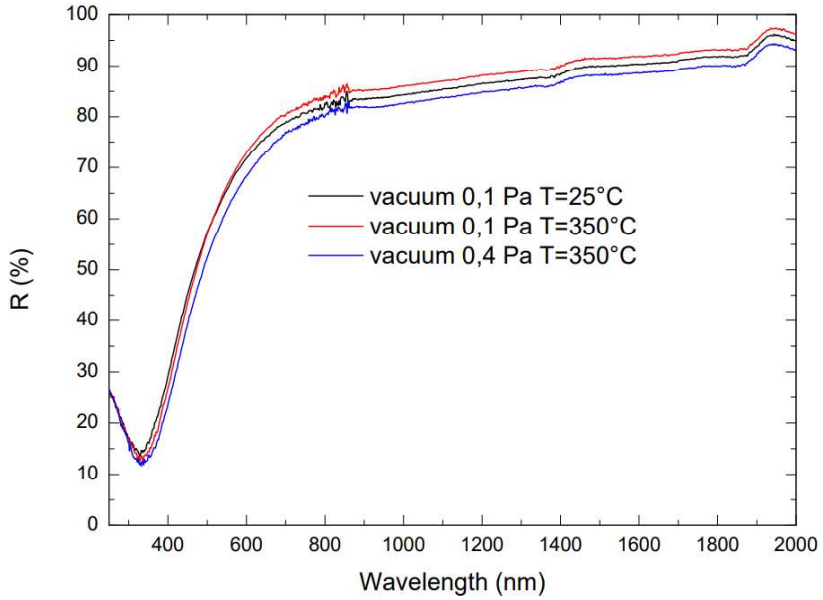

Figure 3.10 Reflectance curves of TiN samples deposited in low vacuum.

Observing the results, it is possible to notice that the position of the minimum reflectance, is around 330 nm. The position and the value of the minimum are not significantly affected by the change in substrate temperature and pressure. While, for large wavelengths, it is possible to notice that reflectance increases with the substrate temperature and decreases with the deposition pressure. Hence, the sample deposited at 0.1 Pa and with a nominal substrate temperature of 500°C has the strongest metallic behaviour.

The dielectric function of the samples has been retrieved through the interpolation of data collected by means of ellipsometric measurements, and the results are presented in Figure 3.11

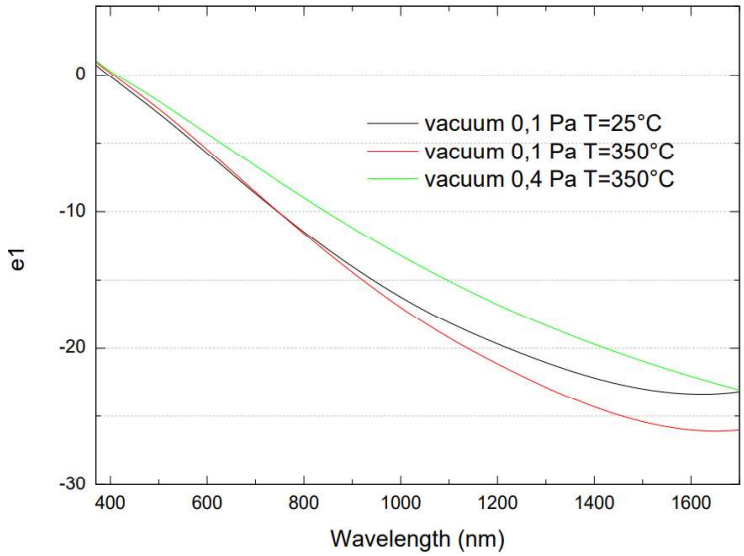

Figure 3.11 Real part of the dielectric function of TiN samples deposited in low vacuum.

Analysing the results, it is possible to notice that the samples deposited at 0.1 Pa are characterized by a minimum of ε_1 around 1650 nm. This probably means that from that point the real part of the dielectric function starts to increase crossing another time the x-axis, obtaining a second plasma frequency. Hence, the results of G.Baiardi are confirmed, but the range of wavelengths in which it occurs is different. This is probably related to a change in the vacuum pumping system that has shifted the threshold value of pressure to higher values, meaning that values of residual air adopted during this thesis are not enough to favour the development of the double epsilon-near-zero behaviour in a smaller range of frequencies.

As expected from the previous analysis, the material that shows the most intense metallic behaviour, and so the most negative ε_1, is the one deposited at 0.1 Pa and at a 350°C. The plasma wavelength, computed as the point in which ε_1 is null, is around 410 nm and it seems to not depend on the substrate temperature and on the value of deposition pressure.

The results related to imaginary part of the dielectric function are presented in Figure 3.12.

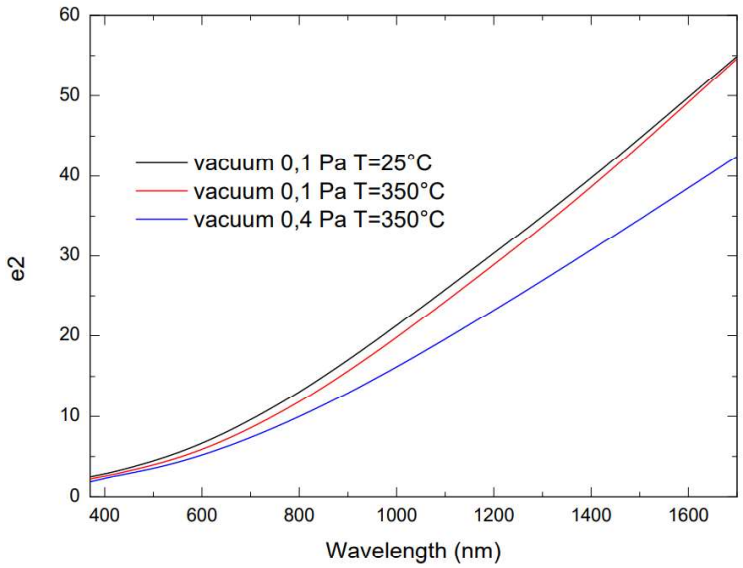

Figure 3.12 Imaginary part of the dielectric function of TiN samples deposited in low vacuum.

Observing the results, it could be assumed that an increase in the substrate temperature or an increase in the deposition pressure allow to obtain a material with a lower imaginary component of the dielectric function, and so a material that, in principle, is characterized by lower optical losses.

The electrical properties of the samples have been investigated by means of Van der Pauw method (four probe), providing the data listed in Table 3.8.

Target	Pressure (Pa)	T_{sub} (°C)	Resistivity (Ωcm)
TiN	0.1	25	$1.22*10^{-3} \pm 7.94*10^{-5}$
TiN	0.4	350	$4.36*10^{-4} \pm 1.23*10^{-5}$

Table 3.8 List of values of resistivity for TiN samples deposited in low vacuum.

Probably due to problems related to the low adhesion of the film on the glass substrate, the measurement of resistivity for the remaining sample could not be performed.

Generally, an increase in the pressure of the residual air present in the vacuum chamber leads to an increase in the degree of oxidation of the film reducing the number of free charges and so the conductivity. According to this hypothesis, it can be assumed that the substrate temperature is able to compensate for the increase in pressure causing a reduction in the resistivity with the respect of the sample deposited at a lower content of residual air.

3.1.3. TiN samples deposited in a reducing atmosphere

According to the data obtained by G.Baiardi during his master thesis work, also the deposition of TiN thin films in presence of a reducing atmosphere, such as N_2-H_2, can promote the development of the double epsilon-near-zero behaviour. Hence, because of the reasons explained in section 3.1.2. I decided to deposit the last set of titanium nitride reference samples in presence of a mixture of nitrogen and hydrogen N_2-H_2 (95% in volume of nitrogen). In general, this type of atmosphere is adopted to compensate for the sub-stoichiometric nature of titanium nitride, promoting the incorporation of nitrogen in the compound and reducing the oxidation of the film.

The reference samples deposited in presence of a reducing atmosphere, with their relative deposition parameters, are listed in Table 3.9.

Target	Atmosphere	Pressure (Pa)	T_{nom} (°C)	T_{sub} (°C)	Fluence (J/cm²)
TiN	N_2-H_2	1	400	250	3.5
TiN	N_2-H_2	1	25	25	3.5
TiN	N_2-H_2	3	500	350	4

Table 3.9 List of TiN samples deposited in a reducing atmosphere with their relative deposition parameters.

For all the samples presented, the background pressure in the chamber at which the gas mixture started to be injected is around $2*10^{-3}$ Pa to ensure a low level of contamination in the deposited films.

The values of fluence used have been retrieved from the previous work carried out by G.Baiardi at Nanolab, because they are considered optimal for the deposition of these types of material.

After the deposition, a vacuum thermal treatment at 500°C has been performed on sample deposited with 1 Pa of N_2-H_2 to investigate the influence of the substrate temperature on the effects of the annealing process.

The cross-section analysis of the samples, performed by means of SEM, confirmed the obtainment of compact and adherent films of TiN with thickness around 200 nm. (Figure 3.13)

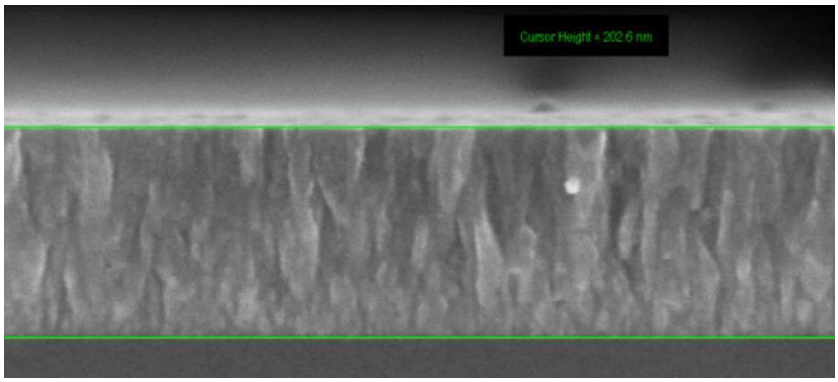

Figure 3.13 Cross-section image of a TiN sample deposited in presence of 1 Pa of N_2-H_2 at 250°C.

After the thermal treatment, several detachments of the films from the substrate have been detected; however, their number is much larger in the case of the sample deposited at room temperature. This phenomenon is probably related to the fact that a higher substrate temperature can partially relax the internal stresses induced during the growth of the film. (Figure 3.14) But, probably a substrate temperature of 350°C is not enough to favour the relaxation of the internal stresses induced during the deposition in presence of N_2-H_2.

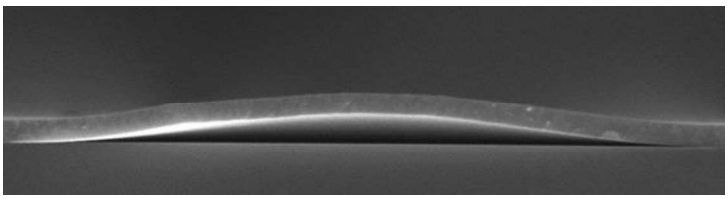

Figure 3.14 Example of the effect of thermal treatment on TiN samples deposited in presence of a reducing atmosphere.

An EDXS analysis have been performed to retrieve information about the stoichiometry of the samples produced, providing the data listed in Table 3.10.

Target	Pressure (Pa)	T_{sub} (°C)	C (%)	N(%)	O(%)	Ti(%)	N/Ti
TiN	1	250	3.63	21.20	34.79	40.38	0.52
TiN	1	25	5.12	18.92	38.58	37.38	0.51
TiN	3	350	1.50	27.39	29.45	41.66	0.66

Table 3.10 List of elemental compositions and atomic ratios of different TiN samples deposited in presence of a reducing atmosphere.

As expected, increasing the pressure of the mixture N_2-H_2 the quantity of nitrogen incorporated rises. Looking at the atomic ratio it is possible to notice that the substrate temperature does not affect the incorporation of nitrogen in titanium nitride thin films.

After the annealing process, another EDXS analysis has been performed to study the effect of the thermal treatment on the stoichiometry of the compound, providing the results listed in Table 3.11.

Target	Pressure (Pa)	T_{sub} (°C)	Status	C (%)	N (%)	O (%)	Ti (%)	N/Ti
TiN	1	250	ann.	6.64	21.68	36.29	35.39	0.61
TiN	1	25	ann.	12.90	13.28	44.25	29.29	0.45

Table 3.11 List of elemental compositions and atomic ratios of different annealed TiN samples deposited in presence of a reducing atmosphere.

Analysing the results, it is noticeable a decrease in the content of titanium. Since a phenomenon of evaporation of Ti at 500°C is practically impossible, the variation of the contents of the sample can be attributed to the limited accuracy, typical of this type of measurement.

Then the reference samples have been analysed by means of Raman spectroscopy, obtaining the spectra represented in Figure 3.15.

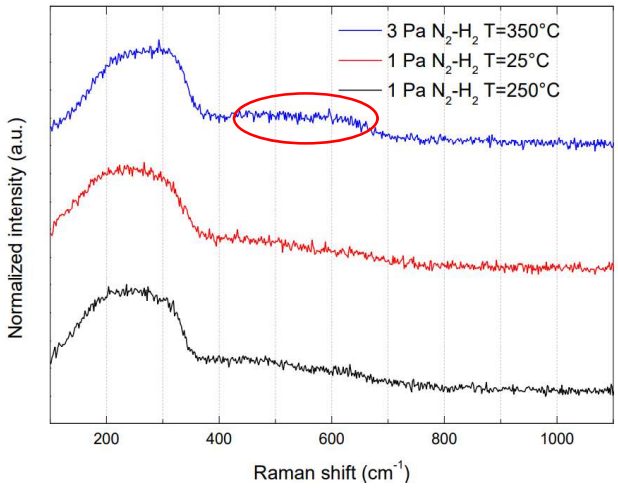

Figure 3.15 Raman spectra of TiN samples deposited at different temperatures in presence of a reducing atmosphere.

Analysing the graph, it is noticeable that the sub-stoichiometric nature of the compound is confirmed by the presence of a broad acoustic band below 400 cm^{-1} that highlights the presence of nitrogen vacancies in the crystalline lattice. As expected, the width of the band is lower in the case of the sample deposited in presence of 3 Pa of N_2H_2 due to a larger incorporation of nitrogen in the film caused by a larger pressure of gas mixture present during the deposition. Another evidence of the larger

concentration of nitrogen, can be found in the slightly visible band around 600 cm^{-1} that is related to the vibration of N^{3-} ions.

In addition, the substrate temperature seems not to affect the results obtained through Raman spectroscopy. This is accordance with the stoichiometric information retrieved by means of EDXS analysis.

After the annealing process, the samples have been analysed by means of Raman spectroscopy to investigate the effects of the thermal treatment, leading to the obtainment of the results presented in Figure 3.16.

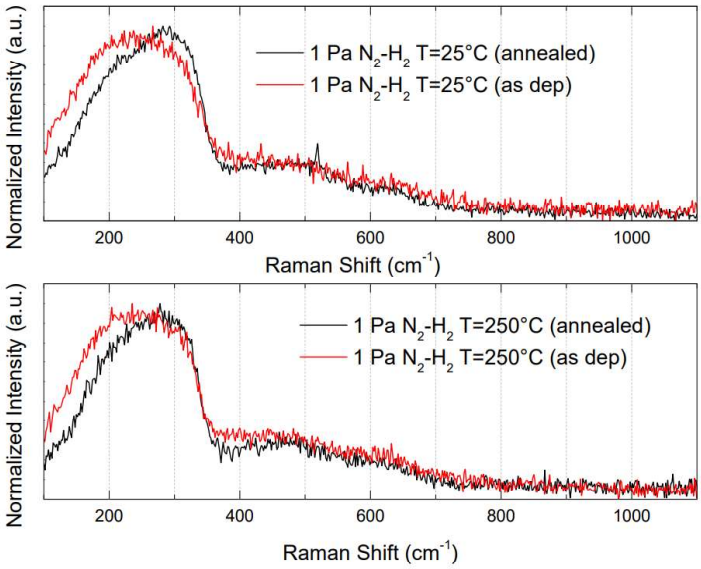

Figure 3.16 Raman spectra of annealed TiN samples deposited at different temperatures in presence of a reducing atmosphere.

In the graph, it can be noticed that the acoustic band (below 400 cm^{-1}) is blue-shifted, probably due to a phenomenon of partial oxidation occurred during the annealing, and narrower, meaning that probably the structure is more ordered, after the thermal treatment. Even after the annealing, the effect of the substrate temperature is practically null for what concerns the Raman spectroscopy.

As for the reference samples deposited in vacuum, the optical properties of the films have been investigated by means of UV-Vis-NIR spectroscopy and ellipsometry.

The data related to the reflectivity of the materials have been obtained through UV-Vis-NIR spectroscopy, providing the results presented in Figure 3.17.

For the samples deposited at 1 Pa of N_2H_2, the minimum is around 350 nm, while, in the case of the sample deposited at 3 Pa of N_2H_2, it can be found around 400 nm. For larger wavelengths, it is evident that the material with the highest reflectance, and the strongest metallic behaviour, is the one deposited at a nominal substrate temperature of 400°C and with 1 Pa of N_2H_2. Making a comparison between the two samples deposited with the substrate heater switched on, it is possible to note that lower is the pressure of the gas mixture and stronger is the metallic behaviour of titanium nitride.

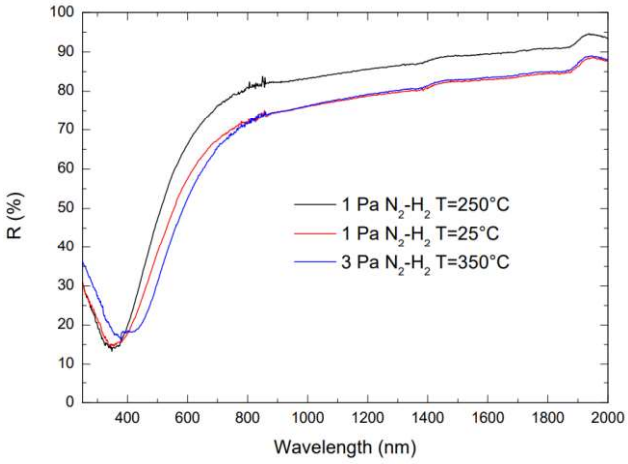

Figure 3.17 Reflectance curves of TiN samples deposited in presence of a reducing atmosphere.

The reflectance of the reference samples has been analysed also after the thermal treatment to examine the effect of annealing on the optical properties. The results obtained are presented in Figure 3.18.

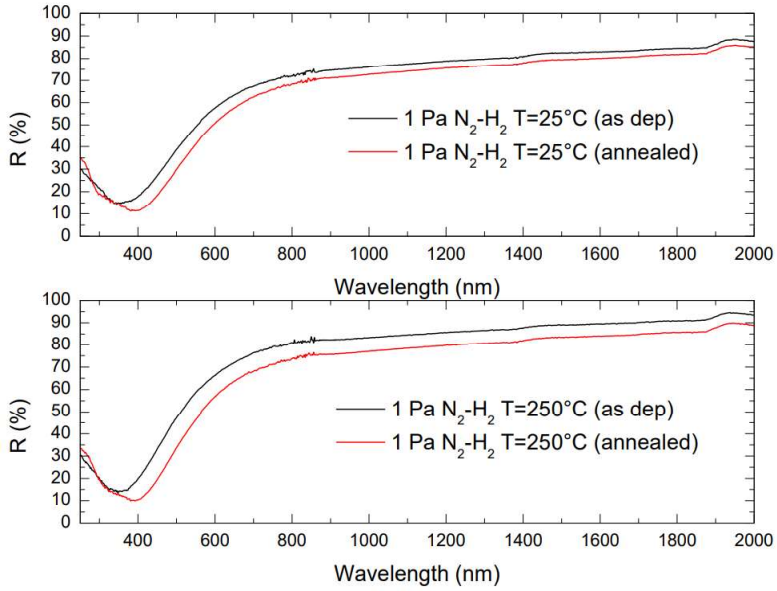

Figure 3.18 Reflectance curves of annealed TiN samples deposited in presence of a reducing atmosphere.

Analysing the results, it has been noticed that the minimum of reflectance has red-shifted from 350 cm^{-1} to 390 cm^{-1}. Moreover, the annealing has caused a reduction in reflectance for larger wavelengths. Since these properties are related to the density of free charges, it could be assumed that during the treatment a partial oxidation has occurred causing a reduction in the number of free charges.

Analysing the results, it has been noticed that the minimum of reflectance has red-shifted from 350 cm^{-1} to 400 cm^{-1}. Moreover, the annealing has caused a reduction in reflectance for larger wavelengths. This could be associated with a possible

phenomenon of oxidation occurred during the annealing that caused a reduction in the metallicity of TiN films.

As described in Chapter 1, the complex dielectric function has been retrieved to model the hyperbolic behaviour of a multilayered structure by means of the effective medium theory. Hence, due to the adhesion problems previously described, that would be detrimental for the development of a multilayered structure, and due to the complexity of the ellipsometric measurements, it has been decided to perform the analysis only on the sample deposited at 3 Pa of N_2H_2 (TiN_9). The final results obtained are presented in Figure 3.19.

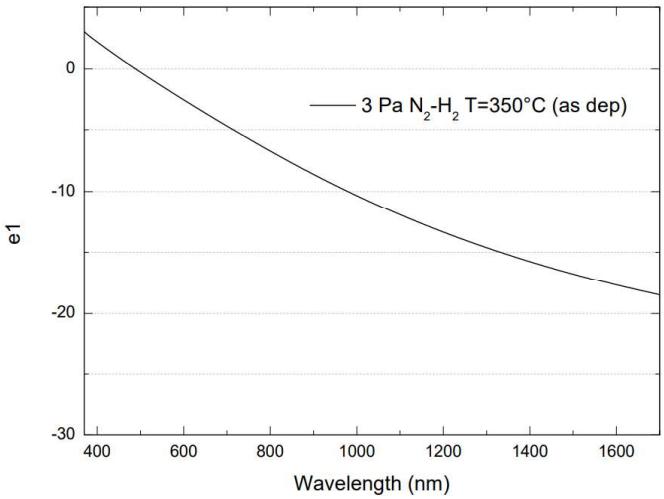

Figure 3.19 Plot of the real part of complex dielectric function of the sample deposited with 3 Pa of N_2-H_2.

The plasma wavelength, that corresponds to the point in which ε_1 is null, is around 500 nm.

Probably due to problems related to the low adhesion of the film on the glass substrate, it was not possible to retrieve results from the electrical measurements of the samples deposited in presence of N2-H2.

3.1.4. Comparison between different deposition atmospheres

In the previous sections, the attention was focused on the effects of the substrate temperature on the properties of several TiN reference samples. Now, in this section, the effects of the deposition atmosphere, maintaining constant the substrate temperature, are presented.

The titanium nitride selected for the description of the effects of the deposition atmosphere are listed in Table 3.12.

Since some samples have been deposited only with the substrate heater switched on, I decided to select the samples presented in the list to guarantee a more precise description of the effects of the deposition atmosphere.

Target	Atmosphere	Pressure (Pa)	T_{nom} (°C)	T_{sub} (°C)	Fluence (J/cm²)
TiN	Vacuum	$1.29*10^{-3}$	500	350	3.5
TiN	Vacuum	0.1	500	350	6.5
TiN	Vacuum	0.4	500	350	6.5
TiN	N_2H_2	1	400	250	3.5
TiN	N_2H_2	3	500	350	4

Table 3.12 List of TiN samples selected to investigate the effect of the deposition pressure and type of atmosphere.

All the data related to the stoichiometry of the samples, obtained by means of EDXS analysis, are collected, and presented in Table 3.13.

Target	Pressure (Pa)	T_{sub} (°C)	C (%)	N(%)	O(%)	Ti(%)	N/Ti
TiN	$1.29*10^{-3}$ (vac)	350	5.35	21.20	33.53	39.92	0.53
TiN	0.1 (vac)	350	6.38	20.71	35.09	37.82	0.55
TiN	0.4 (vac)	350	2.81	20.98	32.84	43.38	0.48
TiN	1 (N_2-H_2)	250	3.63	21.20	34.79	40.38	0.52
TiN	3 (N_2-H_2)	350	1.50	27.39	29.45	41.66	0.66

Table 3.13 List of elemental compositions and atomic ratios for different TiN samples.

Analysing the results presented in Table 3.13, it is noticeable that the films deposited in high and low vacuum are characterized by practically the same elemental compositions and atomic ratios. This could be related to the vacuum pumping system that is enough efficient to guarantee the same level of contamination (oxygen) in low and high vacuum. In addition, it is evident that, only in the case of the sample deposited in presence of 3 Pa of N_2-H_2, an increase in the nitrogen content is noticed. Hence, depositing in an atmosphere of 1 Pa of N_2-H_2 is not enough to promote the incorporation of nitrogen with the respect to the samples deposited in vacuum.

Stoichiometry is also investigable by means of Raman spectroscopy. All the data previously described are collected in the graph presented in Figure 3.20

Looking at the graph, it is possible to observe that there is only one sample (TiN_9) that shows a different Raman spectrum, confirming the results obtained by means of EDXS. The sample deposited with 3 Pa of N_2-H_2 is characterized by a narrower acoustic band below 400 cm^{-1}, that indicates a lower concentration of nitrogen vacancies. Another evidence of the larger concentration of nitrogen can be found in more intense band at around 600 cm^{-1} related to the vibration of nitrogen ions.

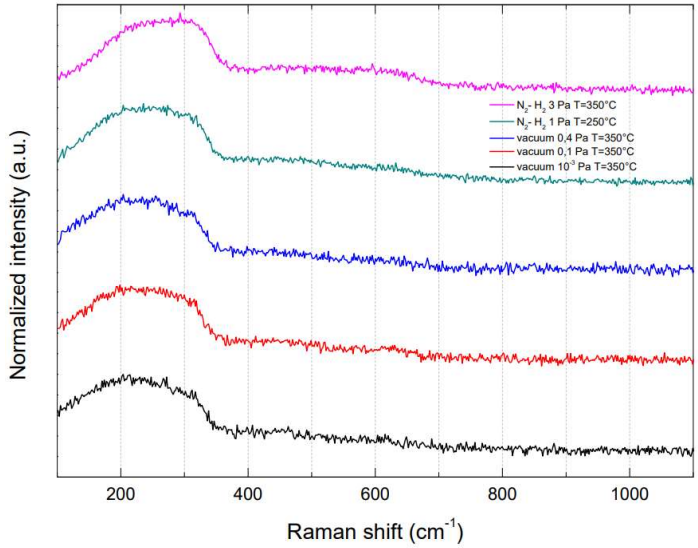

Figure 3.20 Raman spectra of TiN samples deposited with different atmoshperes.

Looking at the graph, it is possible to observe that there is only one sample that shows a different Raman spectrum, confirming the results obtained by means of EDXS. TiN deposited with 3 Pa of N_2-H_2 is characterized by a narrower acoustic band below 400 cm^{-1}, that indicates a lower concentration of nitrogen vacancies. Another evidence of the larger concentration of nitrogen can be found in more intense band at around 600 cm^{-1} related to the vibration of nitrogen ions.

The data regarding the reflectance of the different samples are collected in Figure 3.21.

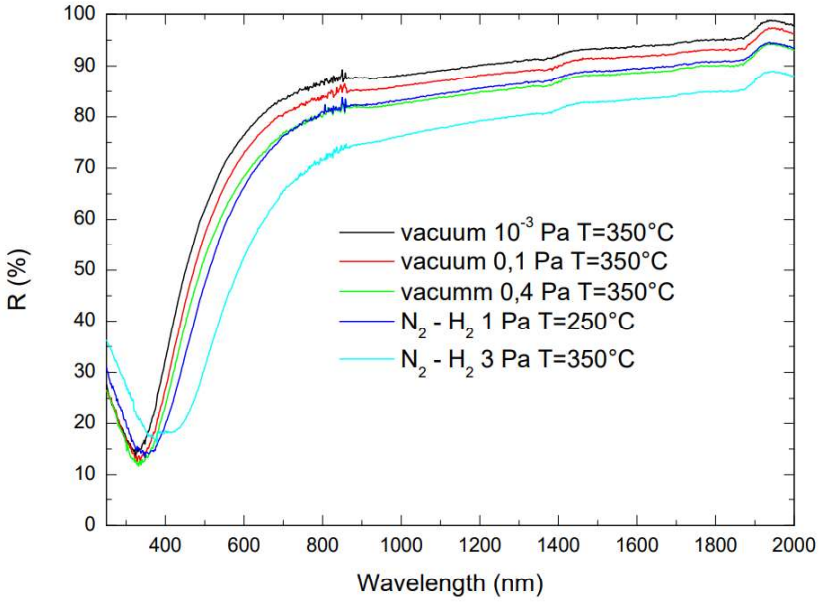

Figure 3.21 Reflectance curves of TiN samples deposited in different atmospheres.

The position of the minimum in reflectance, that corresponds to the plasma wavelength, is practically the same (320 nm) for the sample except for the ones deposited with N_2-H_2 (340 nm-370 nm). Hence, even the presence of 1 Pa of N_2-H_2 can

have an influence on the optical properties of titanium nitride thin films. For larger wavelengths, it is evident for the first time an effect of the deposition pressure for what concerns the samples deposited in vacuum. In particular, the higher is the deposition pressure the lower is the reflectance, and so the weaker is the metallic behaviour of TiN. In conclusion, due to the lower reflectance at large wavelengths and due to the lower plasma frequency, it is possible to assert that the deposition of titanium nitride films in presence of N_2-H_2 promote the development of a weaker metallic behaviour with respect of the ones fabricated in vacuum.

All the data available that describe the real part of the dielectric function of the samples produced are represented in Figure 3.22.

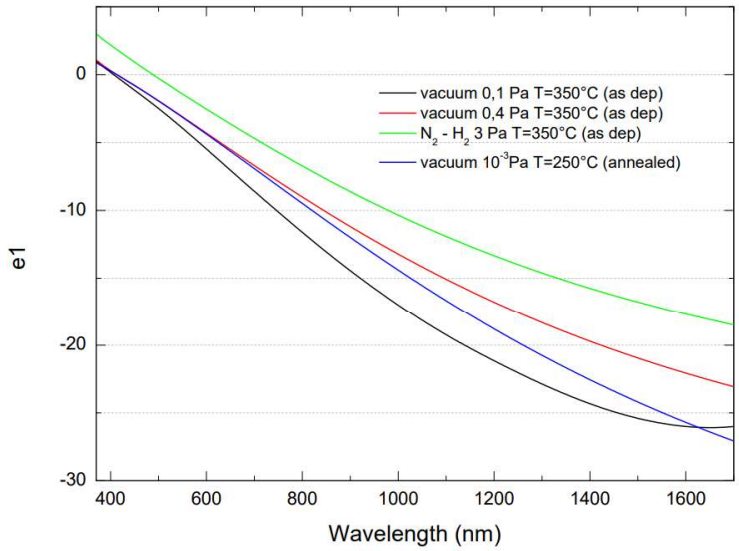

Figure 3.22 Plot of the real component of dielectric function for some TiN samples deposited in presence of different atmospheres.

The data presented in Figure 3.22 confirm what just described regarding the reflectance curves. Indeed, for the samples deposited in vacuum, increasing the pressure also ε_1 rises, meaning that the material deposited in vacuum at 0.4 Pa is less metallic than the one deposited at 0.1 Pa. The plasma wavelength, computed as the point in which ε_1 is null, is equal to around 410 nm for the samples deposited in vacuum and around 510 nm for the sample deposited in presence of N_2-H_2. In addition, the effect of the reducing atmosphere is corroborated by the larger real part of ε and by the larger plasma wavelength.

All the results available regarding the electrical properties of titanium nitride thin films are collected and presented in Table 3.14.

Target	Atmosphere	Pressure (Pa)	T_{sub} (°C)	Resistivity (Ωcm)
TiN	Vacuum	10^{-3}	350	$3.24*10^{-4} \pm 2.77*10^{-5}$
TiN	Vacuum	0.4	350	$4.36*10^{-4} \pm 1.23*10^{-5}$

Table 3.14 List of resistivity for different TiN samples.

It has been possible to perform the electrical analysis on the two samples presented in Table 3.19. This could be related to problems of adhesion of the film to the glass substrate that made the measurement unpracticable.

From the data provided by means of electrical measurements based on Van der Pauw method, it is evident that an increase in the deposition pressure in vacuum causes a lower metallicity of the film, that is proved by the larger resistivity.

To summarize, stoichiometry seems not to be influenced by the different deposition atmospheres, except for gas mixture pressures larger than 1 Pa. Regarding optical and electrical properties, it is possible to assert that the larger is the pressure, the lower is the metallicity of the film deposited. Finally, it has been found that the materials with the lowest metallicity are the TiN films deposited in presence of N_2-H_2, and the metallic behaviour is stronger for smaller pressure of the gas mixture.

3.1.5. Final remarks on the effect of the substrate temperature

In conclusion, analysing all the data presented in the previous sections, it is possible to assert that the substrate temperature is a parameter that can affect the optical and electrical properties of titanium nitride thin films. In particular, increasing the substrate temperature the material is characterized by a larger reflectance and by a lower resistivity. Hence, the temperature of the substrate can be used to control the metallicity of TiN. Regarding the stoichiometry of the samples, it has been noticed that a nominal substrate temperature of 500 °C (≈ 350°C from the thermocouple) is not enough to promote the incorporation of nitrogen and to promote the oxidation of the film. Indeed, by means of EDXS analysis and Raman spectroscopy, it has been verified that the elemental composition of the samples is practically unchanged after an increase in the substrate temperature. In addition, the sub-stoichiometric nature of the compound has been confirmed by the data obtained, and the presence of nitrogen vacancies, detectable by means of Raman spectroscopy, seems not to be affected by the substrate temperature.

Summarizing, the substrate temperature can be used to tune the metallicity of titanium nitride thin films, while the stoichiometry probably needs a higher temperature to be significantly modulated.

3.2. Tantalum doped titanium oxide (Ta:TiO_2)

Tantalum doped titanium oxide (Ta:TiO_2) has been selected as the dielectric component for the development of HMMs multilayered structures for its dielectric behaviour in the visible and NIR range, but also for its peculiar plasmonic behaviour in the IR range, that could lead to the obtainment of multilayers with unexplored optical and plasmonic properties. For this reason, it has been necessary to deposit and characterize different reference samples to investigate the principal properties of

$Ta:TiO_2$. In the following sections, the data obtained during the characterization are presented.

The objective of the deposition and of the characterization of $Ta:TiO_2$ mainly consists in studying the effect of the substrate temperature and dopant content on the morphology, stoichiometry and optical properties of the samples. Due to the duration of the cooling process after the deposition, it has not been possible to deposit the reference samples also at room temperature but only at 350°C. The data used for the comparison with samples deposited at room temperature have been retrieved from previous works carried out at the Nanolab research group laboratories [69].

Before starting with the presentation of the samples and the description of their properties, it may be useful to list the deposition parameters that are in common between all the reference samples produced:

- Deposition atmosphere: 1 Pa of oxygen
- Substrate: silicon wafer (110 crystal plane) and glass. The substrates have been heated through a substrate heater, as described in section 2.1.
- Target to substrate distance: 5 cm.
- Laser fluence: ≈ 2 J/cm^2.
- Laser: pulsed green laser (532nm) with a frequency of 10 Hz.
- Sample thickness: ≈ 200 nm and ≈ 20 nm.

The deposition atmosphere and the value of the pressure have been selected according to previous studies performed by the Nanolab research group, in which these parameters have been found as optimal for the deposition of a conductive tantalum doped titanium oxide film. While, I decided to deposit thin films with thicknesses in the order of the ones typically used for the development of HMMs multilayers, due to the characteristic influence of the thickness on the properties of transparent conductive oxides (TCOs). The value of energy laser has been set in accordance with previous works carried out at the Nanolab laboratories, to reach a value of fluency around 2 J/cm^2, that is considered optimal for the deposition of this kind of material.

To investigate the effect of the tantalum content, different targets have been used during the depositions:

- $Ta:TiO_2$, with diameter of 2 inches and with a content of tantalum equal to 5% in mass.
- $Ta:TiO_2$, with diameter of 2 inches and with a content of tantalum equal to 10% in mass.

To avoid any modifications of the films and too excessive phenomenon of oxidation, the samples have been extracted from the vacuum chamber only when the substrate temperature detected by the thermocouple, mounted on the substrate holder, was below 50°C.

The reference samples of tantalum doped titanium oxide produced during this master thesis project are listed in Table 3.15.

Target	Ta content (%)	Thickness (nm)	T_{nom} (°C)	T_{sub} (°C)
Ta:TiO_2	5	20	500	350
Ta:TiO_2	5	200	500	350
Ta:TiO_2	10	20	500	350
Ta:TiO_2	10	200	500	350

Table 3.15 List of Ta:TiO_2 samples with their relative deposition parameters.

After the deposition, an annealing process, in vacuum at around 500°C, has been performed to promote the crystallization of the films. This process is considered necessary for this type of material for the reasons described in Chapter 1.

The cross section of every sample has been analysed by means of scanning electron microscopy (SEM), confirming the obtainment of compact and adherent films, with thicknesses around 20 nm and 200 mn. (Figure 3.23)

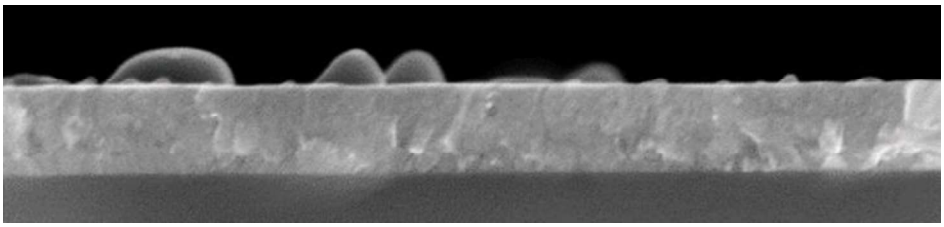

Figure 3.23 Example of cross-section image of tantalum doped titanium oxide sample (10% of Ta and 200 nm).

After the thermal treatment, no changes have been observed in the morphology of the cross-section. In addition, problems of detachment of the films have not been observed both in the as deposited and annealed samples. (Figure 3.24)

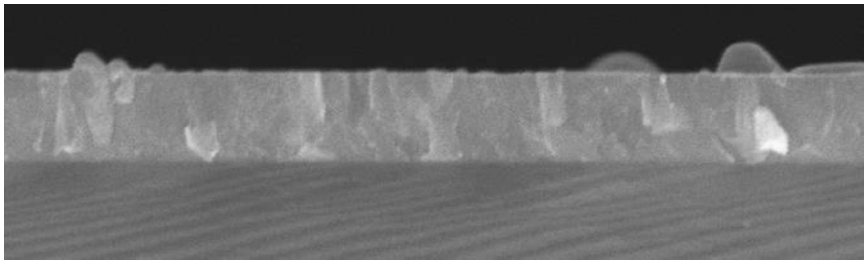

Figure 3.24 Example of cross-section image of Ta:TiO_2 sample after the thermal treatment (10% of Ta and 200 nm).

Information about the stoichiometry of the deposited films have been retrieved by means of EDXS analysis. The results obtained for the sample with 200nm of thickness are listed in Table 3.16. The ones of the samples with 20 nm are not presented due to a too strong contribution of Si and C that is probably related to the small thickness.

Target	Ta content (%)	T_{sub} (°C)	C (%)	O (%)	Ti (%)	Ta (%)
Ta:TiO_2	5	350	3.23	65.63	29.57	1.57
Ta:TiO_2	10	350	3.74	65.26	28.72	2.29

Table 3.16 List of elemental compositions for different Ta:TiO_2 samples.

As for the TiN reference samples, the data presented in Table 3.20 have been normalized with the respect of the content of silicon to obtain more precise information about the stoichiometry of the films.

As expected, the content of tantalum is higher in the case of the sample obtained ablating the target with the largest content of dopant agent.

The elemental composition of the samples has been investigated also after the annealing process, providing the results listed in Table 3.17.

Status	Ta content (%)	T_{sub} (°C)	C (%)	O (%)	Ti (%)	Ta (%)
annealed	5	350	3.23	65.63	29.57	1.57
annealed	10	350	3.74	65.26	28.72	2.29

Table 3.17 List of elemental compositions for different annealed Ta:TiO2 samples.

Since an evaporation of tantalum is practically impossible at temperatures around 500°C, it is possible to assume that the variations of the elemental composition could be related to the normalization with the respect of silicon and to the limited accuracy of the measurement. In addition, the condition for which the highest content of Ta has been detected in the sample deposited ablating the target with the largest content of dopant agent has been verified also after the thermal treatment.

As described in Chapter 1, the crystallinity of tantalum doped titanium oxide can be investigated by means of Raman spectroscopy (Figure 3.25)

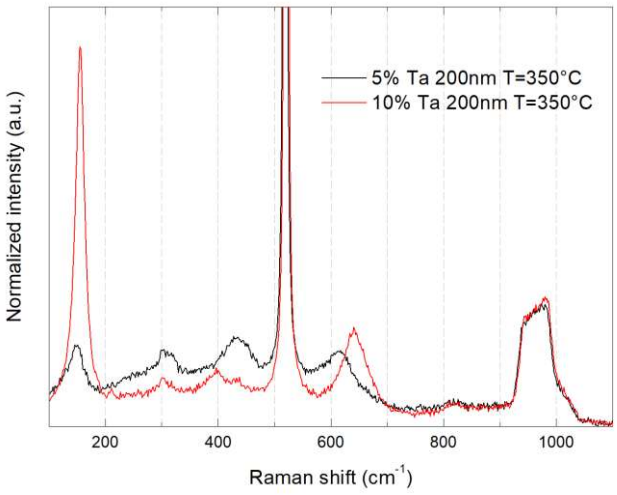

Figure 3.25 Raman spectra of different Ta:TiO_2 reference samples.

Considering the sample with 10% of Ta in mass, four peaks can be noticed at around 150 cm^{-1} (E_g), at around 300 cm^{-1}, at around 400-450 cm^{-1} (B_{1g}) and around 630 cm^{-1} (E_g), meaning that the film is already crystalline, in the anatase phase, after the deposition at around 350°C. Considering the sample with 5% of Ta in mass, four peaks can be noticed at around 150 cm^{-1} (E_g), at around 300 cm^{-1}, at around 450 cm^{-1} (E_g) and around 610 cm^{-1} (A_{1g}), meaning that the film is already crystalline, with a probable coexistence of anatase and rutile phase, after the deposition at around 350°C.

Focusing on the principal peak at around 150 cm^{-1}, it has been observed that the sample with 10% of Ta in mass presented a peak slightly blue-shifted with the respect to the one with 5% of Ta. This is accordance with the experimental results found by Mazzolini et al. [32], for which an increasing density of free charges, that is directly related to the content of the dopant agent, causes a progressive blue-shift of the principal peak at around 150 cm^{-1}.

In addition, it is possible to notice that the intensity of the peak is larger for the samples with 10% of Ta, meaning that this sample has a more ordered and crystalline structure with the respect to the one with 5% of Ta. Crystallization of Ta:TiO_2 never occurred during the deposition at room temperature, meaning that the use of a substrate heater could be very important and crucial for the obtainment of crystalline Ta:TiO_2 during the process of deposition.

On the sample with 20 nm of thickness no peaks have been detected and this could be related to the small thickness of the film that did not permit the development of a more intense and detectable signal.

During this project, a sample of pure titanium oxide has been deposited with the same deposition parameters of the Ta:TiO_2 ones, being characterized by the Raman spectrum presented in Figure 3.26.

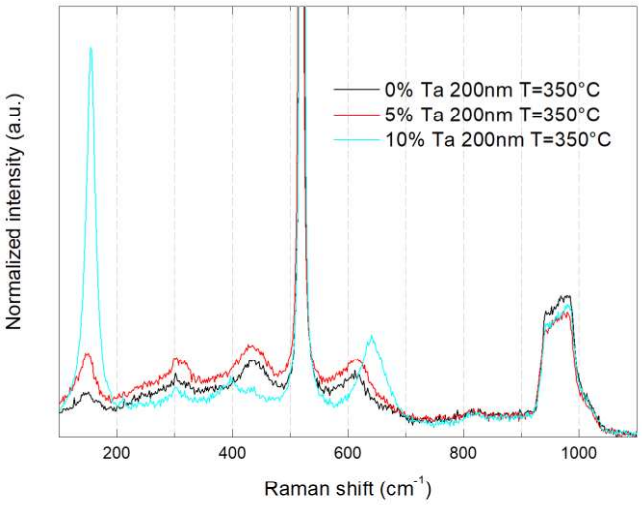

Figure 3.26 Raman spectra of TiO_2 and Ta:TiO_2 samples.

From the graph, it is evident that the titanium oxide sample is practically amorphous with the respect to the remaining Ta:TiO_2 samples. This is another evidence of the effect of the tantalum content on the process of crystallization of thin films.

After the thermal treatment, Raman spectroscopy performed on the reference samples provided the results presented in Figure 3.27.

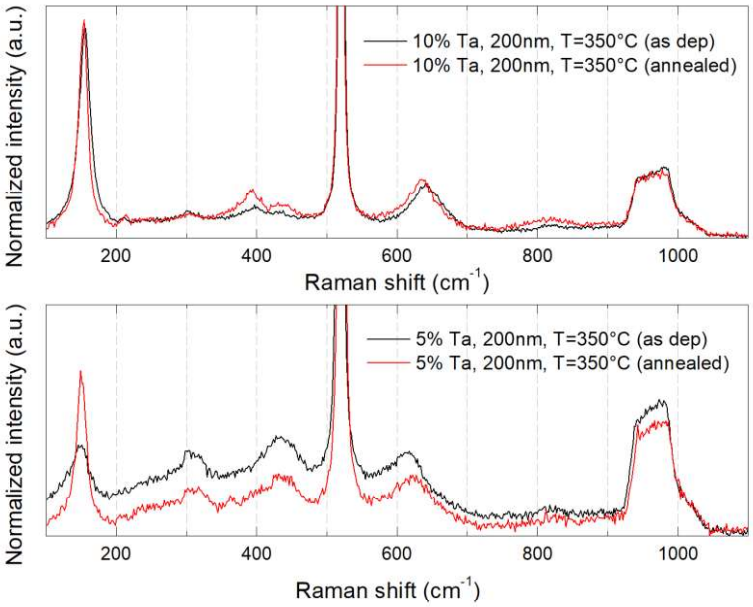

Figure 3.27 Raman spectra of annealed Ta:TiO_2 samples with thickness of 200 nm.

Raman spectra of the 20 nm annealed samples are not presented because the signal is too weak probably due to the limited thickness of the films.

it is noticeable in Figure 3.28 that the thermal treatment favoured a process of crystallization in the sample with the lowest content of tantalum . Indeed, the characteristic peak at around 150 cm^{-1} is narrower and more intense. On the contrary, the Raman spectrum of the sample with 10% of Ta is practically unchanged after the annealing, meaning that the crystalline structure obtained after the deposition is equal to the one obtainable after the thermal treatment. Fitting the data, it is possible to determine approximately the position of the characteristic peak. In particular, for the sample with 5% of Ta the peak is positioned at 150.4 cm^{-1}, while the peak of the sample with 10% of tantalum is positioned at 154.3 cm^{-1}. This is in accordance with what have been noticed for the samples with lower thickness and with the results obtained by Bricchi [40] and Mazzolini [32] during their research works.

The dielectric function of the tantalum doped titanium oxide thin films has been computed through an interpolation of data obtained during ellipsometric measurements, providing the results presented in Figure 3.28 and 3.29.

Due to the complexity of the measurement, it has been possible to perform the measurement only on the annealed sample with the largest thickness and content of tantalum. The data presented in the graphs, that are related to the sample deposited at

room temperature, have been retrieved from a previous work carried out by C. Mancarella during her PhD thesis project [69].

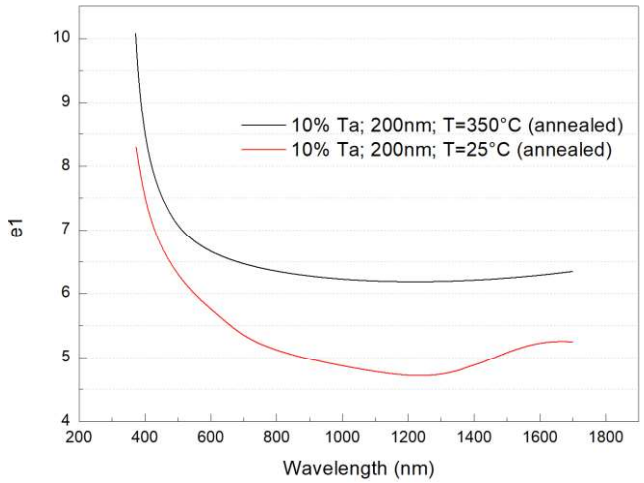

Figure 3.28 Real part of dielectric function computed for different Ta:TiO_2 samples.

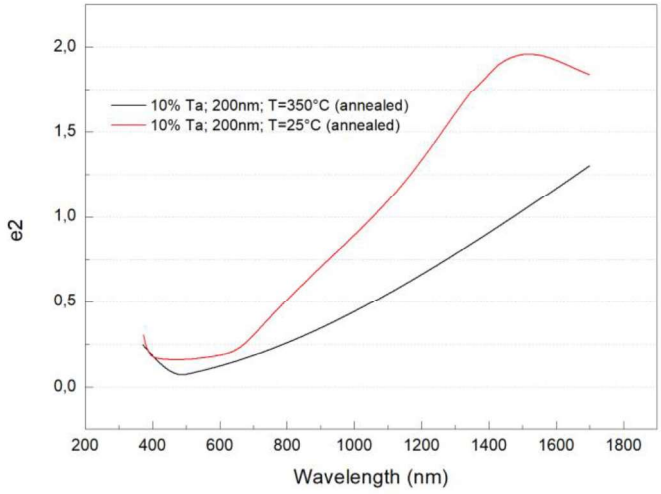

Figure 3.29 Imaginary part of dielectric function computed for different Ta:TiO_2 samples.

Analysing the results, it can be observed that the material deposited at room temperature shows a smaller real part of the dielectric function and a larger imaginary part. Hence, theoretically, the deposition of tantalum doped titanium oxide, with a substrate temperature around 350°C, can lead to the obtainment of a film with a stronger dielectric behaviour and with a lower dispersion coefficient. On the other hand, there exists a possibility that this variation is mainly related to the model used for the interpolation of the data obtained during the ellipsometric analysis. This could be explained by the fact that the model used is a combination of Drude and Lorent models in which the plasma frequency is considered. Hence, since the plasma frequency of Ta:TiO_2 with 5% or 10% of Ta in mass belongs to the IR range (≈4100 nm), an interpolation of the data related to Ta:TiO_2 in a range of wavelengths between 370 nm and 1700 nm could represent a limitation for the accuracy of the interpolation.

3.2.1. Final remarks

To summarize, during this master thesis work it has been verified that is possible to obtain crystalline, or partially crystalline, tantalum doped titanium oxide thin films directly during deposition, increasing the substrate temperature at values around 350 °C. The possibility of reaching a complete crystalline structure instead of a partial one seems to be related to the content of the doping agent. Indeed, it has been noticed that, for a constant substrate temperature, the larger is the content of tantalum the higher is the crystallinity of the film. In addition, it has been verified that for a content of Ta of 5% in mass, the deposition at around 350 °C promotes the obtainment of a crystalline structure in which the anatase and rutile phase coexist.

Considering the optical properties of tantalum doped titanium oxide films, it has been noticed that an increase in the substrate temperature caused an increase in the real part of the dielectric function and a decrease in the imaginary, obtaining a film with a better dielectric behaviour. However, this variation could be not the related to the substrate temperature, but to the model used for the interpolation of the data.

In conclusion, the substrate temperature, the content of doping agent are surely parameters that can control the process of crystallization of tantalum doped titanium oxide films. Regarding the optical properties, the substrate temperature seems to affect positively the dielectric function, but this effect needs to be investigated more precisely to exclude the errors related to the model adopted for the interpolation of the data.

4 Ta:TiO_2/TiN multilayers

After the deposition and characterization of the reference samples, two sets of multilayered structures have been developed and analysed to investigate the effect of the substrate temperature and of the geometry on the morphology and on the optical properties of the multilayers.

The first set is composed of multilayer structures in which the dielectric part consists of tantalum doped titanium oxide with a content of Ta equal to 5% in mass, while for the metallic component, titanium nitride deposited in high vacuum has been selected. The multilayers have been deposited at different substrate temperatures (at room temperature and around 350°C) to investigate the effects on the morphology and on the optical properties of the structures. The thickness of the layers deposited has been maintained constant and equal to 20 nm, while the number of layers has been set to 10 and 11 also changing the order of deposition of the layers.

For the second set it has been decided to adopt a different approach for the development of the multilayered structure. Firstly, several simulations based on the effective medium, described in Chapter 1, have been performed to define the best configurations in terms of materials and geometry that can guarantee the widest range of wavelengths in which the multilayered structures assume a hyperbolic behaviour. The data used for the simulations are the ones obtained through the characterization of the reference samples. According to the simulations carried out, the materials selected for the development of the multilayered structures are Ta:TiO_2 with 10% of tantalum in mass for the dielectric, and TiN deposited in low vacuum (0.1 Pa) and high vacuum (10^{-3} Pa) for the metal part. Ta:TiO_2 has been selected because it behaves as dielectric material in the range of wavelengths investigated during this project (visible and NIR). For what concerns the geometry of the structure, it has been noticed that the largest range of hyperbolicity is achievable with multilayers that have the metallic part thicker than the dielectric one. In particular, two different configurations for each metallic material have been deposited, in which the metallic part is characterized by a thickness of 30 nm and 20 nm and the dielectric part is characterized by a thickness of 20 nm and 10 nm, respectively. The number of layers deposited has been maintained constant and equal to 11, in which the dielectric part constitutes the first and the last layer produced. This type of configuration has been adopted in order to put directly in contact with the external environment the less reactive component to avoid modifications of the properties of the multilayered structures. All the structures belonging to the second set have been deposited with the substrate heater switched on and set at a nominal temperature of 500°C (the effective temperature is around 350°C) to focus the attention on the effects of the geometry on the morphology and on the optical properties of the samples produced.

Both for the first and second set, the dielectric part has been deposited in presence of 1 Pa of oxygen to guarantee the growth of a more conductive oxide. This choice has been made in order to guarantee the obtainment of a Ta:TiO_2 that behaves as a metal in the infrared range and so, in combination with a double-epsilon-near-zero metal (titanium oxynitride), could lead to the development of a HMMs that is capable to show a hyperbolic behaviour also in the infrared range.

After the deposition, an annealing process in vacuum at around 500°C has been performed on all the samples produced to investigate the effects of the thermal treatment on the morphology and on the optical properties of the samples.

In conclusion, in this chapter are presented all the samples deposited and the all the results obtained during the characterization of the structures produced.

4.1. Ta:TiO_2/TiN multilayers (Ta:TiO_2 with 5% of Ta)

In this section, a description of the principal properties of Ta:TiO_2/TiN multilayers (Ta:TiO_2 with 5% of Ta in mass) is presented. The multilayered structures have been obtained by means of pulsed laser deposition, with the targets configuration described in Section 2.1. The metallic part consists of titanium nitride deposited in high vacuum (10^{-3} Pa), while the dielectric component is tantalum doped titanium oxide with a content of Ta equal to 5% in mass and deposited in presence of 1 Pa of oxygen.

The deposition parameters that have not been changed during the fabrication process are listed below:

- Target: TiN (99% pure with a dimeter of 1 inches) mounted on a target of Ta:TiO_2 (5% of Ta in mass and with a diameter of 2 inches)
- Substrate: silicon wafer (110 crystal plane)
- Target to substrate distance: 5 cm.
- Laser: pulsed green laser (532nm) with a frequency of 10 Hz.
- Laser fluence: 2 J/cm^2 for Ta:TiO_2 layers and 3.5 J/cm^2 for TiN layers.

All the multilayered structures described in this section are listed in Table 4.1 with their relative geometries and deposition parameters.

Structure	Geometry	t_{layer} (nm)	t_{tot} (nm)	T_{sub} (°C)
Ta:TiO_2 / TiN	10 layers	20	200	25
TiN / Ta:TiO_2	10 layers	20	200	25
Ta:TiO_2 / TiN	11 layers	20	220	350
TiN / Ta:TiO_2	11 layers	20	220	350

Table 4.1 List of multilayers deposited with their relative deposition parameters.

The order of the layer is presented in the first column of Table 4.1, starting with the first layer deposited directly in contact with the silicon substrate. The number of layers has been changed from 10 to 11 to investigate the effect of having an odd number of layers instead of an even one.

After the deposition, an annealing process in vacuum at around 500°C has been performed on all the samples produced.

A visual inspection analysis performed by means of scanning electron microscopy (SEM) has been necessary to investigate the morphology of the multilayers deposited.

A typical cross-section image of a multilayer is presented in Figure 4.1, where it is possible to notice the presence of several layers that constitute the final multilayered structure.

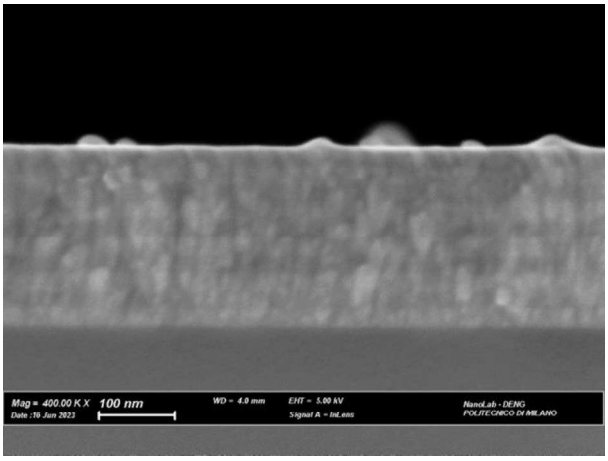

Figure 4.1 Example of cross-section image of a multilayered structure (11 layers TiN / Ta:TiO_2 T=350°C).

Through SEM it has been possible to confirm the deposition of a compact and adherent multilayered structure with thicknesses around 200 nm and 220 nm. After the annealing, the samples have been analysed by means of scanning electron microscopy to investigate the effects of the treatment on their morphology. During this analysis, it has been possible to notice several detachments of the film from the silicon substrate only on the samples deposited at room temperature, as presented in Figure 4.2.

Figure 4.2 Example of detachment of the film present in the annealed samples deposited at room temperature.

It is possible to assume that the absence of detachments in the samples deposited at a nominal substrate temperature of 500°C could be related to a partial relaxation of the

internal stresses typically induced during the growth of the film caused by the higher deposition temperature. Considering the multilayered structure, the problems related to the development of residual internal stresses is more severe than in the case of a single layer due to the presence of many interfaces that intensifies the stresses induced during the deposition.

The influence of the substrate temperature on the crystallinity of the different single layers that form the multilayers has been analysed by means of Raman spectroscopy, providing the results presented in Figure 4.3.

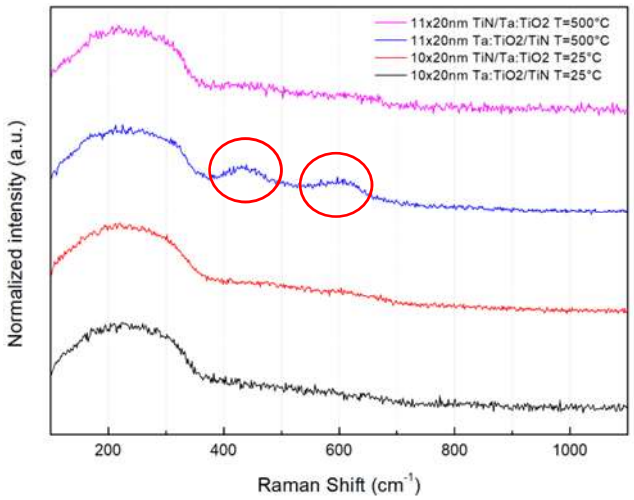

Figure 4.3 Raman spectra of different multilayers deposited at different substrate temperatures.

Analysing the results, it is possible to notice that the sample deposited at higher temperature and with Ta:TiO_2 as the last layer shows a slightly different Raman spectrum. In particular, two bands at around 400 cm^{-1} and 600 cm^{-1} are present. These signals could be related to the anatase phase of titanium oxide, indicating that a phenomenon of crystallization of the tantalum doped titanium oxide layers has already started during the deposition. The typical signal of Ta:TiO_2 present at around 150 cm^{-1} is probably covered by the broad acoustic band of TiN below 400 cm^{-1} that is related to the presence of nitrogen vacancies in the lattice of the metallic layers. Hence, it is possible to assume that a substrate temperature of 350°C is enough to promote the crystallization of the tantalum doped titanium oxide embedded as the dielectric component of a metal-dielectric multilayer. Due to the similar structure and deposition temperature, it is possible to assume that also in the case of the sample with titanium nitride as last layer a crystallization process of Ta:TiO_2 has already started during the deposition, but the signals are probably screened by the presence of 20 nm of titanium nitride above the last layer of tantalum doped titanium oxide.

After the thermal treatment, a Raman spectroscopy analysis has been performed to investigate the effect of the annealing the crystallinity and morphology of the samples deposited, obtaining the data presented in Figure 4.4. and 4.5.

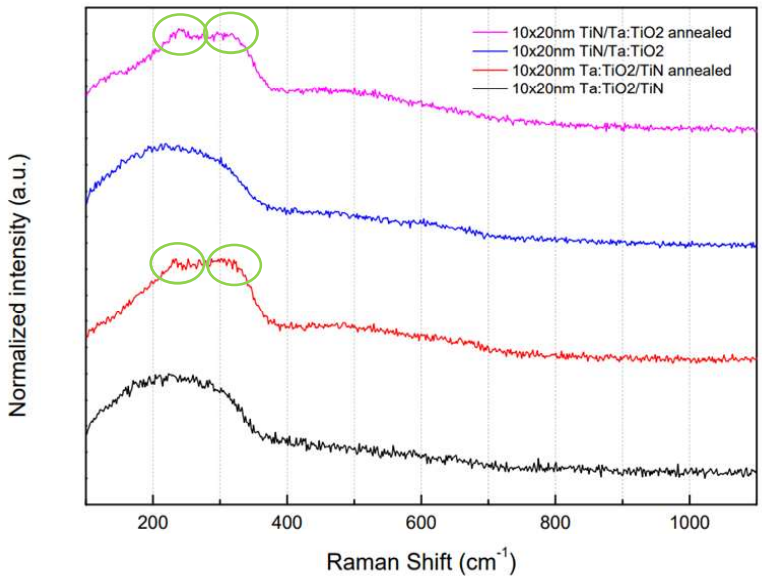

Figure 4.4 Effect of thermal treatment on multilayers deposited at room temperature.

After the annealing, the samples deposited at room temperature show an acoustic band below 400 cm^{-1} related to TiN nitrogen vacancies that is slightly blue-shifted with the respect to the as deposited ones. This is in accordance with the data found during the characterization of the reference samples and with the results of a previous work carried out by the Nanolab research group, meaning that a phenomenon of oxidation could has occurred during the thermal treatment [66]. In addition, it is possible to notice the beginning of a separation of the acoustic band in two bands (transversal at around 220 cm^{-1} and longitudinal at a 330 cm^{-1}) indicating the achievement of a more ordered structure of titanium nitride.

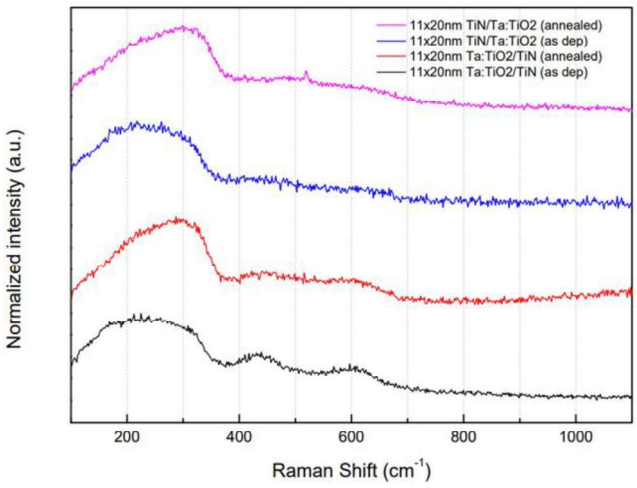

Figure 4.5 Effect of annealing on the Raman spectra of samples deposited at 350°C.

In Figure 4.5 are presented the Raman spectra of the samples deposited with the substrate heater switched on at 500°C before and after the thermal treatment. Also in this case, it is evident that the acoustic band related to the nitrogen vacancies of titanium nitride is blue shifted after the annealing whit the respect to the as deposited

samples and this could be related to a phenomenon of oxidation occurred during the annealing.

All the data related to the Raman analysis of the annealed samples have been collected and represented in Figure 4.6.

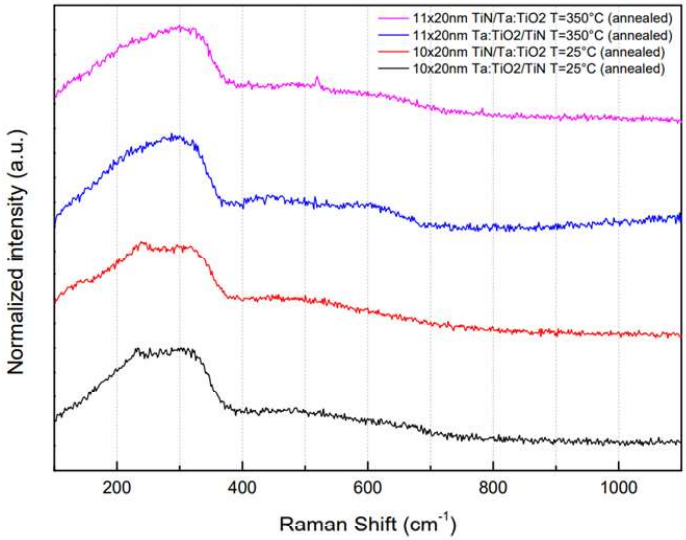

Figure 4.6 Raman spectra of annealed multilayers deposited at different temperatures.

Analysing all the results, it is evident that the shape of the acoustic band of titanium nitride below 400 cm^{-1} varies changing the temperature of deposition. In particular, the annealed samples deposited at room temperature show an acoustic band that is more similar to the typical one of TiN presented in Chapter 1 with the respect to the annealed samples deposited at 350°C. Indeed, the separation between the transversal and longitudinal acoustic band seems to be glimpsed.

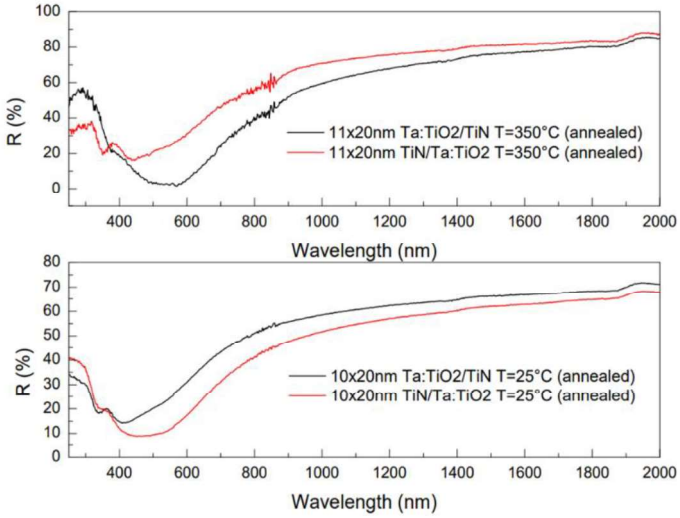

Figure 4.7 Reflectance curves of annealed multilayered structure deposited at different temperatures.

The optical properties of the multilayered structures have been investigated by means of UV-Vis-NIR spectroscopy, retrieving the values of reflectance represented in Figure 4.7.

Since the thermal treatment must be performed on the multilayered structure to promote the crystallization of tantalum doped titanium oxide, it has been decided to perform the analysis of the optical properties only on the annealed samples. From the results obtained, it is noticeable that the samples with the same last layer deposited (TiN or Ta:TiO_2) show similar reflectance curves. In particular, the bands related to phenomena of interference present below 400 nm are more evident in the case in which the last layer deposited is the tantalum doped titanium oxide. This is probably related to the greater contribution of the first metal-dielectric interface that is not screened by a highly reflecting layer, such as titanium nitride. As expected, the configuration that shows the highest reflectance is the one in which TiN is the last layer deposited. This configuration shows reflectance curves that are similar to the ones of the reference samples described in Chapter 3, but the values of wavelength at which the curves reach the minimum are different with the respect to the case of the reference sample. Indeed, for a single layer of TiN deposited in high vacuum (10^{-3} Pa) the position of the minimum is around 330 nm, while in a multilayered structure the position of the minimum shifts to values around 500 nm and 550 nm. This phenomenon is probably related to the implementation of TiN in multilayered structure in combination with Ta:TiO_2 that has completely different optical properties.

The hyperbolic behaviour of the multilayered structures deposited has been investigated by means of a Matlab code, developed by Professor A. De Luca from the University of Calabria, that is based on the effective medium theory described in Chapter 1. Through this code it is possible to derive the effective parallel and perpendicular component of the dielectric function, that can be used to define the range of wavelengths in which the material assumes a hyperbolic behaviour. Due to the detrimental problems related to the low adhesion of the multilayers deposited at room temperature, it has been decided to perform the simulation only for the samples deposited at 350°C, retrieving the results presented in Figure 4.8.

During the simulation it was not possible to consider the order of deposition of the layers and an even number of the layers, so it has been possible to perform the calculation only for the configurations with 10 layers of 20 nm.

Due to the configuration of a metal-dielectric multilayered structure, in principle the movement of free electrons is favoured on a direction that is parallel to the surface of the layers inside the metallic layers and forbidden in a perpendicular direction because they must pass through a dielectric material. For these reasons, it was reasonable to expect negative values for the real parallel component of the effective dielectric function and positive for the perpendicular one. As described, in Chapter 1, the material shows a hyperbolic behaviour when the two components represented in

Figure 4.8 have opposite sign. Hence, it can be asserted that theoretically a multilayered structure composed of TiN and Ta:TiO_2 a can be considered an hyperbolic metamaterial (HMM) in a range of wavelengths between 650 nm and 1700 nm. The range of validity of the simulation is limited by the range of wavelengths in which the data used for the calculation have been retrieved through ellipsometric measurements.

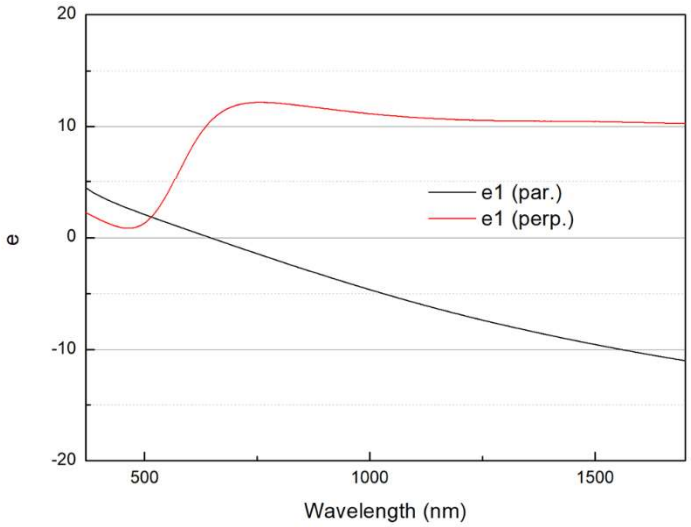

Figure 4.8 Representation of the theoretical real parallel and perpendicular components of the effective dielectric function of a multilayered structure deposited at 350°C after annealing.

4.1.1. Final remarks

Summarizing what has been just described in the previous section, different multilayered structures have been developed and characterized to investigate the effects of the deposition temperature and the order of the layers on the morphology and on the optical properties of the samples produced.

Starting from the morphology, it has been noticed that the deposition of multilayers at substrate temperatures around 350°C can favour the partial relaxation of the residual internal stresses induced during the growth of the structure, avoiding the development of detachment of the films from the substrate afterwards the necessary thermal treatment. In addition, it has been found that a substrate temperature of 350°C is enough to promote the crystallization of the 20 nm layer of tantalum doped titanium oxide, confirming the results obtained during the characterization of the reference samples of Ta:TiO_2.

Considering the optical properties, the order of the layers can affect the shape of the reflectance curves of the multilayered structures. In particular, the samples that have Ta:TiO_2 as the last layer show more evident band of interference, below 400 nm. While, in the case of samples that have TiN as the last layer, the reflectance curves are similar in shape to the ones of the single layers reference samples described in Chapter 3.

Analysing the position of the minimum of reflectance, it is noticeable that this point has shifted towards larger wavelengths with the respect to the single layer case. This effect cannot directly imply a variation of a plasma frequency of the structure because the multilayers is composed of several layers of different materials that have completely different optical behaviour in the visible and NIR range.

Finally, a simulation based on the effective medium theory has been performed to determine the range of wavelengths in which the material assumes a hyperbolic behaviour, obtaining that a multilayered structure composed of Ta:TiO_2 and TiN with 11 layers of 20 nm can be considered a hyperbolic metamaterial in the visible and NIR range, in particular between 650 nm and 1700 nm.

4.2. Ta:TiO_2/TiN multilayers (Ta:TiO_2 with 10% of Ta)

The first set of multilayers has been developed and deposited to explore the feasibility of depositing multilayered structure composed of Ta:TiO_2 and TiN. Hence, the strategy adopted for the deposition of the second set of multilayers has been changed with the respect to the one described in Section 4.1. Now, the first step for the development of multilayered structures consists in performing several simulations based on the effective medium theory, using the data presented in Chapter 3, to determine the material combinations and geometry of the structure that can guarantee the widest range of wavelengths in which the multilayer shows a hyperbolic behaviour. Regarding the possible material combinations, I decided to select for the metallic component the compounds that during the characterization of the reference samples have shown the strongest metallic behaviour. The materials selected are listed in Table 4.2.

Target	Atmosphere	Pressure (Pa)	T_{sub} (°C)	Fluence (J/cm²)
TiN	Vacuum	$1.29*10^{-3}$	350	3.5
TiN	Vacuum	0.1	350	6.5

Table 4.2 List of titanium nitride selected for the simulation of the hyperbolic behaviour.

While the materials selected for the dielectric component of the multilayered structure are presented in Table 4.3.

Target	Content Ta (%)	Atmosphere	Pressure (Pa)	T_{sub} (°C)	Fluence (J/cm²)
Ta:TiO_2	5	O_2	1	350	2
Ta:TiO_2	10	O_2	1	350	2

Table 4.3 List of tantalum doped titanium oxide selected for the simulation of the hyperbolic behaviour.

Considering the geometry of the structures, all the possibilities investigated during the simulations are listed in Table 4.4.

Structure	Content Ta (%)	Geometry	Atmosphere	Pressure (Pa)
Ta:TiO_2/TiN	5	20 nm + 20 nm	O_2 / vacuum	1 / 10^{-3}
Ta:TiO_2/TiN	5	10 nm + 20 nm	O_2 / vacuum	1 / 10^{-3}
Ta:TiO_2/TiN	5	20 nm + 30 nm	O_2 / vacuum	1 / 10^{-3}
Ta:TiO_2/TiN	5	20 nm + 10 nm	O_2 / vacuum	1 / 10^{-3}
Ta:TiO_2/TiN	5	30 nm + 20 nm	O_2 / vacuum	1 / 10^{-3}
Ta:TiO_2/TiN	5	20 nm + 20 nm	O_2 / vacuum	1 / 0.1
Ta:TiO_2/TiN	5	10 nm + 20 nm	O_2 / vacuum	1 / 0.1
Ta:TiO_2/TiN	5	20 nm + 30 nm	O_2 / vacuum	1 / 0.1
Ta:TiO_2/TiN	5	20 nm + 10 nm	O_2 / vacuum	1 / 0.1
Ta:TiO_2/TiN	5	30 nm + 20 nm	O_2 / vacuum	1 / 0.1
Ta:TiO_2/TiN	10	20 nm + 20 nm	O_2 / vacuum	1 / 10^{-3}
Ta:TiO_2/TiN	10	10 nm + 20 nm	O_2 / vacuum	1 / 10^{-3}
Ta:TiO_2/TiN	10	20 nm + 30 nm	O_2 / vacuum	1 / 10^{-3}
Ta:TiO_2/TiN	10	20 nm + 10 nm	O_2 / vacuum	1 / 10^{-3}
Ta:TiO_2/TiN	10	30 nm + 20 nm	O_2 / vacuum	1 / 10^{-3}
Ta:TiO_2/TiN	10	20 nm + 20 nm	O_2 / vacuum	1 / 0.1
Ta:TiO_2/TiN	10	10 nm + 20 nm	O_2 / vacuum	1 / 0.1
Ta:TiO_2/TiN	10	20 nm + 30 nm	O_2 / vacuum	1 / 0.1
Ta:TiO_2/TiN	10	20 nm + 10 nm	O_2 / vacuum	1 / 0.1
Ta:TiO_2/TiN	10	30 nm + 20 nm	O_2 / vacuum	1 / 0.1

Table 4.4 List of all the possible configurations investigated during the simulations.

After the simulations, it has been possible to derive the range of wavelengths in which the material assumes a hyperbolic behaviour. The best structures are presented in Table 4.5

The configurations that show a wider range of hyperbolicity are highlighted in Table 4.5. It is evident that these geometries are characterized by a thickness of TiN is larger than the one of Ta:TiO_2. Due to the duration of the cooling process, it was possible to deposit only 4 multilayered structures. Hence, since it has been proved that the Ta:TiO_2, with 10% in mass of tantalum, crystallizes better that Ta:TiO_2 with 5% of Ta in mass during the deposition process carried out at 350°C, it has been decided to fabricate four multilayered structures with this type of material for the dielectric component.

Structure	Content Ta (%)	Geometry	Atmosphere	Pressure (Pa)	λ (nm)
Ta:TiO_2/TiN	5	10 nm + 20 nm	O_2 / vacuum	1 / 10^{-3}	630-1700
Ta:TiO_2/TiN	5	20 nm + 30 nm	O_2 / vacuum	1 / 10^{-3}	580-1700
Ta:TiO_2/TiN	5	10 nm + 20 nm	O_2 / vacuum	1 / 0.1	540-1700
Ta:TiO_2/TiN	5	20 nm + 30 nm	O_2 / vacuum	1 / 0.1	560-1700
Ta:TiO_2/TiN	10	10 nm + 20 nm	O_2 / vacuum	1 / 10^{-3}	590-1700
Ta:TiO_2/TiN	10	20 nm + 30 nm	O_2 / vacuum	1 / 10^{-3}	570-1700
Ta:TiO_2/TiN	10	10 nm + 20 nm	O_2 / vacuum	1 / 0.1	550-1700
Ta:TiO_2/TiN	10	20 nm + 30 nm	O_2 / vacuum	1 / 0.1	570-1700

Table 4.5 Best structures according to the simulations performed.

The configurations that show a wider range of hyperbolicity are highlighted in Table 4.5. It is evident that these geometries are characterized by a thickness of TiN is larger than the one of Ta:TiO_2. Due to the duration of the cooling process, it was possible to deposit only 4 multilayered structures. Hence, since it has been proved that the Ta:TiO_2, with 10% in mass of tantalum, crystallizes better than Ta:TiO_2 with 5% of Ta in mass during the deposition process carried out at 350°C, it has been decided to fabricate four multilayered structures with this type of material for the dielectric component.

The results obtained during the simulations for the selected geometries are presented in Figure 4.9 and 4.10.

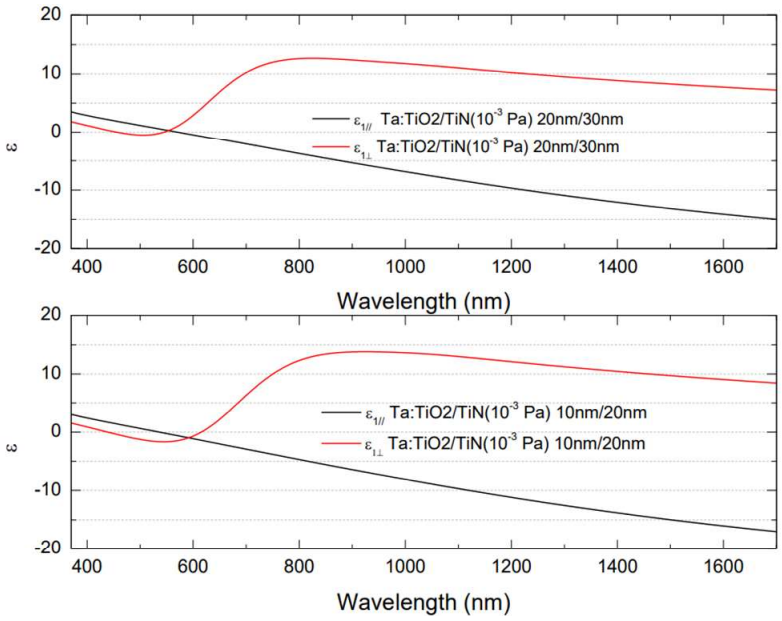

Figure 4.9 Representation of the theoretical real part of the effective dielectric function for multilayered structure in which TiN has been deposited in high vacuum.

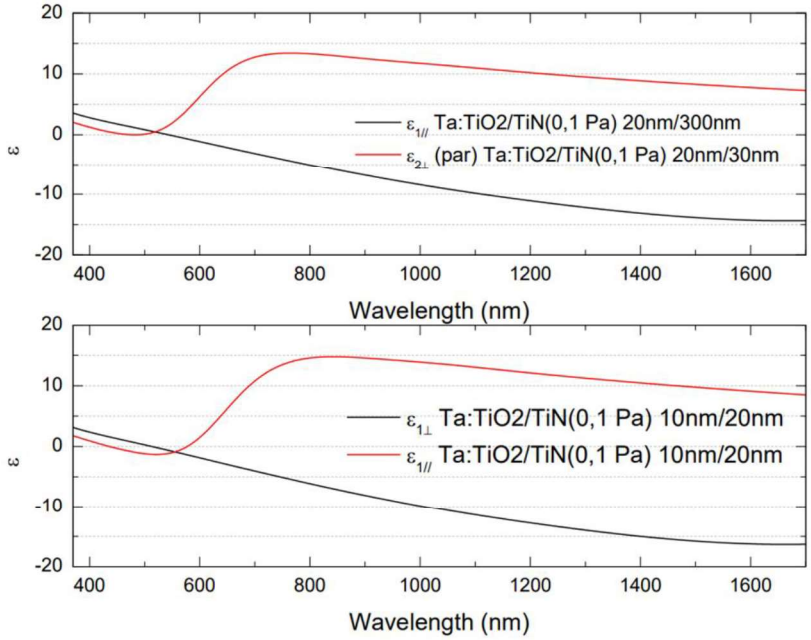

Figure 4.10 Representation of the theoretical real part of the effective dielectric function for multilayered structure in which TiN has been deposited in low vacuum.

The configurations that have been deposited during this master thesis project are presented in Table 4.6.

Structure	Content Ta (%)	Geometry	Atmosphere	Pressure (Pa)	Number layers
Ta:TiO_2/TiN	10	10 nm + 20 nm	O_2 / vacuum	1 / 10^{-3}	11
Ta:TiO_2/TiN	10	20 nm + 30 nm	O_2 / vacuum	1 / 10^{-3}	11
Ta:TiO_2/TiN	10	10 nm + 20 nm	O_2 / vacuum	1 / 0.1	11
Ta:TiO_2/TiN	10	20 nm + 30 nm	O_2 / vacuum	1 / 0.1	11

Table 4.6 List of multilayered structures deposited.

After the deposition, a thermal treatment in vacuum at around 500°C has been performed on all the samples produced to investigate the effect of the annealing on the morphology and on the optical properties of the multilayered structure.

A visual inspection through scanning electron microscopy (SEM) has been conducted, confirming the obtainment of compact and adherend multilayered structures with the desired total thickness. (Figure 4.11)

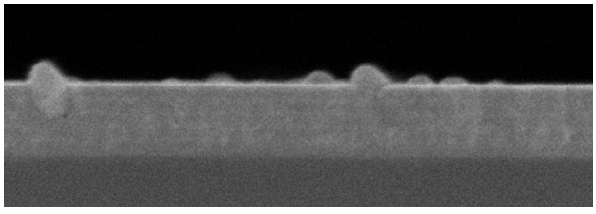

Figure 4.11 Example of cross-section image of a multilayered structure deposited at 350°C (Ta:TiO_2/TiN (10^{-3}Pa) 20nm/30nm).

In Figure 4.11 it is possible to notice the different layers that form the final multilayered structure.

After the thermal treatment, no modifications of the film have been detected by means of scanning electron microscopy (Figure 4.12). In addition, no detachment has been encountered during the visual inspection analysis, confirming the positive effect of the substrate heater related to the promotion of the relaxation of the residual internal stresses induced during the deposition.

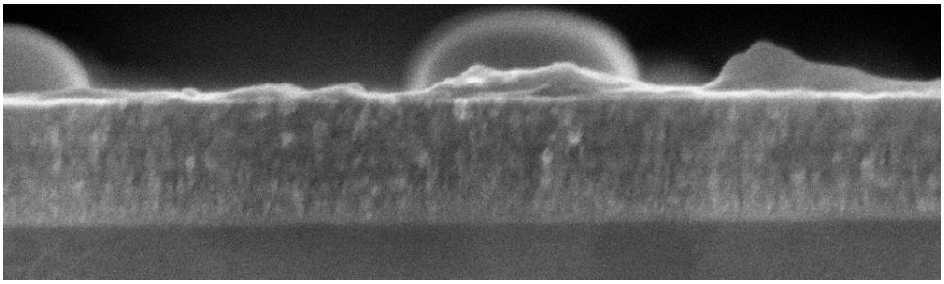

Figure 4.12 Example of cross-section image of an annealed multilayered structure deposited at 350°C. (annealed Ta:TiO_2/TiN (10^{-3}Pa) 20nm/30nm)

The crystallinity of the layers that compose the multilayered structure has been analysed by means of Raman spectroscopy, obtaining the results presented in Figure 4.13

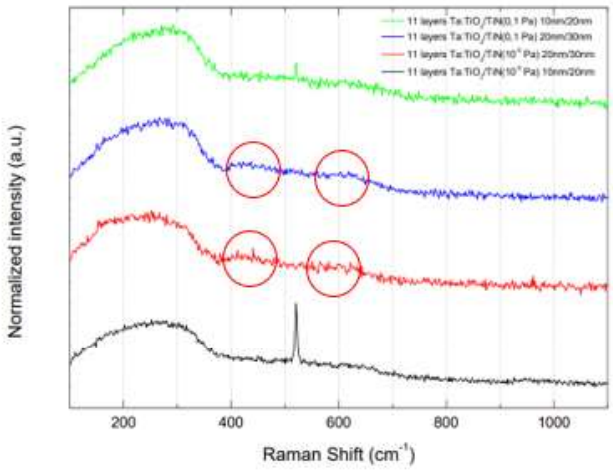

Figure 13 Raman spectra of different multilayers deposited at 350°C

Figure 4.13 Raman spectra of different multilayers deposited at 350°C

Observing the results, it is possible to notice two weak signals around 400 $cm^{-1}$and around 600 cm^{-1} on the samples characterized by larger thicknesses. The signals could be associated with the characteristic ones of the anatase phase of titanium oxide (B_{1g} at 400 cm^{-1} and E_g at around 600 cm^{-1}), indicating that a process of crystallization of the last layer of Ta:TiO_2 has occurred during the deposition. In addition, the acoustic band below 400 cm^{-1} of the samples in which titanium nitride has been deposited in low vacuum (0.1 Pa) is slightly blue-shifted with the respect to the case in which TiN has

been deposited in high vacuum (10^{-3} Pa). This variation has been noticed for the first time during the characterization of the multilayered structure. Indeed, as presented in Chapter 3, during the characterization of the reference, no differences have been detected in these signals changing the deposition pressure. Hence, it is possible to assume that the implementation of titanium nitride in metal-dielectric multilayered structure can change the influence that the deposition pressure has on the Raman spectra of titanium nitride films.

After the annealing, a Raman spectroscopy analysis has been performed to investigate the effect of the treatment on the morphology and on the crystallinity of the layers that form the multilayered structures, retrieving the data presented in Figure 4.14 and 4.15.

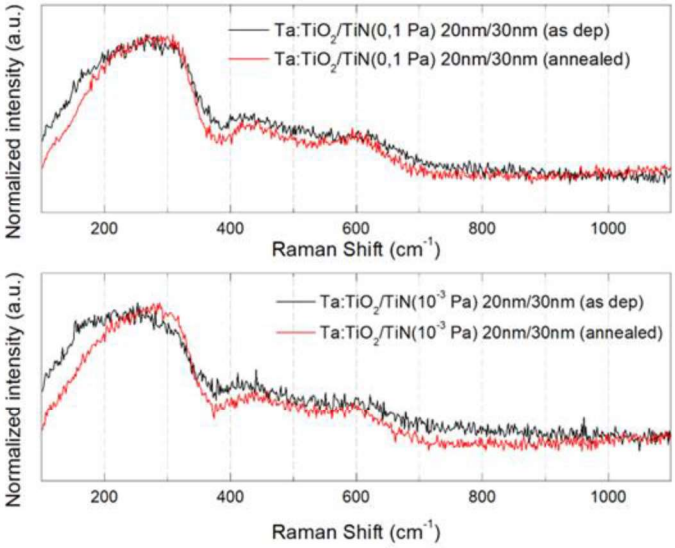

Figure 4.14 Raman spectra of samples deposited with different pressures before and after the annealing.

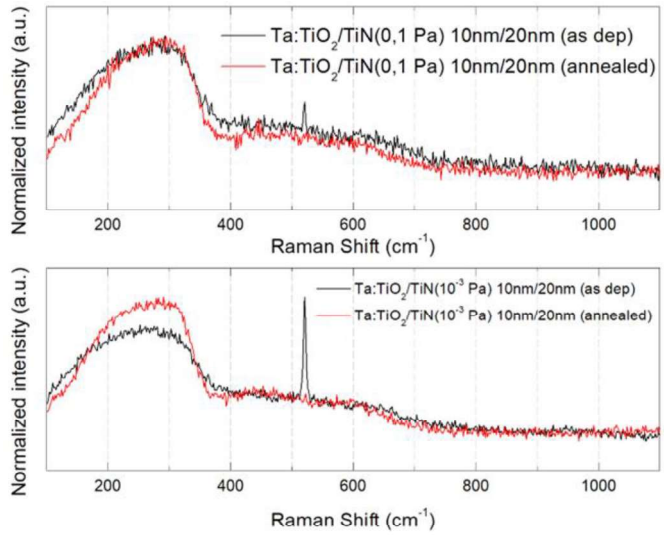

Figure 4.15 Raman spectra of samples deposited with different pressures before and after the annealing.

Looking at the results, it is observable that the shape of the acoustic band below 400 cm^{-1} is practically the same after the annealing, instead of the case of the as deposited samples in which the shape of this signal has been found to be influenced by the deposition pressure and by the thicknesses of the layers. After the thermal treatment, is possible to notice a better signal-to-noise ratio, meaning that layers are characterized by a more ordered and crystalline structure. In addition, it is possible to notice that a strong peak at around 520 cm^{-1} is present in the as deposited samples. This signal could be associated to the characteristic peak of silicon that composes the substrate of the multilayers. The measurements have been performed in three different point of the multilayers and in all the results the peak related to Si is present. After the treatment the signal disappears, this is probably related to a change in the microstructure of the layers that modified the contribution of silicon to the Raman spectra.

The optical properties of the multilayered structures have been investigated by means of UV-Vis-NIR spectroscopy, obtaining the values of reflectance presented in Figure 4.16.

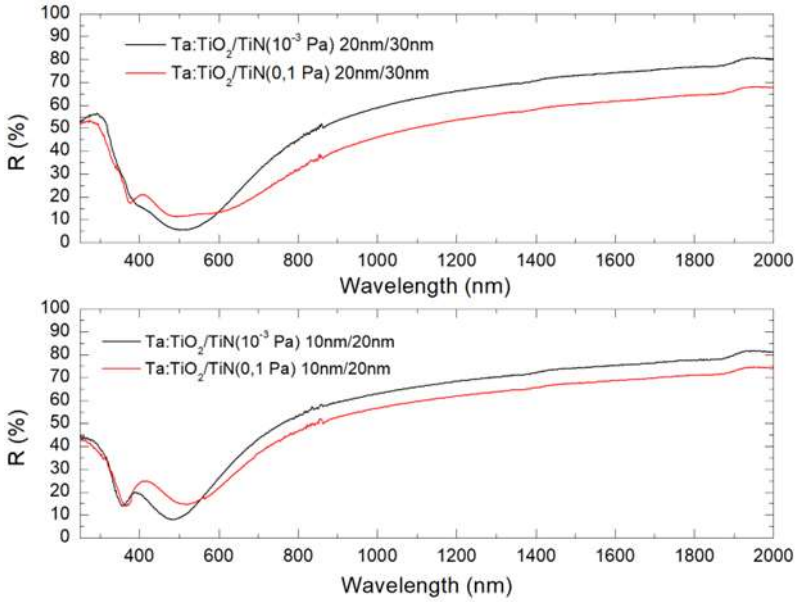

Figure 4.16 Reflectance curves for different multilayers deposited at 350°C.

Analysing the results, it is possible to notice that the bands of interference are more evident in the case of the samples with the lowest thicknesses.

Considering the position of the minimum of reflectance, from which is possible to derive some information about the plasma frequency of the material, it is evident that in the case of the sample in which TiN has been deposited at 10^{-3} Pa the position of the minimum seems to be influenced by the thickness of the layers. Indeed, increasing the thickness of the layers the position of the minimum moves towards larger values of wavelengths, meaning is possible to assert that the optical properties of a multilayered structure are affected by the thickness of the layers deposited. In addition, for large wavelengths it is observed that the multilayers in which the TiN has been deposited

at 0.1 Pa show lower values of reflectance, confirming the results obtained during the characterisation of the single layer reference samples. The values of reflectance reached by the multilayers at high wavelengths are smaller than the ones reached by the single layer samples. This phenomenon can be related to the presence of a thin film of Ta:TiO_2 on the surface of TiN reducing its reflectivity.

The effects of the thermal treatment on the values of reflectance of the multilayers deposited are presented in Figure 4.17 and 4.18.

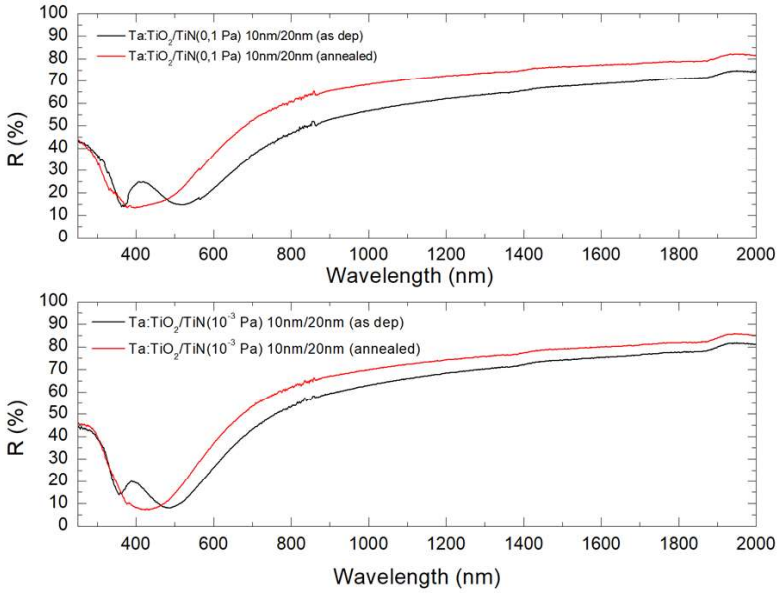

Figure 4.17 Representation of the effect of annealing on the reflectance curves of multilayers deposited at 350°C.

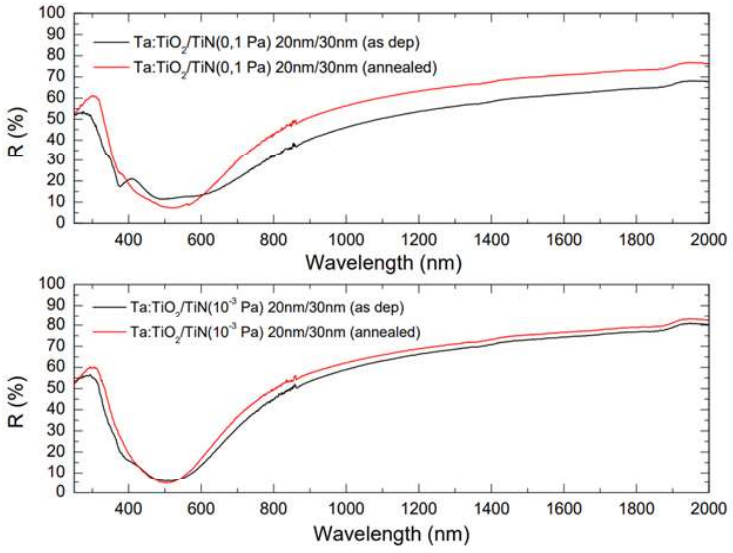

Figure 4.18 Representation of the effect of annealing on the reflectance curves of multilayers deposited at 350°C.

After the annealing, the bands related to phenomena of interference disappeared and the shape of the reflectance curves became very similar to the ones of the single layer

of titanium nitride, described in Chapter 3. This effect could be related to a process of crystallization of the superficial layer of Ta:TiO_2, that caused a variation of its refractive index changing the optical response of the multilayers. This effect can be observed for all the samples deposited independently on the geometry and on the deposition pressure of TiN. In addition, the values of reflectance for large wavelengths of every sample increased after the thermal treatment confirming the results obtained during the characterization of the single layer reference samples of titanium nitride. Moreover, it can be noticed that the increase in reflectance is larger if TiN has been deposited at 0.1 Pa than in the case of a deposition in high vacuum at around 10^{-3} Pa.

To investigate the effect of the implementation of TiN in a metal-dielectric multilayer on its optical properties, a comparison between the reflectance curves of the multilayered structure and the ones of the single layers reference samples has been performed, providing the results presented in Figure 4.19.

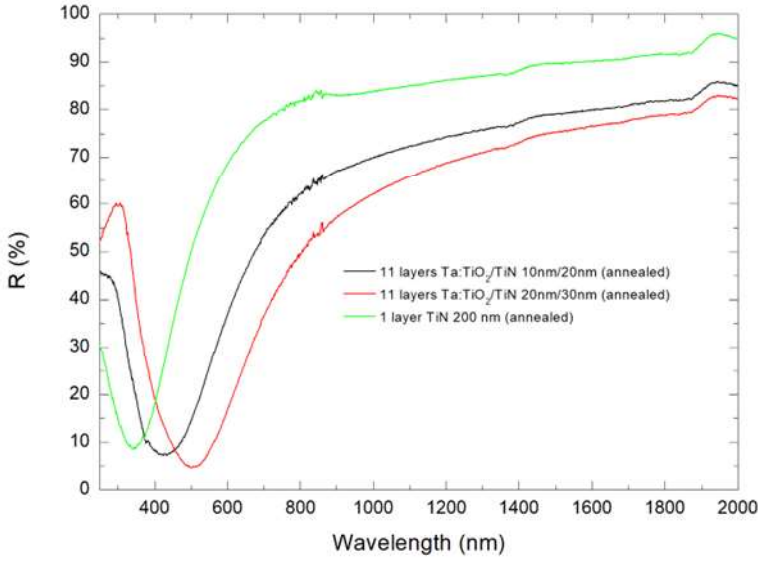

Figure 4.19 Comparison between reflectance curves of multilayers and a single layer of titanium nitride.

Since the annealing has been performed only on the reference sample deposited in high vacuum, the comparison has been executed only using the data retrieved by the characterization of the samples deposited at pressures around 10^{-3} Pa, maintaining constant the deposition temperature (T=350°C). Observing the results of the comparison, it is evident that the minimum of reflectance is significantly influenced by the geometry of the structure and the values of reflectance for large wavelengths decreases, as expected, increasing the thickness of the superficial layer of Ta:TiO_2.

To analyse the effects of the geometry on the optical properties of the multilayers, it has been necessary to carry out different simulations using a Matlab code, developed by Professor F. Scotognella from "Politecnico di Torino", based on the transfer matrix method, permitting the obtainment of reflectance values starting from the optical

properties of the single layers (the refractive index n and the absorption coefficient k). The results retrieved during these simulations are presented in Figure 4.20 and 4.21.

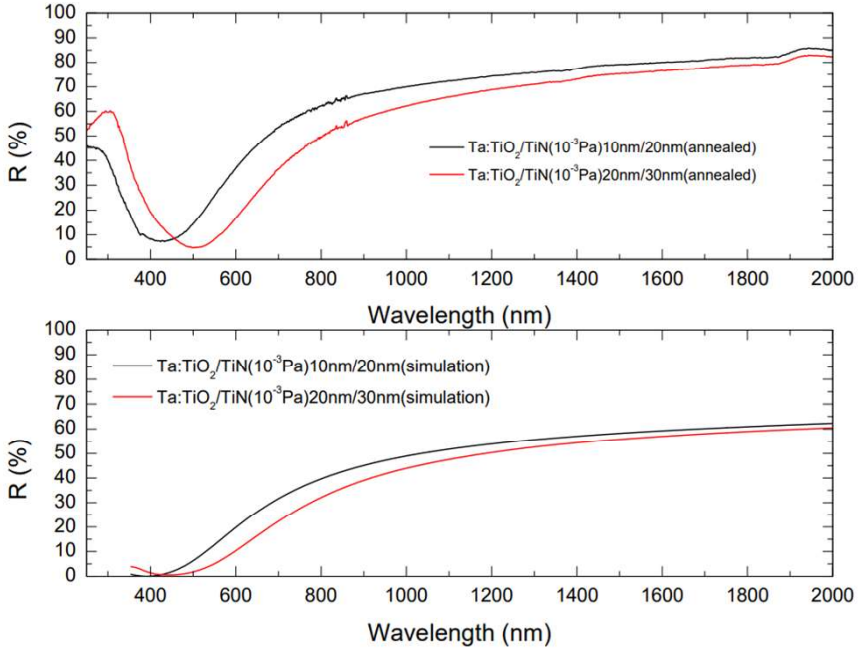

Figure 4.20 Representation of the theoretical and experimental values of reflectance for multilayers deposited at 350°C.

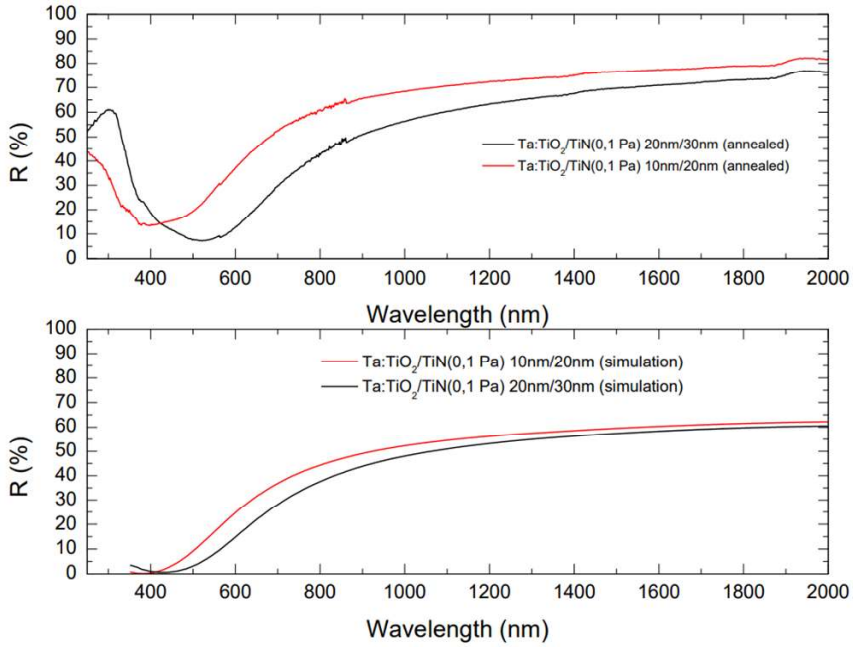

Figure 4.21 Representation of the theoretical and experimental values of reflectance for multilayers deposited at 350°C.

Studying the results retrieved during the simulations, a trend of the values of reflectance with the respect to the thickness of the layers can be detected. Indeed, increasing the thickness of the layers the position of the minimum of reflectance shifts towards larger values of wavelengths. In addition, for high wavelengths, an increase

in the thickness of the layers is related to a decrease in the values of reflectance. This last effect can be simply explained by the presence of a thicker layer of Ta:TiO_2 that reduces the reflectivity of the multilayered structure.

Looking at the results obtained experimentally by means of UV-Vis-NIR spectroscopy, it is possible to assert that the trend theoretically defined has been respected also by the experimental results, confirming the possibility to tune the optical response of a multilayer controlling its geometry. In addition, it is noticeable that the trend has been respected only qualitatively and not quantitatively, and this could be related to the approximation made by the model used for the simulation.

4.2.1. Final remarks

Executing several simulations by means of a suitable Matlab code, based on effective medium theory, it has been possible to identify the materials combinations and the geometries that can guarantee the widest range of wavelengths in which a multilayered material assumes a hyperbolic behaviour. The data obtained show that the best geometries are the ones in which the metallic component is thicker than the dielectric one, independently on the type of dielectric selected. In this way it has been possible to select four geometries to deposit during this master thesis project that in principle can show a hyperbolic behaviour in a range of wavelengths between around 500nm and 1700 nm. The upper limit of this range is limited by the range of validity of the ellipsometric measurements, used to retrieve the data necessary for the simulations.

All the samples have been deposited at the same temperature (T=350°C) to focus the attention on the effects of the geometry on the optical properties of the multilayers.

A visual inspection analysis carried out by means of SEM has confirmed the positive effect of the substrate heater related to the relaxation of the residual internal stresses induced during the deposition that can cause the detachment of the film from the substrate afterwards an annealing process.

By means of Raman spectroscopy, it has been possible to observe that the multilayers with thicker layers present a superficial layer of Ta:TiO_2 already crystalline after the deposition at 350°C, confirming what have been found during the characterization of the single layers reference samples. After the thermal treatment, the crystalline structure of the superficial Ta:TiO_2 seems to be unchanged, meaning that it is possible to obtain a structure similar to an annealed one only by depositing the multilayers at 350°C. Due to the complexity of the structure, it is not possible to confirm that all the tantalum doped titanium oxide are already crystallized after the deposition, so a thermal treatment could be necessary to be sure that the crystallization occurs in every dielectric layer.

Considering the optical properties, it has been proved that the geometry of the structure and the deposition pressure of titanium nitride can influence the values of

reflectance of the multilayers. In particular, it has been noticed that reducing the deposition pressure of the metallic layers the values of reflectance for large wavelengths increase, while increasing the thickness of the layers these values of reflectance decrease. In addition, it has been found that the reflectivity of the multilayers is lower with the respect to the single layer reference samples of TiN probably due to the presence of a dielectric layer of Ta:TiO_2 on top of the multilayers. Since the metallic behaviour shown by Ta:TiO_2 in the infrared range, it is reasonable to expect a change in the optical properties of the multilayers in this range, but new measurements in the IR range are needed to investigate this possible phenomenon.

Finally, different simulations, by means of a suitable Matlab code based on transfer matrix theory, have been performed to define a relationship between the thickness of the layers and the optical properties of the multilayered structure. The results obtained consist of theoretical reflectance curves showing that increasing the thickness of the layers the position of the minimum of reflectance shifts towards larger wavelengths and the values of R at high wavelengths decrease. This theoretical trend has been confirmed by the experimental data obtained through UV-Vis-NIR spectroscopy confirming that the optical response of a multilayered structure can be modulated controlling its geometry.

5 Conclusions and future perspectives

During this master thesis project, multilayered structures composed of titanium nitride (TiN) and tantalum doped titanium oxide (Ta:TiO_2) have been developed and characterized with the objective of investigating their applicability in the field of plasmonics as hyperbolic metamaterials (HMMs) in the visible and near-infrared (NIR) range of wavelengths.

Titanium nitride (TiN) has been selected for the metal component of the multilayered structure because of its peculiar plasmonic properties, that allow to consider it as a promising material capable of substituting traditional plasmonic materials, such as noble metals. While for the dielectric component, tantalum doped titanium oxide has been selected because of its good compatibility with the metal part (TiN) without causing a depletion of the quality and optical properties of the final multilayers. Another reason of the selection of this type of material lies in the will of studying the effects related to the implementation of a doped semiconductor as a dielectric component of a possible hyperbolic metamaterial, that is something never investigated by the Nanolab research group. In addition, Ta:TiO_2 behaves as a metal in the infrared range, meaning that its combination with a metal that shows double-epsilon-near-zero behaviour, such as titanium oxynitride, for the development of HMMs could, in principle, lead to the obtainment of a hyperbolic behaviour in the IR range, where Ta:TiO_2 acts as the metal component.

All the samples produced during this work have been deposited on silicon and glass substrates by means of Pulsed Laser Deposition (PLD) and characterized using several experimental techniques, such as Scanning Electron Microscopy (SEM), Raman spectroscopy, Van der Pauw method (four probe), UV-Vis-NIR spectroscopy and ellipsometry.

Several geometries (changing the order and the thickness of the layers), different dielectric (with different content of the dopant agent) and metallic (changing the pressure of deposition) materials and different substrate temperatures (using a substrate heater) have been explored to establish their influence on the morphology and on the electrical, optical properties of the samples fabricated.

For the development of the multilayers, it has been necessary to deposit and characterize single layers of the different components.

Single layers of titanium nitride have been widely investigated during previous works carried out in the Nanolab laboratories by B. Bricchi [65], G. Baiardi [67] and S. Garattoni [83]. They have studied and defined the optimal conditions for the obtainment of a compact and adherent film of titanium nitride deposited at room temperature starting from a stochiometric target of TiN in vacuum or in presence of

background reducing atmosphere composed of nitrogen and hydrogen (N_2-H_2 95%-5% respectively in volume), with laser fluences that belong to the range between 2 and 6.5 J/cm^2. During this master thesis project, a substrate heater has been used during the deposition through PLD for the first time in the Nanolab laboratories. Hence, during this project the deposition parameters have been retrieved from previous work but changing the temperature of substrate to investigate its influence on the morphology, optical and electrical properties of TiN single layer films. Nine different reference samples of titanium nitride have been deposited at different substrate temperatures, in presence of different kinds of atmosphere (vacuum or N_2-H_2) and at different pressures with the aim of analysing the effects of these parameters on the main properties of the films. By means of scanning electron microscopy the morphology of the films deposited has been explored, confirming the obtainment of compact, columnar, and adherent films with thicknesses around 200 nm. On some samples, a thermal treatment in vacuum at around 500°C has been performed causing the detachment of the films deposited in presence of a reducing atmosphere, independently on the substrate temperature. The sub-stoichiometric nature of titanium nitride has been verified by means of Raman spectroscopy and EDXS analysis, highlighting the fact that a substrate temperature around 350°C is not enough to modify the stoichiometry of the compound. Considering the optical properties, it has been noticed that the position of the minimum of reflectance, that is associated with the plasma frequency, has not been influenced by the temperature of the substrate, while for larger wavelengths it has been observed that the values of reflectance, which are linked to the metallicity of the compound, increase with the substrate temperature. Hence, it is possible to assert that an increase in the deposition temperature can cause the obtainment of a titanium nitride film with a stronger metallic behaviour. In addition, an opposite effect on the metallicity has been found characteristic of the deposition pressure, in particular increasing the pressure the values of reflectance drop. Considering only the plasma frequency of the materials deposited in vacuum, it has been verified by means of reflectance measurements and ellipsometric measurements that this parameter seems not to be influenced by the degree of vacuum at which the reference samples have been produced. Indeed, the sample deposited in vacuum at 10^{-3} Pa has shown the same plasma frequency of the one deposited in vacuum at 0.1 and 0.4 Pa. Moreover, it has been verified that also the type of deposition atmosphere can influence the optical behaviour of TiN. Indeed, depositing a titanium nitride film in presence of a mixture of nitrogen and hydrogen leads to the obtainment of a material with a lower plasma frequency and lower values of reflectance, and so with a weaker metallic behaviour. This effect has been confirmed also by ellipsometric measurements performed on samples deposited in different conditions. Regarding the electrical properties of the reference samples, it is possible to notice an accordance with what have been discovered during the characterization of the optical properties, confirming the positive effect related to the adoption of substrate heater to control the metallicity of the titanium nitride films.

Thin films of Ta:TiO_2 have been deeply studied by B.Bricchi [40], [65], P. Mazzolini [32], C. Mancarella [69] and L. Ornago [68] at the Nanolab laboratories. They studied and defined the optimal deposition conditions to obtain a compact and adherent transparent conductive oxide. According to these previous studies, it has been decided to deposit the single layer films with a laser fluency equal to 2 J/cm^2 in presence of 1 Pa of oxygen to obtain a better conductivity of the oxide. In addition, after the deposition a thermal treatment in vacuum at around 500°C has been executed to promote the crystallization of the material. But, as for the titanium nitride, they had the possibility to deposit the samples only at room temperature, so during this project the effect of the substate temperature on the fabrication of Ta:TiO_2 has been investigated for the first time. Four different reference samples have been produced changing the content of the dopant agent (5% of Ta and 10% of Ta in mass) and the thickness of the layers deposited. Due to the duration of the cooling process after the deposition with the substrate heater switched on, it has not been possible to fabricate reference samples at room temperature. Hence, the data used for the comparison with the results obtained during this thesis have been retrieved from previous studies [69]. The visual inspection by means of scanning electron microscopy have confirmed the obtainment of compact and adherent films characterized by the desired thicknesses (200nm and 20nm). The crystallinity of the samples before and after the thermal treatment have been investigated through Raman spectroscopy. During this analysis, it has been observed that on the samples of 200 nm a process of crystallization has already started during the deposition at 350°C. In particular, it has been noted that the sample with the larger content of tantalum (10%) was characterized by a more ordered and crystalline structure with the respect to the sample with the same thickness, but lower content of Ta (5%). In addition, it has been verified that the crystalline structure of the sample with 10% of Ta and with a thickness of 200 nm has not been influenced by the thermal treatment performed after the deposition. This is an important result because it means that is possible to avoid the performing of an annealing process to obtain a crystalline film of Ta:TiO_2. Considering the sample with 5% of Ta, it has been observed that after the annealing the crystalline structure is more ordered, meaning that the treatment promoted the complete crystallization of the materials that was not able to be fulfilled during the deposition. Considering the optical properties of Ta:TiO_2, the dielectric nature of the material has been confirmed by the positive values of the real part of the dielectric function, obtained interpolating with a combination of Drude and Lorentz model the data retrieved during the ellipsometric measurements.

After the characterization of the single layer reference samples, two different sets of multilayered structures have been developed with the objective of studying the effects of the substrate temperature and of the geometry of the structure on the optical response of the multilayer.

For the first set, Ta:TiO_2 (5% of Ta) and TiN deposited in vacuum at 10^{-3} Pa have been chosen as component of the multilayered structures. Four different multilayers have

been deposited changing the deposition temperature and maintaining constant the thickness of the layers. The deposition conditions adopted for the fabrication of the different layers were the ones used for the deposition of the reference samples. After the deposition a thermal treatment has been performed on all the samples fabricated to promote the crystallization of Ta:TiO_2. Two multilayers have been deposited at room temperature and the remaining two at around 350°C changing the order of the layers on the structure. A visual inspection performed after the annealing by means of SEM, highlighted the development of detachment of the films from the silicon substrate only the samples deposited at room temperature, meaning that the deposition at around 350°C could favour the relaxation of the internal residual stresses induced during the deposition of the different layers. The detachments have been observed independently on the order of deposition of the layers. By means of Raman spectroscopy, it has been possible to observe that for the sample that presented Ta:TiO_2 as final layer signals that could be related to the anatase phase of TiO_2 were evident in its Raman spectrum, meaning that also in the case of a multilayered structure, a deposition temperature of 350°C is enough to promote the crystallization of Ta:TiO_2. Considering the optical properties of the multilayers, it has been possible to notice that the shape of the reflectance curves was similar to the ones observed for TiN, but with the minimum of reflectance shifted towards larger wavelengths and with lower values of reflectance with the respect to the single layer. This means that implementing TiN in a metal-dielectric multilayered structure can be considered a way to modulate its optical properties. The hyperbolic behaviour of these kinds of structures has been studied by means of simulations based on the effective medium theory. Since the problems of detachment could be detrimental for plasmonic applications, it has been decided to investigate the hyperbolicity only of the samples deposited at 350°C, obtaining that these materials can theoretically assume a hyperbolic behaviour for values of wavelengths larger than 650nm.

The strategy for the deposition of the second set of multilayers has been changed with the respect to the one described before. Firstly, several simulations based on the effective medium theory have been executed to compute the geometries and materials combinations that can guarantee the widest range of wavelengths in which the multilayers assume a hyperbolic behaviour. The results obtained show that the best geometries are the ones in which the metal is thicker than the dielectric independently on the type of metal and dielectric used for the simulation. Since it has been demonstrated that the crystallization of Ta:TiO_2 is easier when the content of Ta is equal to 10%, this material has been selected for the dielectric component. While for the metal one, the two most metallic TiN according to the characterization of the reference samples have been chosen (deposited in vacuum at 0.1 Pa and 10^{-3} Pa). In total, four different multilayers have been deposited at 350°C with different materials and geometries. The two geometries explored are 20 nm of metal with 10 nm of dielectric and 30 nm of metal with 20nm of dielectric. The number of layers has been

maintained constant and equal to 11. The even number of layers has been adopted to encapsulate the metallic layers with the dielectric ones exposing the materials less reactive with the external environment. Raman spectroscopy has been performed to analyse the crystallinity of the films, highlighting that the samples with the larger thicknesses of the layers (20nm/30nm) shew Raman signals that are typical of the anatase phase of TiO_2, meaning that the superficial of Ta:TiO_2 can be considered already partially crystalline after the deposition at 350°C. After the thermal treatment performed on all the samples in vacuum at 500°C, the Raman spectra of the multilayers became practically equal, meaning that the annealing can compensate the differences in morphology related to the different geometries. Considering the optical properties, it has been observed that in the as deposited samples some bands of interference were present, but they disappeared after the annealing process. This phenomenon could be related to a complete crystallization of the superficial layer of Ta:TiO_2 that caused a change in the refractive index in the material modifying the optical response of the multilayers. In addition it has been verified the effect of the deposition pressure on the optical properties of titanium nitride highlighted during the characterization of the reference samples. Indeed, increasing the pressure of deposition of the metallic layer the reflectance of the multilayer decreased. The position of the minimum of reflectance for the annealed sample can be considered dependent on the geometry, but independent on the materials combinations. In particular, increasing the thickness of the layers the position of the minimum shifted to larger wavelengths, meaning that the optical response of a multilayered structure composed of Ta:TiO_2 (10% of Ta) and TiN can be modulated controlling its geometry. Finally, different simulations based on the transfer matrix theory have been executed to define a theoretical relationship between the optical response of the multilayer and its geometry. The results obtained shew a trend, according to which larger are the thicknesses and lower is the plasma frequency and lower are the values of reflectance at large wavelengths. This trend has been respected by the experimental data retrieved by means of UV-Vis-NIR spectroscopy.

Considering the results obtained during this project, it is possible to think about possible future developments that are listed below:

- The possibility of developing a multilayered structure that shows a hyperbolic behaviour in the far-infrared rang exploiting the double-epsilon-near-zero behaviour characteristic of titanium nitride deposited in low vacuum and the metallic behaviour of tantalum doped titanium oxide.
- Ellipsometric measurements should be performed step-by-step after the deposition of each layer to obtain a more precise description of the hyperbolic behaviour of the multilayered structure, without the need for executing simulations based on the effective medium theory.

- The use of the substrate heater should be extended to other structures and materials to exploit the positive effects related to the increase in metallicity of the samples deposited and to the relaxation of the internal stresses induced during the deposition.
- Other geometries should be explored to have a more complete vision of its effects on the optical properties of multilayers.
- Lasty, specific techniques capable of assessing the hyperbolic behaviour of HMMs experimentally should be developed.

Bibliography

[1] S. A. Maier, *Plasmonics: Fundamentals and applications*. 2007. doi: 10.1007/0-387-37825-1.

[2] Y. Guo, Z. Xu, A. G. Curto, Y. J. Zeng, and D. Van Thourhout, "Plasmonic semiconductors: materials, tunability and applications," *Progress in Materials Science*, vol. 138. 2023. doi: 10.1016/j.pmatsci.2023.101158.

[3] W. P. Guo *et al.*, "Titanium Nitride Epitaxial Films as a Plasmonic Material Platform: Alternative to Gold," *ACS Photonics*, vol. 6, no. 8, 2019, doi: 10.1021/acsphotonics.9b00617.

[4] L. Ferrari, C. Wu, D. Lepage, X. Zhang, and Z. Liu, "Hyperbolic metamaterials and their applications," *Progress in Quantum Electronics*, vol. 40. 2015. doi: 10.1016/j.pquantelec.2014.10.001.

[5] J. Zhang, L. Zhang, and W. Xu, "Surface plasmon polaritons: Physics and applications," *Journal of Physics D: Applied Physics*, vol. 45, no. 11. 2012. doi: 10.1088/0022-3727/45/11/113001.

[6] S. Franzen, "Surface plasmon polaritons and screened plasma absorption in indium tin oxide compared to silver and gold," *Journal of Physical Chemistry C*, vol. 112, no. 15, 2008, doi: 10.1021/jp7097813.

[7] P. R. West, S. Ishii, G. V. Naik, N. K. Emani, V. M. Shalaev, and A. Boltasseva, "Searching for better plasmonic materials," *Laser and Photonics Reviews*, vol. 4, no. 6. 2010. doi: 10.1002/lpor.200900055.

[8] P. Patsalas and S. Logothetidis, "Optical, electronic, and transport properties of nanocrystalline titanium nitride thin films," *J Appl Phys*, vol. 90, no. 9, 2001, doi: 10.1063/1.1403677.

[9] G. V. Naik, J. L. Schroeder, X. Ni, A. V. Kildishev, T. D. Sands, and A. Boltasseva, "Titanium nitride as a plasmonic material for visible and near-infrared wavelengths," *Opt Mater Express*, vol. 2, no. 4, 2012, doi: 10.1364/ome.2.000478.

[10] E. Petryayeva and U. J. Krull, "Localized surface plasmon resonance: Nanostructures, bioassays and biosensing-A review," *Analytica Chimica Acta*, vol. 706, no. 1. 2011. doi: 10.1016/j.aca.2011.08.020.

[11] W. Lin, L. Bi, D. Liu, and K. Zhang, "Use of Debye's series to determine the optimal edge-effect terms for computing the extinction efficiencies of spheroids," *Opt Express*, vol. 25, no. 17, 2017, doi: 10.1364/oe.25.020298.

[12] Y. Chen and H. Ming, "Review of surface plasmon resonance and localized surface plasmon resonance sensor?," *Photonic Sensors*, vol. 2, no. 1. 2012. doi: 10.1007/s13320-011-0051-2.

[13] T. T. Nguyen, N. Van Sau, Q. M. Ngo, G. Eppe, N. Q. Tran, and N. T. P. Anh, "Enhanced sensitivity and detection of near-infrared refractive index sensor with plasmonic multilayers," *Sensors*, vol. 21, no. 21, 2021, doi: 10.3390/s21217056.

[14] G. Singh and S. S. Verma, "Plasmon enhanced light trapping in thin film GaAs solar cells by Al nanoparticle array," *Physics Letters, Section A: General, Atomic and Solid State Physics*, vol. 383, no. 13, 2019, doi: 10.1016/j.physleta.2019.02.008.

[15] X. Zhang, Y. L. Chen, R. S. Liu, and D. P. Tsai, "Plasmonic photocatalysis," *Reports on Progress in Physics*, vol. 76, no. 4, 2013, doi: 10.1088/0034-4885/76/4/046401.

[16] J. Theiss, P. Pavaskar, P. M. Echternach, R. E. Muller, and S. B. Cronin, "Plasmonic nanoparticle arrays with nanometer separation for high-performance SERS substrates," *Nano Lett*, vol. 10, no. 8, 2010, doi: 10.1021/nl904170g.

[17] J. B. Khurgin, "How to deal with the loss in plasmonics and metamaterials," *Nat Nanotechnol*, vol. 10, no. 1, 2015, doi: 10.1038/nnano.2014.310.

[18] I. Kriegel, F. Scotognella, and L. Manna, "Plasmonic doped semiconductor nanocrystals: Properties, fabrication, applications and perspectives," *Physics Reports*, vol. 674. 2017. doi: 10.1016/j.physrep.2017.01.003.

[19] P. Patsalas, N. Kalfagiannis, and S. Kassavetis, "Optical properties and plasmonic performance of titanium nitride," *Materials*, vol. 8, no. 6, 2015, doi: 10.3390/ma8063128.

[20] E. Budke, J. Krempel-Hesse, H. Maidhof, and H. Schüssler, "Decorative hard coatings with improved corrosion resistance," *Surf Coat Technol*, vol. 112, no. 1–3, 1999, doi: 10.1016/S0257-8972(98)00791-9.

[21] A. Trenczek-Zajac *et al.*, "Structural and electrical properties of magnetron sputtered Ti(ON) thin films: The case of TiN doped in situ with oxygen," *J Power Sources*, vol. 194, no. 1, 2009, doi: 10.1016/j.jpowsour.2008.12.112.

[22] C. Stampfl, W. Mannstadt, R. Asahi, and A. J. Freeman, "Electronic structure and physical properties of early transition metal mononitrides: Density-functional theory LDA, GGA, and screened-exchange LDA FLAPW calculations," *Phys Rev B Condens Matter Mater Phys*, vol. 63, no. 15, 2001, doi: 10.1103/PhysRevB.63.155106.

[23] P. Patsalas *et al.*, "Conductive nitrides: Growth principles, optical and electronic properties, and their perspectives in photonics and plasmonics," *Materials Science and Engineering R: Reports*, vol. 123. 2018. doi: 10.1016/j.mser.2017.11.001.

[24] Z. H. Ding, B. Yao, L. X. Qiu, and T. Q. Lv, "Raman scattering investigation of nanocrystalline δ-TiNx synthesized by solid-state reaction," *J Alloys Compd*, vol. 421, no. 1–2, 2006, doi: 10.1016/j.jallcom.2005.11.017.

[25] A. Perego *et al.*, "Hierarchical TiN Nanostructured Thin Film Electrode for Highly Stable PEM Fuel Cells," *ACS Appl Energy Mater*, vol. 2, no. 3, 2019, doi: 10.1021/acsaem.8b02030.

[26] D. Rasic, R. Sachan, M. F. Chisholm, J. Prater, and J. Narayan, "Room temperature growth of epitaxial titanium nitride films by pulsed laser deposition," *Cryst Growth Des*, vol. 17, no. 12, 2017, doi: 10.1021/acs.cgd.7b01278.

[27] W. Spengler, R. Kaiser, A. N. Christensen, and G. Müller-Vogt, "Raman scattering, superconductivity, and phonon density of states of stoichiometric and nonstoichiometric TiN," *Phys Rev B*, vol. 17, no. 3, 1978, doi: 10.1103/PhysRevB.17.1095.

[28] U. Guler, V. M. Shalaev, and A. Boltasseva, "Nanoparticle plasmonics: Going practical with transition metal nitrides," *Materials Today*, vol. 18, no. 4. 2015. doi: 10.1016/j.mattod.2014.10.039.

[29] J. Yu *et al.*, "Titanium Nitride Electron-Conductive Contact for Silicon Solar Cells by Radio Frequency Sputtering from a TiN Target," *ACS Appl Mater Interfaces*, vol. 12, no. 23, 2020, doi: 10.1021/acsami.0c04439.

[30] R. P. Sugavaneshwar, S. Ishii, T. D. Dao, A. Ohi, T. Nabatame, and T. Nagao, "Fabrication of Highly Metallic TiN Films by Pulsed Laser Deposition Method for Plasmonic Applications," *ACS Photonics*, vol. 5, no. 3, 2018, doi: 10.1021/acsphotonics.7b00942.

[31] P. D. C. King and T. D. Veal, "Conductivity in transparent oxide semiconductors," *Journal of Physics Condensed Matter*, vol. 23, no. 33. 2011. doi: 10.1088/0953-8984/23/33/334214.

[32] P. Mazzolini, P. Gondoni, V. Russo, D. Chrastina, C. S. Casari, and A. L. Bassi, "Tuning of electrical and optical properties of highly conducting and transparent Ta doped TiO2 polycrystalline films," *Journal of Physical Chemistry C*, vol. 119, no. 13, 2015, doi: 10.1021/jp5126156.

[33] T. Zhu and S. P. Gao, "The stability, electronic structure, and optical property of tio 2 polymorphs," *Journal of Physical Chemistry C*, vol. 118, no. 21, 2014, doi: 10.1021/jp412462m.

[34] M. S. Prévot and K. Sivula, "Photoelectrochemical tandem cells for solar water splitting," *Journal of Physical Chemistry C*, vol. 117, no. 35, 2013, doi: 10.1021/jp405291g.

[35] M. Shakeel Ahmad, A. K. Pandey, and N. Abd Rahim, "Advancements in the development of TiO2 photoanodes and its fabrication methods for dye sensitized solar cell (DSSC) applications. A review," *Renewable and Sustainable Energy Reviews*, vol. 77. 2017. doi: 10.1016/j.rser.2017.03.129.

[36] Y. Furubayashi *et al.*, "A transparent metal: Nb-doped anatase TiO2," *Appl Phys Lett*, vol. 86, no. 25, 2005, doi: 10.1063/1.1949728.

[37] T. Hitosugi *et al.*, "Fabrication of highly conductive Ti1-x Nbx O2 polycrystalline films on glass substrates via crystallization of amorphous phase grown by pulsed laser deposition," *Appl Phys Lett*, vol. 90, no. 21, 2007, doi: 10.1063/1.2742310.

[38] P. Mazzolini *et al.*, "Vibrational-Electrical Properties Relationship in Donor-Doped TiO2 by Raman Spectroscopy," *Journal of Physical Chemistry C*, vol. 120, no. 33, 2016, doi: 10.1021/acs.jpcc.6b05282.

[39] B. R. Bricchi *et al.*, "Integration of plasmonic Au nanoparticles in TiO2 hierarchical structures in a single-step pulsed laser co-deposition," *Mater Des*, vol. 156, 2018, doi: 10.1016/j.matdes.2018.06.051.

[40] B. R. Bricchi *et al.*, "Optical and electronic properties of transparent conducting Ta:TiO2thin and ultra-thin films: The effect of doping and thickness," *Mater Adv*, vol. 2, no. 21, 2021, doi: 10.1039/d1ma00584g.

[41] G. V. Naik, J. Liu, A. V. Kildishev, V. M. Shalaev, and A. Boltasseva, "Demonstration of Al:ZnO as a plasmonic component for near-infrared metamaterials," *Proc Natl Acad Sci U S A*, vol. 109, no. 23, 2012, doi: 10.1073/pnas.1121517109.

[42] M. Y. Abdelatty, M. M. Badr, and M. A. Swillam, "Compact silicon electro-optical modulator using hybrid ITO Tri-coupled waveguides," *Journal of Lightwave Technology*, vol. 36, no. 18, 2018, doi: 10.1109/JLT.2018.2863571.

[43] V. E. Babicheva, A. Boltasseva, and A. V. Lavrinenko, "Transparent conducting oxides for electro-optical plasmonic modulators," *Nanophotonics*, vol. 4, no. 1. 2015. doi: 10.1515/nanoph-2015-0004.

[44] A. Agrawal, R. W. Johns, and D. J. Milliron, "Control of Localized Surface Plasmon Resonances in Metal Oxide Nanocrystals," *Annu Rev Mater Res*, vol. 47, 2017, doi: 10.1146/annurev-matsci-070616-124259.

[45] A. Agrawal, S. H. Cho, O. Zandi, S. Ghosh, R. W. Johns, and D. J. Milliron, "Localized Surface Plasmon Resonance in Semiconductor Nanocrystals," *Chemical Reviews*, vol. 118, no. 6. 2018. doi: 10.1021/acs.chemrev.7b00613.

[46] G. Li, S. Liu, Y. Piao, B. Jia, Y. Yuan, and Q. Wang, "Joint improvement of conductivity and Seebeck coefficient in the ZnO:Al thermoelectric films by tuning the diffusion of Au layer," *Mater Des*, vol. 154, 2018, doi: 10.1016/j.matdes.2018.05.019.

[47] J. Borges *et al.*, "Thin films of Ag-Au nanoparticles dispersed in TiO2: Influence of composition and microstructure on the LSPR and SERS responses," *J Phys D Appl Phys*, vol. 51, no. 20, 2018, doi: 10.1088/1361-6463/aabc49.

[48] E. Shamonina and L. Solymar, "Metamaterials: How the subject started," *Metamaterials*, vol. 1, no. 1. 2007. doi: 10.1016/j.metmat.2007.02.001.

[49] K. V. Sreekanth *et al.*, "Hyperbolic metamaterials-based plasmonic biosensor for fluid biopsy with single molecule sensitivity," *EPJ Applied Metamaterials*, vol. 4, 2017, doi: 10.1051/epjam/2016015.

[50] Z. Guo, H. Jiang, and H. Chen, "Hyperbolic metamaterials: From dispersion manipulation to applications," *J Appl Phys*, vol. 127, no. 7, 2020, doi: 10.1063/1.5128679.

[51] A. A. Govyadinov and V. A. Podolskiy, "Metamaterial photonic funnels for subdiffraction light compression and propagation," *Phys Rev B Condens Matter Mater Phys*, vol. 73, no. 15, 2006, doi: 10.1103/PhysRevB.73.155108.

[52] A. Drozdov, M. Andreev, M. Kozlov, D. Petukhov, S. Klimonsky, and C. Pettinari, "Lycurgus cup: the nature of dichroism in a replica glass having similar composition," *J Cult Herit*, vol. 51, 2021, doi: 10.1016/j.culher.2021.07.002.

[53] A. J. Hoffman *et al.*, "Negative refraction in semiconductor metamaterials," *Nature Materials*, vol. 6, no. 12. 2007. doi: 10.1038/nmat2033.

[54] A. Fang, T. Koschny, and C. M. Soukoulis, "Optical anisotropic metamaterials: Negative refraction and focusing," *Phys Rev B Condens Matter Mater Phys*, vol. 79, no. 24, 2009, doi: 10.1103/PhysRevB.79.245127.

[55] C. Chen, Z. Wang, K. Wu, H. Chong, Z. Xu, and H. Ye, "ITO-TiN-ITO Sandwiches for Near-Infrared Plasmonic Materials," *ACS Appl Mater Interfaces*, vol. 10, no. 17, 2018, doi: 10.1021/acsami.8b01760.

[56] J. Rho *et al.*, "Spherical hyperlens for two-dimensional sub-diffractional imaging at visible frequencies," *Nat Commun*, vol. 1, no. 9, 2010, doi: 10.1038/ncomms1148.

[57] B. D. F. Casse, W. T. Lu, Y. J. Huang, E. Gultepe, L. Menon, and S. Sridhar, "Super-resolution imaging using a three-dimensional metamaterials nanolens," *Appl Phys Lett*, vol. 96, no. 2, 2010, doi: 10.1063/1.3291677.

[58] Y. Xiong, Z. Liu, and X. Zhang, "A simple design of flat hyperlens for lithography and imaging with half-pitch resolution down to 20 nm," *Appl Phys Lett*, vol. 94, no. 20, 2009, doi: 10.1063/1.3141457.

[59] D. Schurig and D. R. Smith, "Spatial filtering using media with indefinite permittivity and permeability tensors," *Appl Phys Lett*, vol. 82, no. 14, 2003, doi: 10.1063/1.1562344.

[60] R. Deshmukh, S. A. Biehs, E. Khwaja, T. Galfsky, G. S. Agarwal, and V. M. Menon, "Long-Range Resonant Energy Transfer Using Optical Topological Transitions in Metamaterials," *ACS Photonics*, vol. 5, no. 7, 2018, doi: 10.1021/acsphotonics.8b00484.

[61] H. Z. Gao *et al.*, "Hyperbolic metamaterials based on multilayer Ag/TiNxOy structure for SPR refractive index sensors," *Opt Laser Technol*, vol. 151, 2022, doi: 10.1016/j.optlastec.2022.108034.

[62] K. V. Sreekanth *et al.*, "Enhancing the Angular Sensitivity of Plasmonic Sensors Using Hyperbolic Metamaterials," *Adv Opt Mater*, vol. 4, no. 11, 2016, doi: 10.1002/adom.201600448.

[63] P. R. Willmott and J. R. Huber, "Pulsed laser vaporization and deposition," *Rev Mod Phys*, vol. 72, no. 1, 2000, doi: 10.1103/revmodphys.72.315.

[64] C. S. Casari and A. Li Bassi, "Pulsed Laser Deposition of nanostructured oxides: From clusters to functional films," in *Advances in Laser and Optics Research*, vol. 7, 2011.

[65] B.R. Bricchi, "Engineering of titanium oxide and nitride nanostructures for plasmonic applications," PhD thesis, Politecnico di Milano, 2020.

[66] L.Tovaglieri, "Tin-based plasmonic multilayer metamaterials," Master thesis, Politecnico di Milano, 2021.

[67] G.Baiardi, "Plasmonic double epsilon-near-zero titanium oxynitrides by pulsed laser deposition," Master thesis, Politecnico di Milano, 2022.

[68] L.Ornago, "Synthesis of tantalum-doped titanium oxide thin films: a bridge to infrared plasmonics," Master thesis, Politecnico di Milano, 2018.

[69] C.Mancarella, "Plasmonic and multifunctional nanostructured metamaterials with tailored electrical and optical properties," PhD thesis, Politecnico di Milano, 2023.

[70] C. A. E. S. W. C. R. Brundle, "SEM: Scanning Electron Microscopy," in *Encyclopedia of Materials Characterization*, Butterworth-Heinemann, Ed., 1992, pp. 70–84.

[71] M. A. Sutton, N. Li, D. C. Joy, A. P. Reynolds, and X. Li, "Scanning electron microscopy for quantitative small and large deformation measurements Part I:

SEM imaging at magnifications from 200 to 10,000," *Exp Mech*, vol. 47, no. 6, 2007, doi: 10.1007/s11340-007-9042-z.

[72] C. A. E. S. W. R. Brundle, "EDS: Energy-Dispersive X-Ray Spectroscopy," in *Encyclopedia of Materials Characterization*, Butterworth-Heinemann, Ed., 1992, pp. 120–134.

[73] D. E. Newbury and N. W. M. Ritchie, "Is scanning electron microscopy/energy dispersive X-ray spectrometry (SEM/EDS) quantitative?," *Scanning*, vol. 35, no. 3, 2013, doi: 10.1002/sca.21041.

[74] F. J. H. S.R.Crouch D.A.Skoog, *Principles of Instrumental Analysis*, 6th ed. 2007.

[75] Y. Il Kim *et al.*, "Endoscopic imaging using surface-enhanced Raman scattering," *European Journal of Nanomedicine*, vol. 9, no. 3–4. 2017. doi: 10.1515/ejnm-2017-0005.

[76] A. Carden, R. M. Rajachar, M. D. Morris, and D. H. Kohn, "Ultrastructural changes accompanying the mechanical deformation of bone tissue: A Raman imaging study," *Calcif Tissue Int*, vol. 72, no. 2, 2003, doi: 10.1007/s00223-002-1039-0.

[77] F. J. H. S.R.Crouch D.A.Skoog, *Principles of Instrumental Analysis*, 6th ed. 2007.

[78] C.Mancarella, "Development of plasmonic gold nanostructures with tunable optical and electrical properties," Master thesis, Politecnico di Milano, 2019.

[79] PerkinElmer Life and Analytical Sciences, "Major considerations in choosing a high performance uv/vis or uv/vis/nir system," 2004.

[80] T. W. H. Oates, H. Wormeester, and H. Arwin, "Characterization of plasmonic effects in thin films and metamaterials using spectroscopic ellipsometry," *Progress in Surface Science*, vol. 86, no. 11–12. 2011. doi: 10.1016/j.progsurf.2011.08.004.

[81] D. V. Likhachev, "Spectroscopic ellipsometry data analysis using penalized splines representation for the dielectric function," *Thin Solid Films*, vol. 669, 2019, doi: 10.1016/j.tsf.2018.10.057.

[82] P.Gondoni, "Nanostructured transparent conducting oxides for advanced photovoltaic applications," PhD thesis, Politecnico di Milano, 2014.

[83] S. Garattoni, "Synthesis of titanium nitride thin films with tunable optical and electrical properties," Master thesis, Politecnico di Milano, 2019.

List of figures

List of tables